Impact of Absorber Rod Material on Bundle Degradation Seen in CORA Experiments

S. Hagen, P. Hofmann, V. Noack, L. Sepold,
G. Schanz, G. Schumacher

Hauptabteilung Ingenieurtechnik
Institut für Materialforschung
Institut für Neutronenphysik und Reaktortechnik
Projekt Nukleare Sicherheitsforschung

Dezember 1996

Impact of absorber rod material on bundle degradation seen in CORA experiments

S. Hagen, P. Hofmann, V. Noack, L. Sepold,
G. Schanz, G. Schumacher

Impact of absorber rod material on bundle degradation seen in CORA experiments

In the CORA program 16 out of 19 tests were performed with absorber rods. Nine tests with (Ag, In, Cd) absorber material should investigate the damage behaviour in PWR-type reactors. For investigation of BWR-type behaviour, seven tests with B_4C/ss absorber were performed. The VVER B_4C/ss absorber arrangement was used in one test.

The absorber materials strongly influence the bundle degradation. In all three reactor types macroscopic degradation starts at about 1200°C (1470 K) by eutectic interactions. For PWR's the (Ag, In, Cd) absorber, molten at about 800°C (1070 K), is released from the absorber rod after failure of the stainless steel absorber cladding, caused by eutectic interaction with the Zry-guide tube. The failure may be influenced by the high vapour pressure of the cadmium. The release normally happens after reaching 1200°C (1470 K). The liquid absorber fills up the space inside the guide tube freezing in the gap at the lower end. The Ag/Zry eutectic interaction dissolves the guide tube and releases the absorber material into the bundle. In conse- quence, the Zry of the cladding starts to be liquefied by the Ag/Zry interaction. The liquefied Zry begins the dissolution of UO_2 far below the melting point of UO_2.

In the BWR absorber blade the boron carbide in contact with stainless steel re- sults in eutectic liquefaction of the blade starting again at about 1200°C (1470 K). The resulting melt destroys the Zry channel box wall by eutectic ss/Zry interactions. After distribution in the bundle the stainless steel melt starts to liquefy the Zry of the cladding. Analogue to the PWR case, also here the liquefied Zry results in the onset of UO_2 dissolution.

For the VVER reactor bundle with similar geometrical arrangement of the ab- sorber rods as in PWR reactors, but with B_4C absorber and stainless steel guide tubes, a similar behaviour was found. The B_4C/ss reaction results in the liquefaction of the absorber rods and guide tubes, starting the liquefaction of the Zr1%Nb fuel rod cladding with the following dissolution of UO_2.

The described behaviour is shown in examples from different tests. The direct comparison of test CORA-W1 without absorber and CORA-W2 with absorber dem- onstrates the strong influence of the absorber material on the melt formation, melt relocation, temperature escalation behaviour and axial temperature distribution.

Einfluß des Absorbermaterials auf die Schadensentwicklung im Reaktor-bündel: Ergebnisse der CORA-Experimente.

Im CORA-Programm wurden 16 der 19 Versuche mit Absorbermaterial durchgeführt. Neun Experimente mit (Ag,In,Cd)-Absorber sollten das Schadensverhalten in druckwasserreaktor-typischen Bündeln untersuchen. Für die Untersuchung des siedewasserreaktor-typischen Verhaltens wurden sieben Versuche mit B_4C/Edelstahl Absorber durchgeführt. Ein Test wurde mit der WER-B_4C/Edelstahl Anordnung durchgeführt.

Das Absorbermaterial hat einen starken Einfluß auf die Schadensentwicklung im Bündel. In allen drei Bündelanordnungen beginnt die Bündelzerstörung oberhalb 1200°C (1470 K) durch eutektische Wechselwirkungen. Im Druckwasserbündel geht das (Ag,In,Cd)-Absorbermaterial bei 800°C (1070 K) in den flüssigen Zustand über. Sein Edelstahlhüllrohr versagt bei gut 1200°C (1470 K) durch eutektische Wechselwirkungen mit dem Zry-Führungsrohr. Das Versagen kann auch durch den sich aufbauenden Cd-Dampfdruck beeinflußt werden. Das geschmolzene Absorbermaterial füllt den Spalt innerhalb des Führungsrohres indem die Schmelze am unteren Ende erstarrt. Die Ag/Zr eutektische Wechselwirkung löst das Hüllrohr auf und entläßt weitere Absorberschmelze ins Bündel. Die sich ausbreitende Absorberschmelze beginnt die Zry-Hülle der Brennstabsimulatoren zu verflüssigen. Das verflüssigte Zry wiederum hat die Auflösung von UO_2 weit unterhalb seiner Schmelztemperatur zur Folge.

Auch beim Siedewasserabsorber beginnt die makroskopische Verflüssigung des B_4C in Kontakt zum Edelstahl bei ca. 1200°C (1470 K). Die resultierende Schmelze zerstört die Zry-Kanalwand durch die eutektische Edelstahl/Zry-Wechselwirkung. Nach Ausbreitung im Bündel beginnt die Edelstahlschmelze das Zry der Brennstabhülle zu verflüssigen, das wiederum mit der chemischen Auflösung des UO_2 beginnt. Für den WER-Reaktor mit ähnlicher Anordnung der Absorberstäbe wie im Druckwasserreaktor, aber mit B_4C-Absorber und Edelstahl-Führungsrohr, ergab sich ein ähnliches Verhalten. Die Borkarbid/Edelstahl-Wechselwirkung resultiert in der Verflüssigung des Absorberstabs und des Führungsrohrs. Die im Bündel verbreitete Schmelze beginnt die Verflüssigung des Zr1%Nb, das daraufhin die Auflösung des UO_2 startet.

Für das oben beschriebene Verhalten werden Beispiele aus verschiedenen Tests angeführt. Der direkte Vergleich des CORA-W1 Versuchs ohne und des CORA-W2 Versuchs mit Absorbermaterial demonstriert deutlich den starken Einfluß der Absorbermaterialien auf die Schmelzenerzeugung, die Schmelzenverlagerung, dasTemperatur-Eskalationsverhalten und die axiale Temperaturverteilung

Contents

1 Introduction

From the early tests in the NIELS facility it is known, that the damage behaviour of the PWR fuel element in loss-of-coolant conditions is strongly influenced by the chemical interactions of the bundle components with each other. Absorber and spacer materials are not thermo-dynamically stable with the Zr of the fuel rod cladding. Also, the Zr interacts with UO_2 at high temperatures. Therefore, in the CORA-program most of the experiments were performed with absorber materials. Nine tests with (Ag, In, Cd) absorber should investigate the damage behaviour of PWR-type bundles. For investigation of the damage behaviour in BWR-type bundles seven tests with B_4C/ss absorber and Zry channel box walls were performed. The VVER B_4C/ss arrangement was used in one test (Table 1).

The arrangement of fuel rods and absorber assemblies of the three considered reactor types is given in Figures 1 to 3. The PWR fuel rod bundle (Figure 1) allows the absorber rods to be lowered inside the Zry-guide tubes. The (Ag,In,Cd) absorber has a stainless steel cladding. About 2,3 t of AgInCd are used in 1000 MWe reactors. The bundle arrangement in a BWR reactor is shown in Figure 2. The absorber blade is placed between 4 bundles and has the shape of a cross. The bundles are surrounded by a Zry channel box wall. Inside the stainless steel cross the boron carbide powder is contained in stainless steel tubes. The region of absorber, channel box walls and bundles, simulated in the CORA bundle, is shown in left lower half of Figure 2. The geometrical arrangement of the VVER-1000 absorber inside the bundle can be seen in Figure 3. The boron carbide is contained in stainless steel tubes which can be moved inside stainless steel guide tubes.

In this paper the strong influence of the absorber material on damage initiation and propagation are discussed and typical examples for the behaviour of the three types of absorber material (PWR, BWR, VVER-1000) are given.

2 Description of the CORA test facility

The CORA out-of-pile facility was designed to investigate the behaviour of LWR fuel elements under severe fuel damage accident conditions. In the experiments the de-

cay heat of the fission products was simulated by electrical heating. Great emphasis was given to the fact that the test bundles contain all materials used in light-water reactor fuel elements to investigate the different material interactions with increasing temperature. Pellets, claddings, grid spacers, absorber rods and the pertinent guide tubes were typical to those of commercial LWRs with respect to their compositions and radial dimensions.

Figure 4 gives a sketch of the facility. The central part of the facility was the fuel rod bundle. The bundle was enclosed in a Zry-shroud with ZrO_2 fibre insulation. A high temperature radiation shield surrounded the bundle, leaving an annular space for moving up the water filled quench cylinder. The bundle was connected to the power supply system at the upper and lower end of the test bundle.

Below the bundle was the quench unit with a water-filled quench cylinder, which could be raised around the bundle with a controlled speed. The cylinder was guided by three rods, which also connected the electric power to the bundle lower end. At the beginning of the test the water level was 220 mm below the "zero elevation" of the bundle. The "zero elevation" corresponded to the lower end of the pellet stack in the heated rods.

The bundle upper end was fixed in the bundle head plate. The plate was connected to the surge condenser by a funnel shaped tube. The surge condenser was double-walled, leaving access to the bundle end fittings above the bundle head funnel.

The steam was produced in the steam generator, superheated and led to the lower end of the bundle, entering at "zero elevation". The steam not consumed within the bundle was condensed in two parallel condensers and the hydrogen produced was given to the off-gas system after dilution to a low H_2 concentration by air.

The arrangements of the fuel rod bundles to study the influence of the different absorber materials are shown in Figures 4 and 4a. In all bundles heated and unheated fuel rods were used. Both types of rods were sheathed with the standard cladding. For the PWR- and BWR-bundles we used Zircaloy-4 (10.75 mm outer diameter) and for the VVER bundles Zr1%Nb (8.2 mm outer diameter). The central part of the

heated fuel rod consisted of a tungsten heater rod (PWR, BWR: 6mm; VVER: 4 mm) and was surrounded by UO_2 annular pellets. The tungsten heater had an effective length of 1024 mm. At top and bottom the tungsten heater was screwed into Mo-electrodes of 300 mm length which fit directly into the Zry cladding. The molybdenum electrodes were connected to copper electrodes by a brazing technique and both were insulated from the Zircaloy cladding by a flame-sprayed ZrO_2 layer. The unheated fuel rod contained solid UO_2 pellets.

The standard PWR bundle consisted of 16 heated, seven unheated and two absorber rods. Test CORA-12 contained only one absorber rod. The absorber rods were composed of original components. The (Ag80,In15,Cd5) absorber material was sheathed in stainless steel, and this rod was surrounded by a Zry-guide tube. Three original spacers were used in the bundle to maintain its geometry. The material of the control spacer was Inconel 718 and the upper and lower ones were made of Zry-4.

The BWR bundle simulated the arrangement of the absorber-cross placed between bundles which are surrounded by a channel box. The original B_4C powder/stainless steel rods inside the stainless steel blade were separated to the fuel rod simulators by the Zry channel box walls.

Two tests were performed with larger bundles. The cross sections of the PWR test CORA-7 and the BWR-test CORA-18 are shown in Figure 4a. No influence of the bundle size on the damage behaviour was found.

The VVER 1000 bundle behaviour (Figure 3) was studied by a 19-rod bundle with hexagonal arrangement of 13 heated and 6 unheated rods. Three original stainless steel spacers were used to maintain the geometry. For the absorber test CORA-W2 one unheated rod was replaced by an original absorber rod inside the stainless steel guide tube.

The bundles were surrounded by a Zry-4 shroud of 1.2 mm thickness. The shroud conducted the steam through the bundle. The steam entered the lower end (0 mm elevation) at 180°C. To minimise the heat losses from the shroud, the test bundle

was surrounded by an insulating layer of ZrO_2 fibre of 19 mm (0.75 inch) thickness. Since the ZrO_2 fibre layer had a low heat conductivity and heat capacity, the shroud temperatures could follow the bundle temperature closely. Since the Zry shroud participated in the interaction with steam, the resulting oxidation energy contributed substantially to the bundle heatup.

To keep the heat losses as low as possible, the bundle was surrounded by an additional high temperature shield. This shield consisted mainly of ceramic fibre plates (inner plates ZrO_2; outer plates Al_2O_3).

The power input was controlled by measuring the currents of the single rods and setting the common voltage necessary to obtain the desired power history. The electric heating was done by direct current to avoid eddy currents in the containment structures.

3 Test conduct

Generally the tests were performed following the same procedure. Three phases (Figure 5) could be recognised:
1. gas preheat phase 0 - 3000 s
2. transient phase 3000 - 4900 s (CIRA.7: 4200 s; CORA-W2: 4500 s)
3. quench or cooling phase.
For the normal bundle in the gas preheat phase there was a flow of 8g/s preheated argon (CORA 7 and 18: 16 g/s; CORA W1 and W2: 6g/s). In addition, a low constant electric power input of about 0.65 kW was used. During this period the temperature in the insulation reached a level which was high enough to avoid steam condensation. To keep the videoscope windows clear an additional flow of 1 g/s argon was directed to the front of the windows of the videoscopes. The system pressure in the facility was controlled to 0.22 MPa.

During the transient phase the temperature increase of initially 1 K/s was produced by rising the electric power input from 6 to 27 kW in the PWR tests and from 6 to 26 kW in the BWR tests (CORA 7 and 18: max. 39 kW; CORA W1 and W2: max. 14

kW). At 3300 s an additional steam flow of 6 g/s for the PWR tests and of 2 g/s for the BWR tests was added to the system (CORA-7: 12 g/s; CORA-18: 4 g/s; CORA-W2: 4 g/s). The electric power input was finished at about 4900 s.

In the non-quench tests the bundles were allowed to cool down by the normal heat losses. In contrast for the quench tests /11/ the water-filled quench cylinder was moved up over the bundle with 1 cm/s. The initiation of quench movement started 30 s before electric energy shutdown (CORA-13) or about 150 s later (CORA-12 and CORA-17).

4 Influence of the chemical interactions between the fuel element components on melt formation

Fuel elements of a reactor are designed to be used at operational temperatures (< 400°C). At the temperatures which are reached under loss of coolant conditions most of the materials are chemically not stable to each other. Preferential eutectic reactions lower the liquefaction temperature of the materials which are in contact. The interactions start in regions where the materials are in local contact. As soon as the eutectic temperature is reached, some material will be liquefied. The molten material general increases the contact and with this the further chemical interactions. At a given critical temperature a fast liquefaction of the components take place.

In Figure 6 the melting temperatures of the reactor components are compared to the temperature regions in which the components in contact to each other are liquefied. For all three reactor types change of the geometry as a result of liquefaction starts at about 1200°C. In the PWR type bundle the stainless steel/Zircaloy and the silver/Zircaloy reaction are responsible for the damage initiation. The (Ag,In,Cd) alloy is already molten at 800°C, but as it is stable against stainless steel, it is kept inside the cladding, as long as the stainless steel/Zircaloy interaction does not chemically fail the cladding. For the BWR- and VVER-type bundle the B_4C/ss reaction starts the liquefaction process. Also here at about 1200°C the liquefied stainless steel attacks the Zircaloy or Zr1%Nb.

The same behaviour as in the integral CORA-tests is also found in the separate effects tests for the interaction between the relevant components. The results of these kinetic studies allow the quantitative description of the reaction rates. In all cases a complete liquefaction of the materials takes place clearly below the melting points of the components.

4.1 Influence of the absorber material in PWR reactors.

In most of the PWR reactors the (Ag,In,Cd) absorber material is contained in stainless steel cladding (Figure 1). The absorber rod is placed inside the Zircaloy guide tube. The guide tubes are positioned by spacers (axial distance of about 50 cm). The spacer material has changed in recent years from Inconel to Zircaloy. But there are still stainless steel springs left inside the Zircaloy spacer.

A schematic presentation of the damage initiation and progression process in the PWR bundle is given in Figure 8. The (Ag,In,Cd) absorber liquefies at about 800°C. As this alloy is stable in contact to stainless steel the melt is kept as long as the cladding is intact. Failure of the cladding below the melting temperature can be produced, if the original central positioned absorber rod is touching the Zircaloy guide tube. The cross sections of the bundle after the test confirm this possibility. The deformation of the absorber rod may also be influenced by the increasing vapour pressure of cadmium.

In all tests it was found that the failure develops after surpassing 1200°C, that means about 200°C below the melting point of the stainless steel. The released absorber melt is filling the gap between absorber rod and guide tube, after forming a blockage at the lower end by "freezing" due to the axial temperature profile. This can be seen for test CORA-5 in Figures 9 to 12. Above 90 mm elevation the gap is completely filled (Figure 9 to 10). Partial filling of the gap by frozen material can be seen down to 0 mm elevation (Figure 11). The absorber melt dissolves the Zry wall of the guide tube, so that further absorber material can spread into the bundle. In the upper part of Figure 12 one can recognise the increasing attack on the Zry wall toward the upper end. Figure 10 shows that in test CORA-5 the Zircaloy wall is destroyed above 250 mm. But partial remnants of the oxidised part of the guide tube have survived.

<u>Figure 10 to 14</u> clearly show the strong chemical attack of the absorber material on the Zry cladding of the surrounding rods. The detail photograph in <u>Figure 13</u> shows the strong dissolution on the right side of the rod and intact parts of the cladding at the same elevation. In the upper part of the cladding on the left side, one can recognise partial attack inside the cladding. Also from other tests we have learned that the absorber melt attacks the remaining metallic layer inside the ZrO_2-layer on the oxidised cladding tube.

The cross sections (<u>Figure 10 to 11</u>) show clearly the increasing dissolution of UO_2 pellets by the liquid Zircaloy. This is confirmed by the high content of uranium in the refrozen melt.

<u>Figure 15 to 18</u> show the influence of the absorber material in test CORA-7. CORA-7 used a large bundle (57 rods including 5 absorber rods). This test was already terminated earlier (4200 s instead at 4900 s; immediately after the escalation) to concentrate on the initial damage of the bundle.

<u>Figure 15</u> shows the preferred melt formation on the left side at the position of the absorber rod. This absorber melt solidified at the outside of the bundle, would attack in the case of a large core the surrounding Zry fuel rod cladding. The picture (<u>Figure 15</u>) also clearly shows the typical deformation of the partially oxidised cladding ("flowering"). The flowering also can be recognised from the cross sections in the upper half of the bundle (<u>Figure 16</u>).

The cross sections between 622 and 1005 mm also show in the inner bundle region the attack of the absorber melt on the Zry cladding. The damage process starts at the absorber positions. In the upper half between 480 mm and 1147 mm all absorber rods have disappeared. The absorber melt has dissolved most of the surrounding Zry cladding. First attack on UO_2 pellets can be recognised.

The molten and dissolved material has relocated down to the central spacer. The spacer is no barrier for the molten material. The horizontal cross section at 465 mm and 426 mm together with the vertical cross section (<u>Figure 18</u>) show, that the melt penetrates through the spacer and freezes according to the axial temperature profile.

The blockage is influenced by the spacer, but the main influence is given by the axial temperature profile. The cross section at -30 mm shows that only a small fraction of the melt fall down as droplets.

In Figures 19 to 21 information about the failure of the absorber rods in test CORA-10 is given. In Figure 19 the failure time determined from the pressure loss of the absorber rods is compared to the first movement of absorber melt as seen by video records. The failure of absorber rod 4.6 and the first melt movement took place within two seconds after 3980 s test time. This means that within 2 s after failure of the absorber cladding, the absorber melt has also penetrated the Zry guide tube and distributes within the bundle. In agreement with the axial temperature distribution the first melt movement is seen at 800 mm elevation.

Absorber rod 6.2 failed at 3990 s. In Figure 20 are shown temperatures measured in the absorber rods and at the guide tubes. One can recognise deviations from the smooth temperature increase again at 3980 s for absorber rod 4.6 and at 3990 s for absorber rod 6.2. We assume that these irregularities are caused by the failure of the absorber rod cladding. According to the temperature profile the absorber is already molten over the corresponding length. After failure of the cladding this melt leaves the absorber tube. The temperature of the absorber rod in the upper part at the time of failure is about 1230°C (1500 K).

The failure time and temperature of heated and unheated rods is shown in Figure 21. In three unheated rods and one heated rod the internal pressure was registered. They failed at about 2.5 bar at the time marked in Figure 21 by the vertical lines. As can be seen form the temperature graphs this corresponds to temperatures between 1280°C to 1450°C.

4.2 Influence of the absorber material in BWR reactors

As is shown in Figure 2 in most BWR reactors the absorber material is arranged in form of a cross between four neighbouring fuel bundles, which are contained in a

Zircaloy box. The B_4C powder is kept in the absorber cross blade inside stainless steel tubes as seen in Figure 4.

The schematical presentation of Figure 22 illustrates the B_4C inside the stainless steel tube and stainless steel blade, surrounded by the Zry channel box wall. The B_4C in contact to the stainless steel tube starts the eutectic interactions. With the melt formation the contact between the materials increases and accelerates the liquefaction process through tube and blade wall. This process starts in the upper part of the bundle at the axial temperature maximum. The liquefied material flows into the gap between absorber blade and channel box wall. The stainless steel melt starts to attack the Zircaloy channel box wall by eutectic interaction. The melt running down within the gap solidifies due to the axial temperature profile. On top of the crust thus formed the melt can pile up within the gap. The eutectic interaction with the Zircaloy liquefies the channel box wall in contact with the melt and releases the melt into the bundle region. In the upper part the absorber blade and the channel box walls disappear completely.

Figure 23 provides the view through the bundle in the direction of the absorber blade. Between 850 and 970 mm elevation one can recognise the background behind the bundle. That means that at these elevations the absorber blade has completely dissappeared.

In Figure 24 the photograph is taken as shown in the schematic view of the cross sections of the bundle. The melt down of absorber blade and channel box wall and strong attack on the fuel rods can be seen. The Zry cladding is liquefied by eutectic interaction to an extent that the pellets can be recognised.

The destruction of the absorber blade and channel box walls in the upper part of the bundle can even better be seen in the horizontal cross sections of Figure 25. At 1145 mm elevation one recognises the intact absorber blade, channel box walls and fuel rod simulators. Due to the low maximum temperature of (1200 °C) at this elevation the interactions between the materials have not yet started. About 100 mm lower below (1052 mm elevation) the B_4C/ss interaction has destroyed the absorber rods and the resulting melt has strongly attacked the Zry channel box walls. At 836 mm

elevation the absorber blade and the channel box walls have practically disappeared and the attack has spread into the bundle onto the fuel rod simulators. At 612 mm elevation one can recognise the increasing attack onto the UO_2 pellets by the liquefied Zry.

In the lower half of the bundle the sintered remnants of the absorber rods can be seen. Below 112 mm the refrozen melt within the gap between the channel box walls and between the rods of the simulator bundle is visible. The vertical cross section in Figure 26 shows that the refrozen melt has piled up to an elevation of about 190 mm.

In Figure 27 the two upper cross sections of the large BWR type bundle CORA-18 are given. They clearly demonstrate the attack of the absorber material on the Zircaloy. At the 1158 mm elevation with a maximum temperature of 1100°C no attack on absorber blade and channel box wall can be recognised. About 140 mm lower, with a maximum temperature of 1530°C the absorber blade is liquefied and the neighbouring part of the channel box walls is nearly dissolved. The other half of the channel box wall, though practically at the same temperature, is fully intact. In the region of the dissolved channel box walls the melt has touched two of the fuel rod simulators and started the attack on the Zry cladding.

Figure 28 gives the temperature measured between the rods of the absorber blade for BWR test CORA-28. In addition the pressure drop of the fuel rod simulator at failure of the cladding is given. The deviation from the smooth regular temperature increase starts at about 4270 s. This corresponds to an absorber temperature of about 1230°C. The fuel rod simulator adjacent to the absorber blade failed between 4340 s and 4490 s.

We assume that the failure of the fuel rod cladding is caused by the interaction with the absorber melt. This means that the time between the beginning of melt formation in the absorber rod and failure of the simulator cladding takes about 70 s.

4.3 Influence of the absorber material in VVER-1000 reactors

As shown in Figure 3 in VVER-1000 reactors the absorber rod (B_4C powder in stainless steel claddings) is placed inside stainless steel guide tubes. A similar behaviour

as in the BWR reactors is therefore expected. The schematical presentation of the attack by the B_4C/stainless steel absorber material on the Zr1%Nb of the fuel rod cladding is given in Figure 29. It is determined by the B_4C/ss eutectic reactions.

As for the influence of the absorber material we can compare the two tests CORA-W2 and CORA-W1, because of almost identical test procedures in CORA-W2 one fuel rod simulator was replaced by an absorber rod (Figure 30). The absorber rod (Figure 31) was made of original components. The comparison of the test conditions is given in Figure 32. Power input, argon flow and steam input was chosen to give the same temperature increase as in the earlier PWR and BWR tests. In test CORA-W2 the power input was stopped earlier at 4500 s.

In Figure 33 the temperatures in the bundle are compared for the two tests. Up to 4200 s the temperature behaviour is the same. The escalation starts in both tests in the upper part of the bundle, at 950 mm elevation. Then, in CORA-W2, the escalation moves much faster to lower elevations. In less than 300 s the escalation has reached the 350 mm elevation. In contrast, in CORA-W1 at the 350 mm elevation no escalation develops at all and the 450 mm elevation was reached by the escalation front only after about 500 s.

The difference in the behaviour of the two tests can be found in the absorber material. The earlier liquefaction of a larger amount of material results in an earlier relocation of molten material. By the heat capacity of the melt the temperature level at the lower elevations is increased which again results in an earlier initiation of the exothermic Zr/steam escalation process.

This strong influence of the melt production by the absorber material against can be seen in Figure 34. There, the non-absorber test CORA-W1 is compared to the absorber tests CORA-29 (PWR) and CORA-28 (BWR). Again we find the much faster progression of the escalation front for the two tests with absorber material. For the BWR test the larger absorber channel favours the movement of the liquefied material.

The much larger melt formation and relocation in the absorber test CORA-W2 - though we had a smaller electric energy input - in comparison to the non-absorber test CORA-W1 is demonstrated in Figures 35a to 35c: The horizontal cross sections of the two tests are directly compared. While in CORA-W1 melt formation and relocation is restricted to above about 400 mm in CORA-W2 the maximum of relocated material is found down to an elevation at about 200 mm elevation.

The axial mass distribution of the two tests is compared in Figure 36. These measurements confirm what we have seen in the cross sections: The relocation of the melts to much lower elevations.

Finally in Figure 37 we have compared for the two tests the axial distribution of the mass to the axial temperature distribution. One can recognise a strong correlation between the axial temperature profile and the melt relocation: The melt relocation to lower elevations in CORA-W2 corresponds to the expansion of high temperatures to the low elevation. We have seen in all our tests that melt relocation and axial temperature distribution are coupled to each other. The melt relocation is determined by the axial temperature distribution, but the axial temperature distribution on the other side is influenced by the melt relocation and the exothermic steam/Zircaloy-reaction triggered by the heat transported with the melt.

The strong influence of the absorber material on the damage initiation and propagation is also confirmed by the post-test analysis of the cross sections. In Figures 39 to 42 some examples of these investigations are given. From different positions of the cross section at the 206 mm elevation the material composition was determined (Figure 39). In position 3 the situation within the cladding of a fuel rod simulator was investigated, which had an intact outer oxide shell, with some missing internal material. Figure 40 shows, that between the outer oxidised cladding and the UO_2 pellet a layer has formed, which contains in addition to the Zr also Fe, Cr, Ni and U. We assume that Fe, Cr, Ni which have liquefied the Zr1%Nb at higher elevations has relocated between outer oxidised skin and pellet. The liquefied Zr1%Nb has dissolved U from the UO_2 pellets. The point measurements show values of about 15 wt% U, 6 wt% Fe, 1.4 wt% Cr, 13 wt% Ni. At some spots even boron is found inside the cladding. A similar layer structure and composition is found on the opposite side of the

bundle (Figure 41). This demonstrates that the absorber material is distributed throughout the whole bundle.

The liquefied ZrNb starts to dissolve the UO_2 of the pellet. Figure 42 shows the attack of the Zr on the UO_2. The enlarged views show the penetration of the Zr melt into the pellet dissolving the UO_2 grains. The view of position 3 shows that there is infiltration of the molten Zr across larger regions of the pellet.

4.4 Summary and conclusions

The results of all CORA experiments show that the degradation of LWR bundles is strongly influenced by interactions of the absorber materials with the other components of the fuel element. With increasing temperatures under loss-of-coolant conditions the materials in contact are no longer chemically stable, with each other.

In PWR reactors the (Ag, In, Cd) absorber, the stainless steel of the absorber cladding and the Inconel of the spacer grids react eutectically with Zircaloy. In BWR and VVER reactors the B_4C powder of the absorber forms eutectic alloys with the stainless steel of its cladding. The liquefied stainless steel reacts with the Zircaloy. In all three reactor types the liquefaction of macroscopic regions of the bundle starts at about 1200°C. The eutectic temperatures of the different reactions are partially below 1000°C, but it takes some time till the diffusion of the initially separated materials start the process on a macroscopic scale. The Zircaloy liquefied by the absorber materials starts the dissolution of the UO_2 pellets over 1000 K below the melting temperature of UO_2.

The comparison of tests with and without absorber rods have shown, that the earlier and stronger melt development and relocation also influences the time behaviour of the escalation of temperature within the bundle. The relocated melt transports also heat, which increases the temperature in the regions of relocated melts, so that the escalation of temperature can start earlier. The changed axial temperature distribution again influences the further relocation. This means, that a strong correlation exists between the axial temperature profile and the melt relocation, which is strongly influenced by the absorber material.

Another aspect of the absorber material relocation is connected with criticality considerations. The early "separation" of absorber material from the fuel to the lower

part of the bundle requires the use of sufficiently borated water for reflooding of the core to avoid recriticality.

For BWR core material behaviour in severe accidents, the use of other material combinations (B_4C/Zircaloy) instead of the present ones (B_4C/stainless steel) would result in greater flexibility for accident management measures. Meltdown would be delayed in time and shifted to higher temperatures.

5 References

/1/ S. Hagen, K. Hain, "Out-of-pile Bundle Experiments on Severe Fuel Damage (CORA-Program): Objectives, Test Matrix and Facility Description", KfK 3677 (1986).

/2/ S. Hagen, P. Hofmann, G. Schanz, L. Sepold, "Interactions in Zry/UO_2 Fuel Rod Bundles with Inconel Spacers at Temperatures above 1200°C; (Post-test Results of Severe Fuel Damage Experiments CORA-2 and CORA-3)", KfK 4378 (1990).

/3/ S. Hagen, V. Noack, L. Sepold, P. Hofmann, G. Schanz, G. Schumacher, "Results of SFD Experiments CORA-13 (OECD International Standard Problem 31)", KfK 5054 (1993).

/4/ M. Firnhaber, K. Trambauer, S. Hagen, P. Hofmann, "ISP-31 OECD/NEA-CSNI International Standard Problem, CORA-13 Experiments on Severe Fuel Damage, NEA/CSNI/R (93) 17, GRS-106, KfK 5287 (1993)

/5/ J. Burbach, "Ergebnisse von REM-Mikrobereichsanalysen des DWR Bünde-labschmelzexperimentes CORA-13" KfK 5162 (1993).

/6/ J. Burbach, "Ergebnisse von REM/EDX-Mikrobereichsanalysen des SWR-Bündelabschmelzexperimentes CORA-16, KfK 4560 (1994).

/7/ S. Hagen, P. Hofmann, V. Noack, G. Schanz, G. Schumacher, L. Sepold; "Dry Core BWR Test CORA-33: Test Results", KfK 5261 (1994).

/8/ S. Hagen, P. Hofmann, V. Noack, G. Schanz, G. Schumacher, L. Sepold; "BWR Slow Heatup Test CORA-31, Test Result", KfK 5383 (1994).

/9/ S. Hagen, P. Hofmann, V. Noack, G. Schanz, G. Schumacher, L. Sepold; "Behaviour of a VVER Fuel Element Tested under Severe Accident Conditions in the CORA Facility (Test Results of Experiment CORA-W1)", KfK 5212 (1994).

/10/ Hagen, P. Hofmann, V. Noack, G. Schanz, G. Schumacher, L. Sepold; "Behaviour of a VVER-1000 Fuel Element with Boron/Steel Absorber Tested under Severe Fuel Damage Conditions in the CORA Facility (Results of Experiment CORA-W2)", KfK 5363 (1994).

/11/ S. Hagen, P. Hofmann, V. Noack, L. Sepold, G. Schanz, G. Schumacher;" Comparison of the Quench Experiments CORA-12, CORA-13, CORA-17", *FZKA* 5679, (1996).

/12/ P. Hofmann, S. Hagen, G. .Schanz, A. Skokan: "Reactor Core Materials Interactions at Very High Temperatures", *Nuclear Technology*, Vol. 87, 146-186(1989).

/13/ S. Leistikow, G. Schanz; "Oxidation Kinetics and Related Phenomena of Zircaloy-4 Fuel Cladding Exposed to High Temperature Steam and Steam-Hydrogen Mixtures Under PWR Accident Conditions". *Nucl. Eng. Des.*, 103, 65-84.(1987).

/14/ P. Hofmann, H.J. Neitzel, E.A. Garcia: "Chemical Interactions of Zircaloy-4 Tubing with UO_2 Fuel and Oxygen at Temperatures between 900 and 2000°C; Experiments and PECLOX Code", *KfK* 4422 (1988)

/15/ P. Hofmann, M. Markiewicz, J. Spino: "Reaction Behaviour of B_4C Absorber Material with Stainless Steel and Zircaloy in Severe LWR Accidents", *Nuclear Technology*, Vol. 90, 226-244 (1990).

/16/ E.A. Garcia, P. Hofmann, A. Denis; "Analysis and Modelling of the Chemical Interactions between Inconel Grid Spacers and Zircaloy Cladding of LWR Fuel Rods; Formation of Liquid Phases due to Chemical Interactions", *Nuclear Materials* 89, 20-33, (1992).

/17/ P. Hofmann, M. Markiewicz: "Compatibility Experiments between Inconel Spacer Grids and Zircaloy Cladding", *KfK* 4729 (1994).

/18/ P. Hofmann, M. Markiewicz: Chemical Behaviour of (Ag, In, Cd) Absorber Rods in Severe LWR Accidents, *KfK 4670 (1990)*.

/19/ P. Hofmann, M. Markiewicz; "Chemical Interactions between As-received and Pre-oxidised Zircaloy-4 and Stainless Steel at High Temperatures", *KfK* 5106 (1994).

/20/ M.S. Veshchunov, P. Hofmann; "Modelling of B_4C Interactions with Zircaloy at High Temperatures", *Journal of Nuclear Materials* 210 (1994) 11-20.

/21/ M.S. Veshchunov, P. Hofmann; "Dissolution of Solid UO_2 by Molten Zircaloy"; *Journal of Nuclear Materials* 209 (1994) 27-40.

/22/ M.S. Veshchunov, P. Hofmann; "Modelling of the Interactions between B₄C and
Stainless Steel at High Temperatures"; *Journal of Nuclear Materials* 226 (1995)
72-91.

/23/ P. Hofmann, M. Markiewicz; Liquefaction of Zircaloy-4 by molten (Ag,In,Cd) ab-
sorber alloy, *Journal of Nuclear Materials 209 (1994) 92-106.*

/24/ M.S. Veshchunov, P. Hofmann; Modelling of Zircaloy dissolution by molten
(Ag,In,Cd) absorber alloy, *Journal of Nuclear Materials 228 (1996) 318-329.*

/25/ M.S. Veshchunov, P. Hofmann, A.V. Berdyshev; Critical evaluation of UO₂ dis-
solution by molten Zircaloy in different crucible tests, *Journal of Nuclear Materi-
als ... (1996), to be published.*

6 Acknowledgements

7 List of Tables

Tab. 1:   CORA Test Matrix

8 List of Figures

Tab. 1: CORA Test Matrix

Test No.	Max. Cladding Temperatures	Absorber Material	Other Test Conditions	Date of Test
2	$\approx 2000°C$	-	UO_2 refer., inconel spacer	Aug. 6, 1987
3	$\approx 2400°C$	-	UO_2 refer., high temperature	Dec. 3, 1987
5	$\approx 2000°C$	Ag, In, Cd	PWR-absorber	Febr. 26, 1988
12	$\approx 2000°C$	Ag, In, Cd	quenching	June 9, 1988
16	$\approx 2000°C$	B_4C	BWR-absorber	Nov. 24, 1988
15	$\approx 2000°C$	Ag, In, Cd	rods with internal pressure	March 2, 1989
17	$\approx 2000°C$	B_4C	quenching	June 29, 1989
9	$\approx 2000°C$	Ag, In, Cd	10 bar system pressure	Nov. 9, 1989
7	$< 2000°C$	Ag, In ,Cd	57-rod bundle, slow cooling	Febr. 22, 1990
18	$< 2000°C$	B_4C	59-rod bundle, slow cooling	June 21, 1990
13	$\approx 2200°C$	Ag, In, Cd	OECD/ISP; quench initiation at higher temperature	Nov. 15, 1990
29*	$\approx 2000°C$	Ag, In, Cd	pre-oxidized,	April 11, 1991
31*	$\approx 2000°C$	B_4C	slow initial heat-up (≈ 0.3 K/s)	July 25, 1991
30*	$\approx 2000°C$	Ag, In, Cd	slow initial heat-up (≈ 0.2 K/s)	Oct. 30, 1991
28*	$\approx 2000°C$	B_4C	pre-oxidized	Febr. 25, 1992
10	$\approx 2000°C$	Ag, In, Cd	cold lower end 2 g/s steam flow rate	July 16, 1992
33	$\approx 2000°C$	B_4C	dry core conditions, no extra steam input	Oct. 1, 1992
W1	$\approx 2000°C$	-	WWER-test	Febr. 18, 1993
W2	$\approx 2000°C$	B_4C	WWER-test with absorber	April 21, 1993

Initial heat-up rate: ≈ 1.0 K/s; Steam flow rate, PWR: 6 g/s, BWR: 2 g/s; quench rate (from the bottom) ≈ 1 cm/s

Tab. 2: Design characteristics of the PWR bundle

Bundle type:		PWR
Bundle size:		25 rods
Number of heated rods:		16
Number of unheated rods:		7
Pitch:		14.3 mm
Rod outside diameter:		10.75 mm
Cladding material:		Zircaloy-4
Cladding thickness:		0.725 mm
Rod length:	- heated rods: (elevation	1960 mm - 489 to 1471 mm)
	- unheated rods (elevation	1672 mm - 201 to 1471 mm)
Heated pellet stack:		1000 mm
Heater material:		Tungsten (W)
Heater	- length	
	- diameter	
Fuel pellets	- heated rods:	UO_2 annular pellets
	- unheated rods:	UO_2 full pellets
Pellet stack	- heated rods: - unheated rods:	O to 1000 mm - 199 to 1295 mm
U-235 enrichment		0.2 %
Pellet outer diameter (nominal)		9.1 mm
Grid spacer	- material:	Zircaloy -4, Inconel 718
	- length:	Zry 42 mm Inc 38 mm
	- location:	lower (Zry) -5 mm center (Inc) + 496 mm top (Zry) + 880 mm
Shroud	- material	Zircaloy -4
	- wall thickness	1.2 mm
	- outside dimensions	89.4 x 90.4 mm
	- elevation	36 mm to 1231 mm
Shroud insulation		ZrO_2 fibre
	- insulation thickness	19 mm
	- elevation	36 mm to 1036 mm

Table 2: (Continuation)

Mo electrode	- length	300 mm
	- diameter	8,6 mm
Cu electrode	- length	189 mm (lower end)
	- length	669 mm (upper end)
	- diameter	8,6 mm
Absorber rod	- number of rods	2
	- material and composition	80Ag,15In,5Cd (wt.%)
	- cladding	Stainless steel
	- cladding OD	11,2 mm
	- cladding ID	10,2 mm
	- length	1660 mm
	- absorber material	-189 mm to +1300 mm
Absorber rod guide tube	- material	Zircaloy-4
	- OD	13,8 mm
	- wall thickness of tube	0,8 mm
Plenum Volume	- heated rods	$12 \cdot 10^{-6}$ m^3
	- unheated rods	$87 \cdot 10^{-6}$ m^3

Tab. 3: Design characteristics of the BWR bundle

Bundle type		BWR
Bundle size		18 rods
Number of heated rods		12
Number of unheated rods		6
Pitch		14.3 mm
Rod outside diameter		10.75 mm
Cladding material		Zircaloy-4
Cladding thickness		0.725 mm
Rod length	- heated rods elevation	1840 mm - 369 to 1471 mm
	- unheated rods elevation	1672 mm - 201 to 1471 mm
Heated pellet stack		0 to 1000 mm
Heater material		Tungsten (W)
Heater	- length	1000 mm
	- diameter	6 mm
Fuel pellets	- heated rods	UO_2 annular pellets
	- unheated rods	UO_2 full pellets
Pellet stack	- heated rods	0 to 1000 mm
	- unheated rods:	- 200 to 1300 mm
U-235 enrichment		0.2 %
Pellet outer diameter (nominal)		9.1 mm
Grid spacer	- material	Zircaloy -4
	- length	42 mm
	- location (upper end)	lower -33 mm center 578 mm top 1167 mm
Shroud	- material	Zircaloy -4
	- wall thickness	1.2 mm
	- outside dimensions	94.4 x 116 mm
	- elevation	40 - 1235 mm

Tab. 3: (Continuation)

Shroud insulation	- material	ZrO_2 fibre
	- insulation thickness	19 mm
	- elevation	40 mm to 1070 mm
Mo electrode	- length	300 mm (upper and lower end, respectively)
	- diameter	8.6 mm
Cu electrode	- length	189 mm (lower end)
	- length	669 mm (upper end)
	- diameter	8.6 mm
Absorber rod	- number of rods	11
	- material	B_4C powder
	- cladding	Stainless steel
	- cladding OD	5.8 mm
	- cladding ID	4.6 mm
	- length	1600 mm
	- absorber material	-270 mm to +1300 mm
Absorber blade	- material	stainless steel
	- dimensions inside	76 x 6 mm
	- wall thickness	1 mm
Channel box wall	- material	Zircaloy -4
	- dimensions inside	13 x 92 mm
	- wall thickness	1.2 mm
Plenum Volume	- heated rods	$19.8 \cdot 10^{-6}$ m^3
	- unheated rods	$39.0 \cdot 10^{-6}$ m^3

Tab. 4: Design characteristics of the VVER bundle

Bundle type:		VVER
Bundle size:		19
Number of heated rods:		13
Number of unheated rods:		5
Pitch:		12.75 mm
Cladding outside diameter		9.13 mm
Cladding inside diameter:		7.72 mm
Cladding material:		Zr-1% Nb
Heater:	- material	Tungsten (W)
	- diameter	4 mm
Fuel pellets:	- heated rods	UO_2 annular pellets
	- outer diameter (nominal)	7.57 mm
	- diameter of central void	4.2 mm
	- unheated rods	UO_2 annular pellets
	- diameter of central void	2.4 mm
Pellets stack:	- heated rods	0 to 1000 mm
	- unheated rods	-142/-192 to 1400 mm
U-235 enrichment		0.3 %
Grid spacer	- material	Stainless steel: 1.4541 (06Ch18N10T and 08Ch18N10T)
	- height	20 mm
	- number	3
	- location by elevation of upper edges (from level 0 mm)	-5; 210; 610 mm
Shroud	- material	Zr-1%Nb
	- wall thickness	1.0 mm
	- outer dimension	68 mm
	- length	1195 mm
Absorber rod	- material	B_4C
	- cladding	Stainless steel
	- cladding OD	8.2 mm
	- cladding ID	7.0 mm
Absorber rod guide tube	- material	Stainless steel
	- OD	12.6 mm
	- ID	11.0 mm

Absorber rods:
Ag In Cd / ss-sheath
2,3 t in 1000 MWe-reactor

SPACER
Inconel
Zry

FUEL RODS:
Zry-4 + UO$_2$

Absorber
Guide
Tubes
Zry
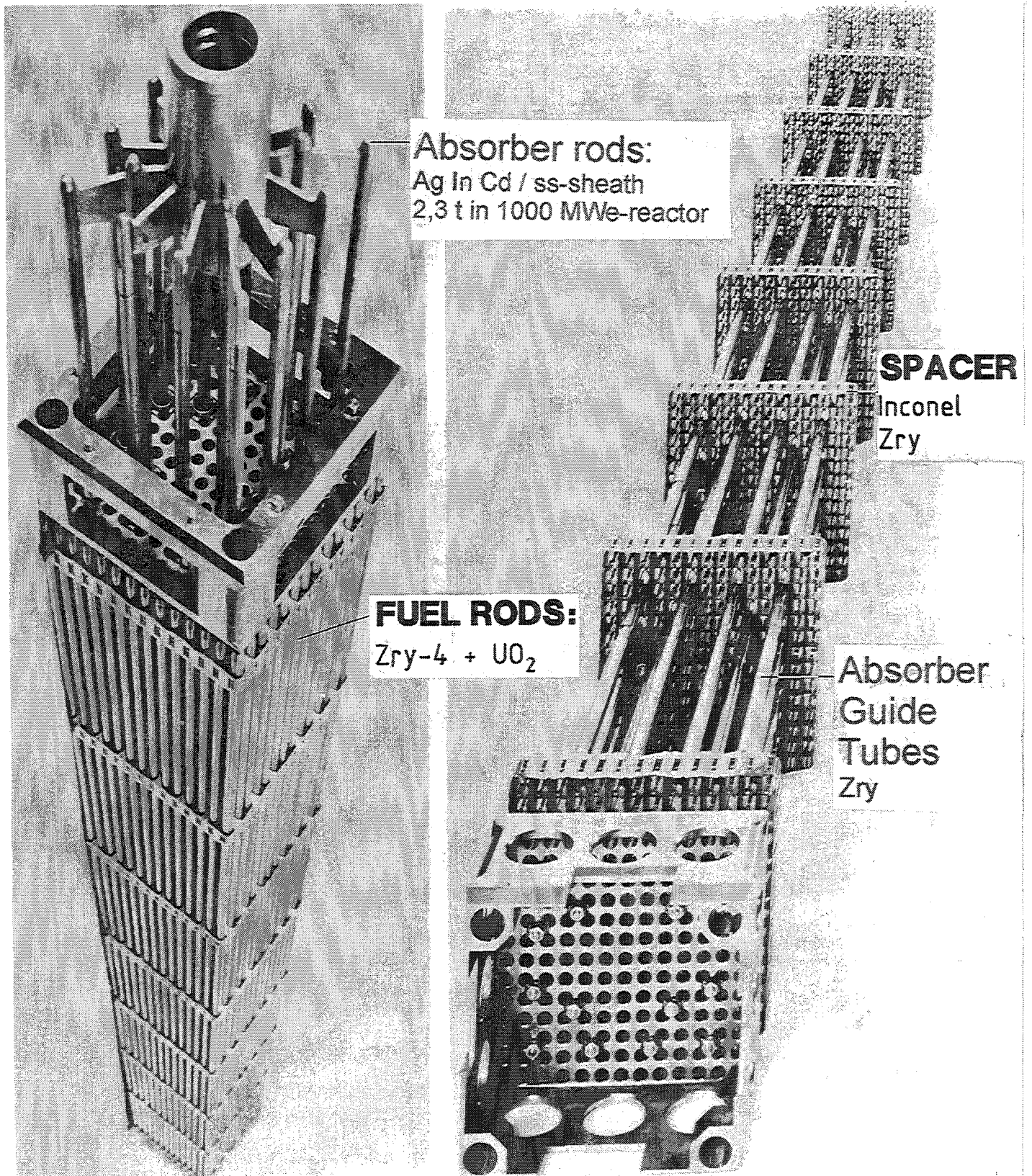
**Fig. 1: PWR - fuel element with absorber rods (left)
and its supporting structure (right)**

- B$_4$C is thermodynamically unstable in contact to stainless steel and Zircaloy

- stainless steel is unstable in contact to Zry

- Zry is unstable in contact to UO$_2$

zircaloy channel box wall

fuel rod
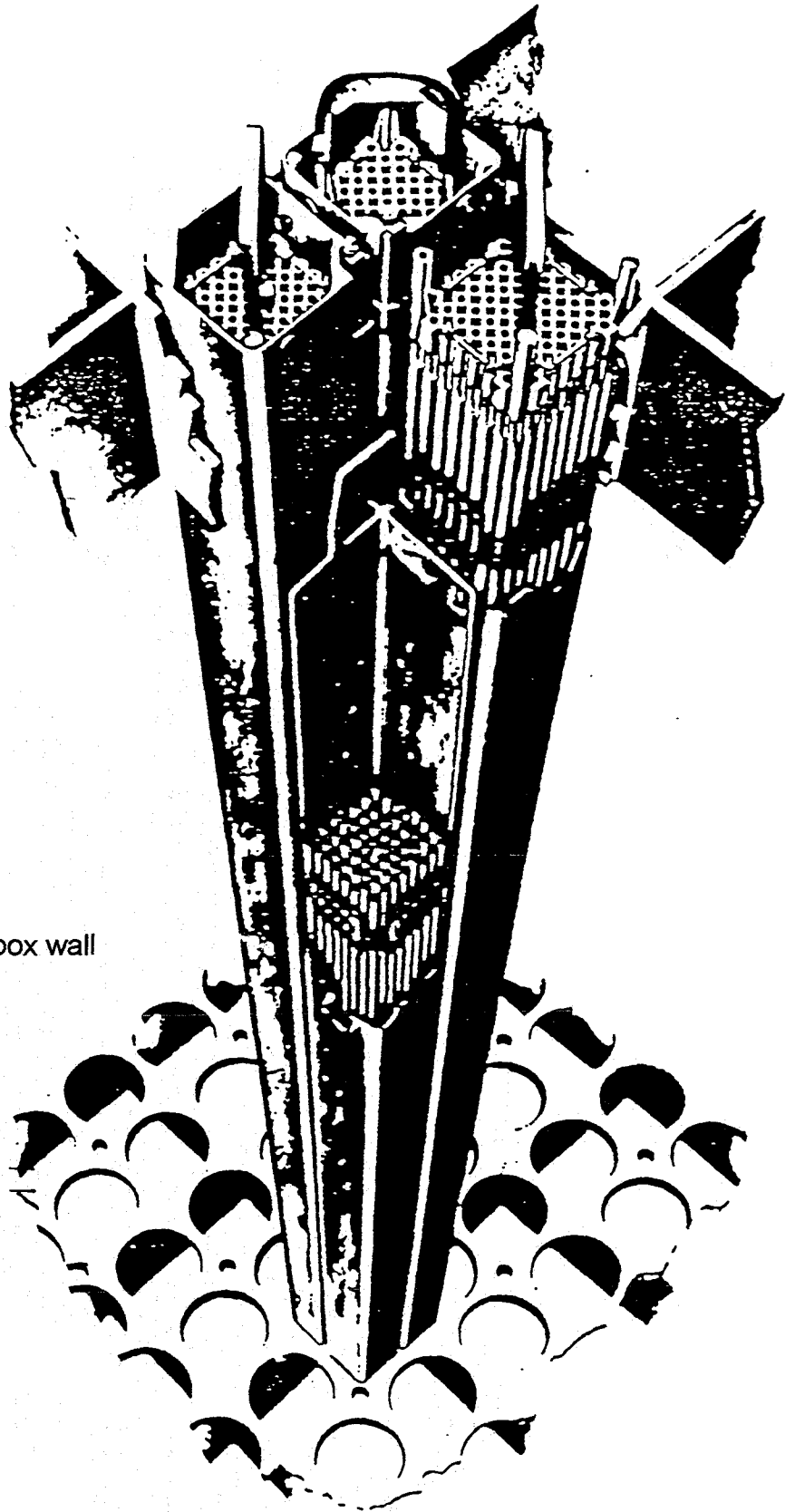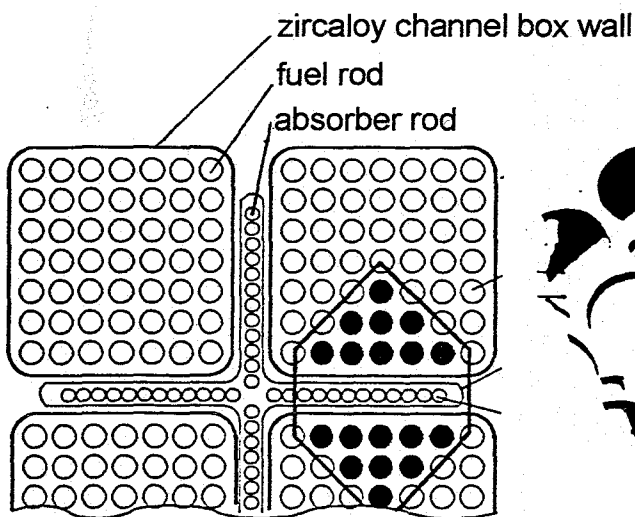
absorber rod

Fig. 2: Absorber arrangement of the BWR fuel elements

B$_4$C-absorber in SS-cladding

SS-guide tube
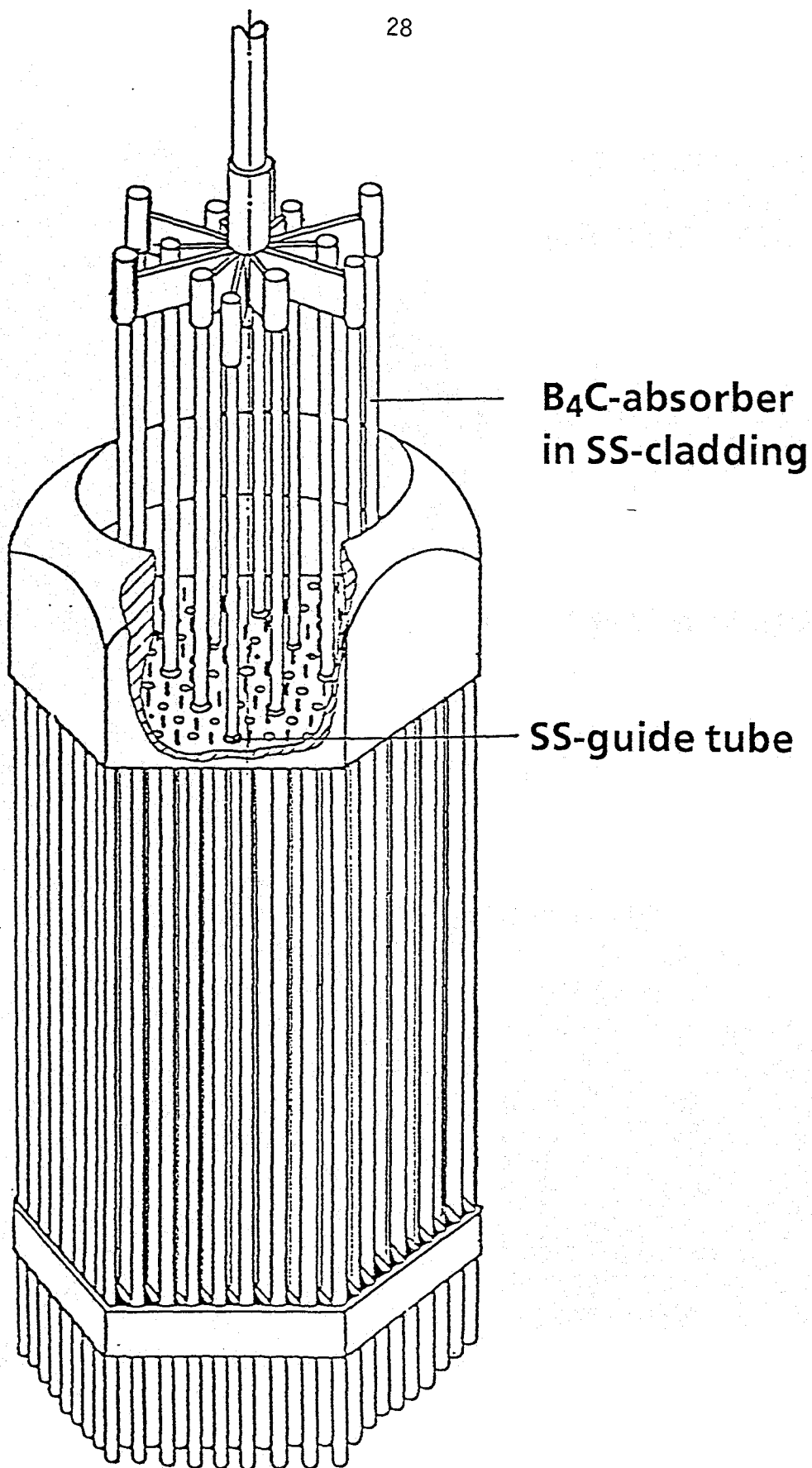
Fig. 3: VVER-1000 fuel bundle

CORA Severe Fuel Damage Test Facility

CONTAINMENT

CONDENSER (2)

AIR

OFF-GAS SYSTEM

TEST BUNDLE

QUENCH-TUBE (WATER FILLED)

WATER

STEAM GENERATOR/ SUPERHEATER

ARGON

MAIN COMPONENTS

1000 mm

TEST BUNDLE

0 mm

STEAM INLET

HIGH-TEMPERATURE SHIELD INSULATION

VIEWPORT FOR VIDEOSCOPE

ELECTRIC POWER CONNECTION

TEST SECTION

Heated rod   Unheated rod   Absorber rod

Cu-electrode

Bundle flange

1471 mm

1471 mm

Mo-electrode

1000 mm

UO_2 annular pellet

1000 mm

Tungsten heater

Mo-electrode

0 mm

Cu-electrode

Zry-4 cladding

UO_2 solid pellet

0 mm

250

201

-200 mm

BWR

ss-blade

B4C absorber rod

Zry-channel (box) wall

fuel rod

PWR

heated rod

unheated rod

shroud

shroud insulation

(Ag, In, Cd)-absorber rods

VVER-1000

heated rod

unheated rod

shroud (Zr, 1% Nb)

B4C absorber rod

Fig.4:

29

CORA-7

- Zircaloy shroud
- Insulation: ZrO_2 - Fiber
- AG / IN / CD - Absorber with Zry guide tube
- Heated
- Unheated

CORA-18

- Zircaloy shroud
- Insulation: ZrO_2 - Fiber
- SS-blade
- B_4C powder Absorber
- Heated
- Unheated

Fig.4a: Cross sections of the large bundles CORA-7 and CORA-18
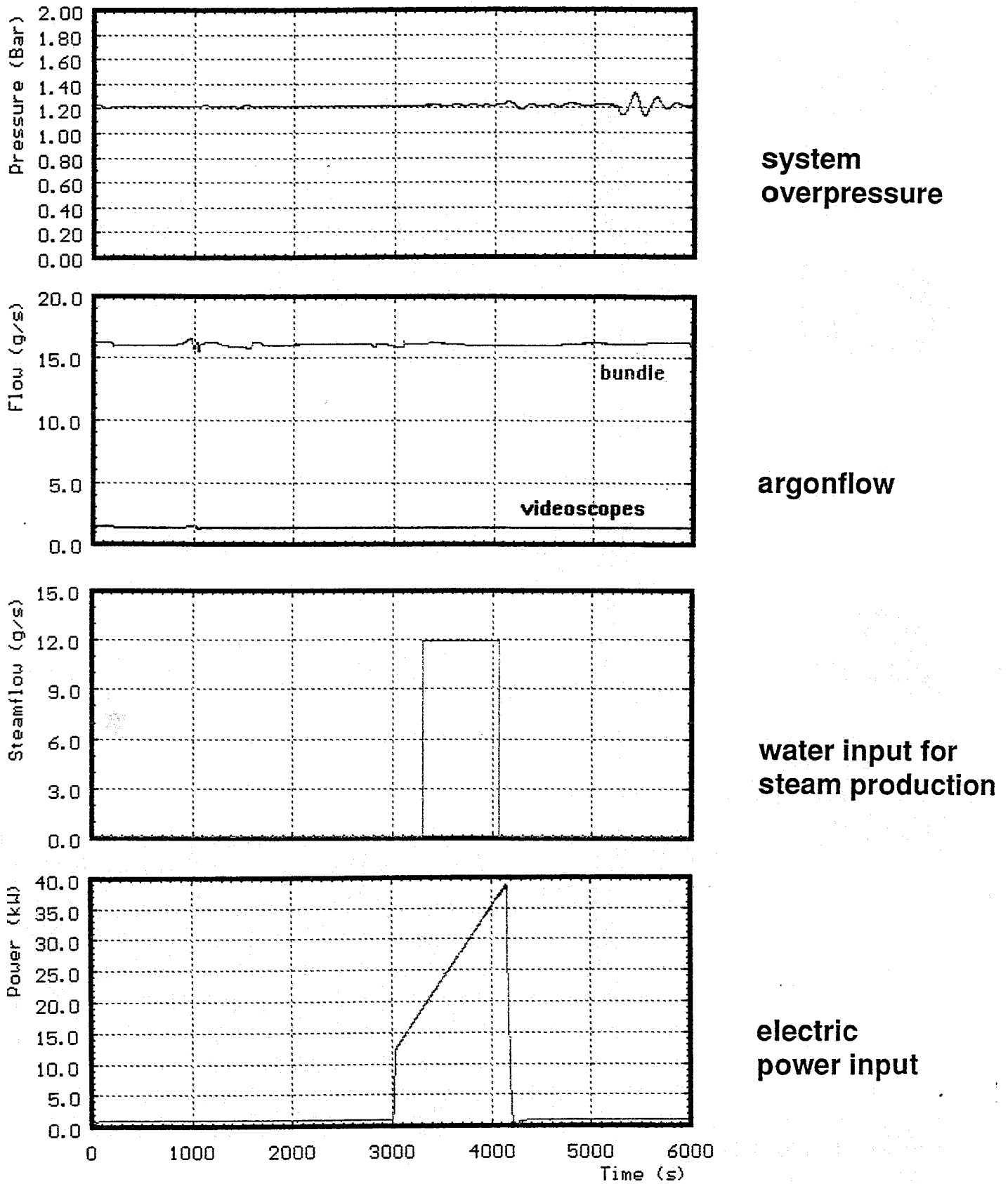
Fig. 5: CORA-7; sytem pressure, argon flow, steam input and power
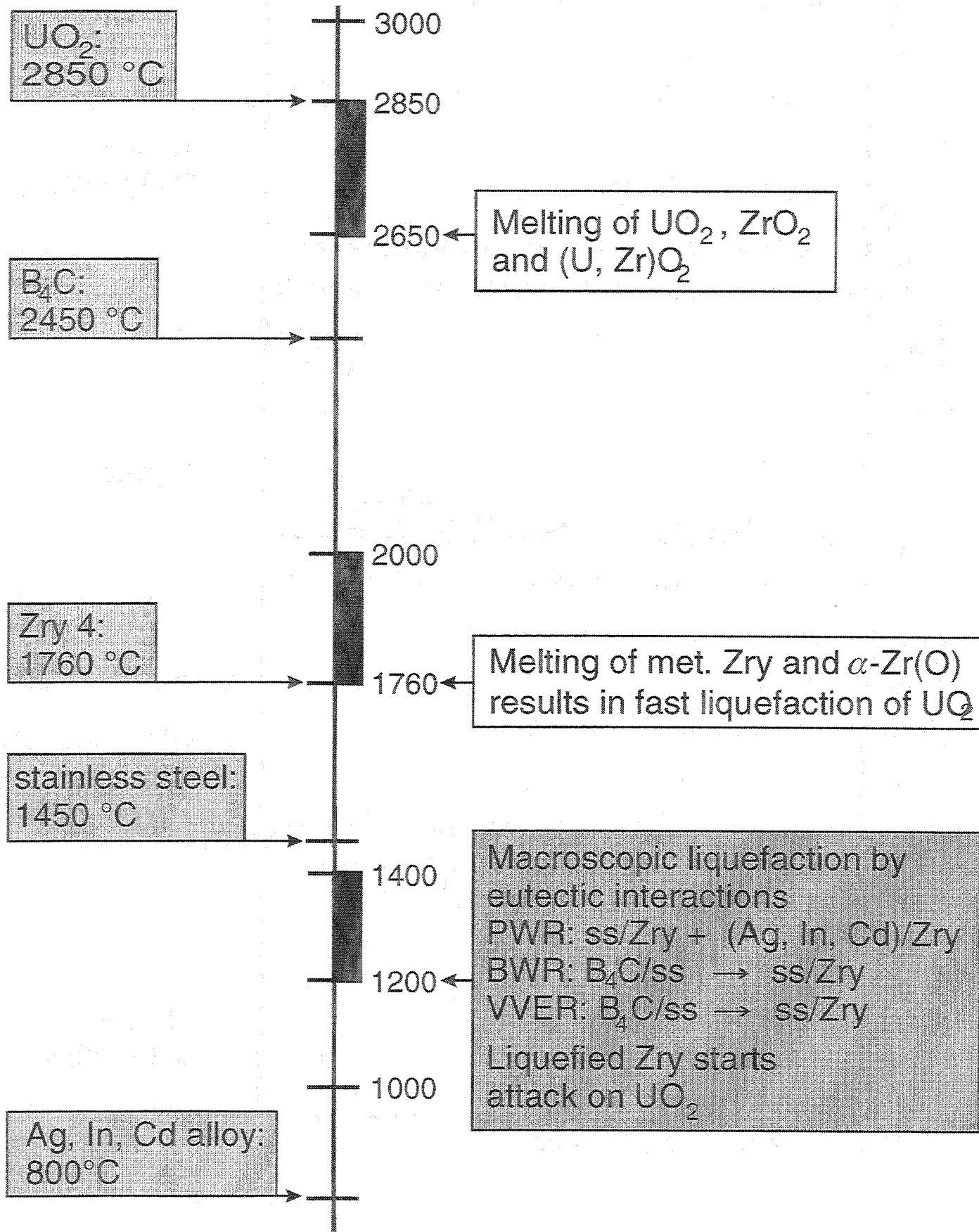
Fig.6: Temperature regimes for liquid-phase formation
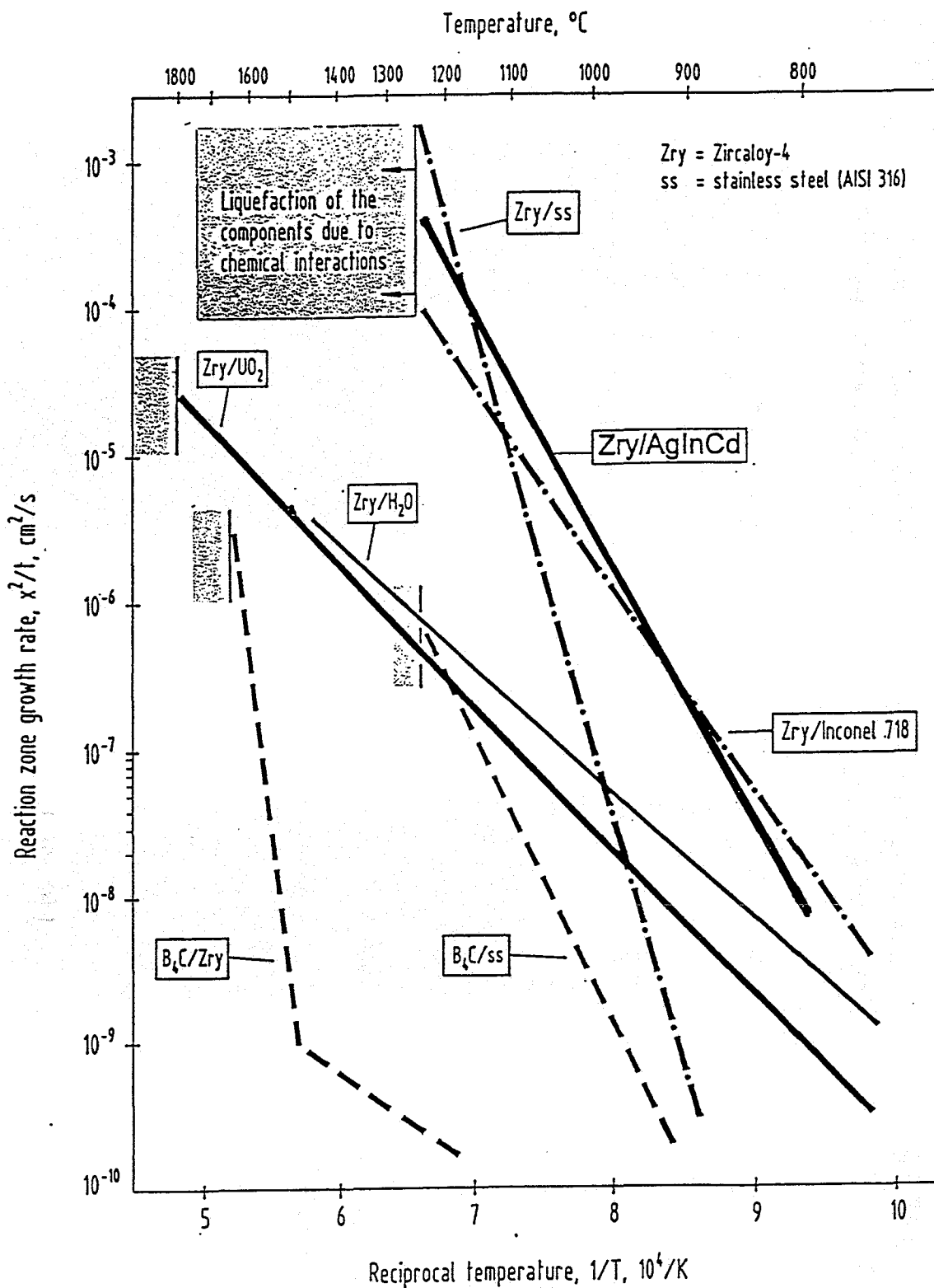
Fig.7: Comparsion of the total reaction zone growth rates of various reaction couples for PWR and BWR bundles.

Interaction:
ss-absorber cladding
Zry-guide tube
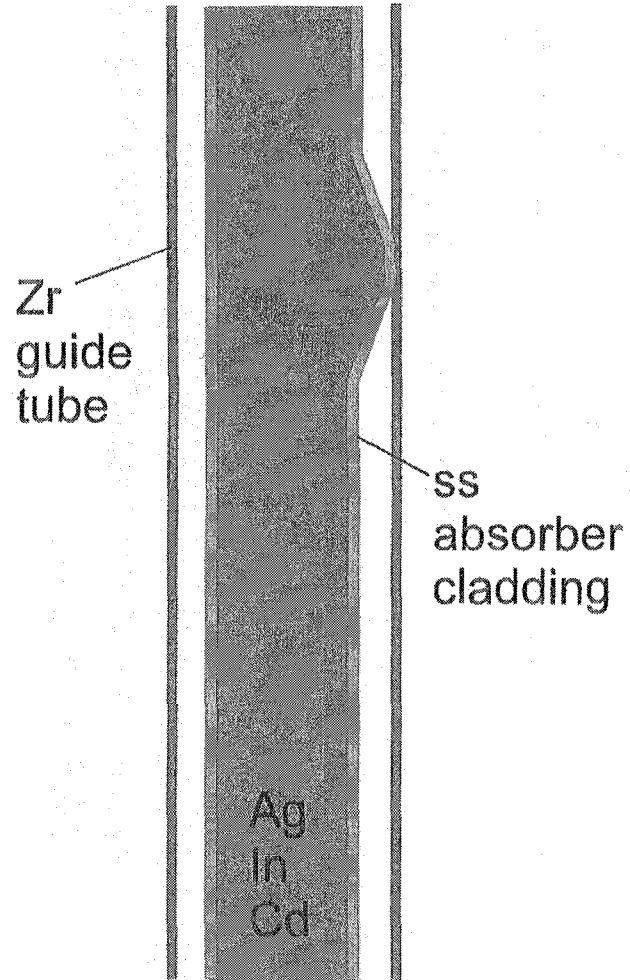
Interaction:
liquid (Ag, In, Cd)
Zry-guide tube
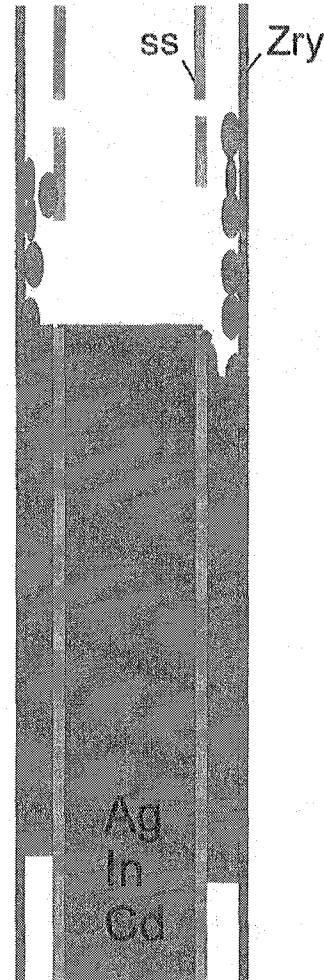
Interaction:
liquid (Ag, In, Cd)
Zry-fuel rod cladding

Zr
guide
tube

ss
absorber
cladding

ss   Zry

Ag
In
Cd

ss

Zry

Ag
In
Cd

Ag
In
Cd

UO₂

34
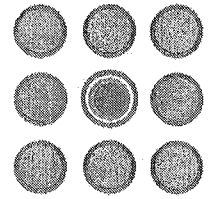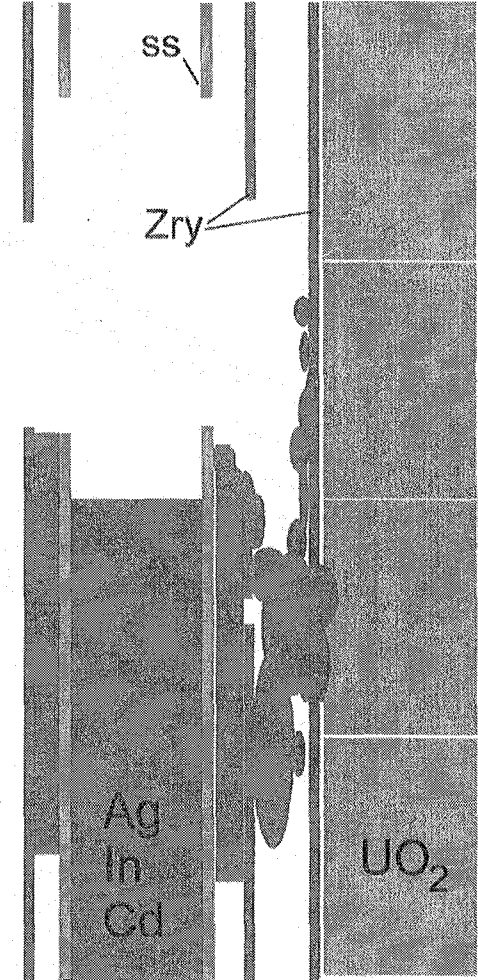
Fig.8: Steps of (Ag, In, Cd) attack on Zry cladding (PWR)

95 mm
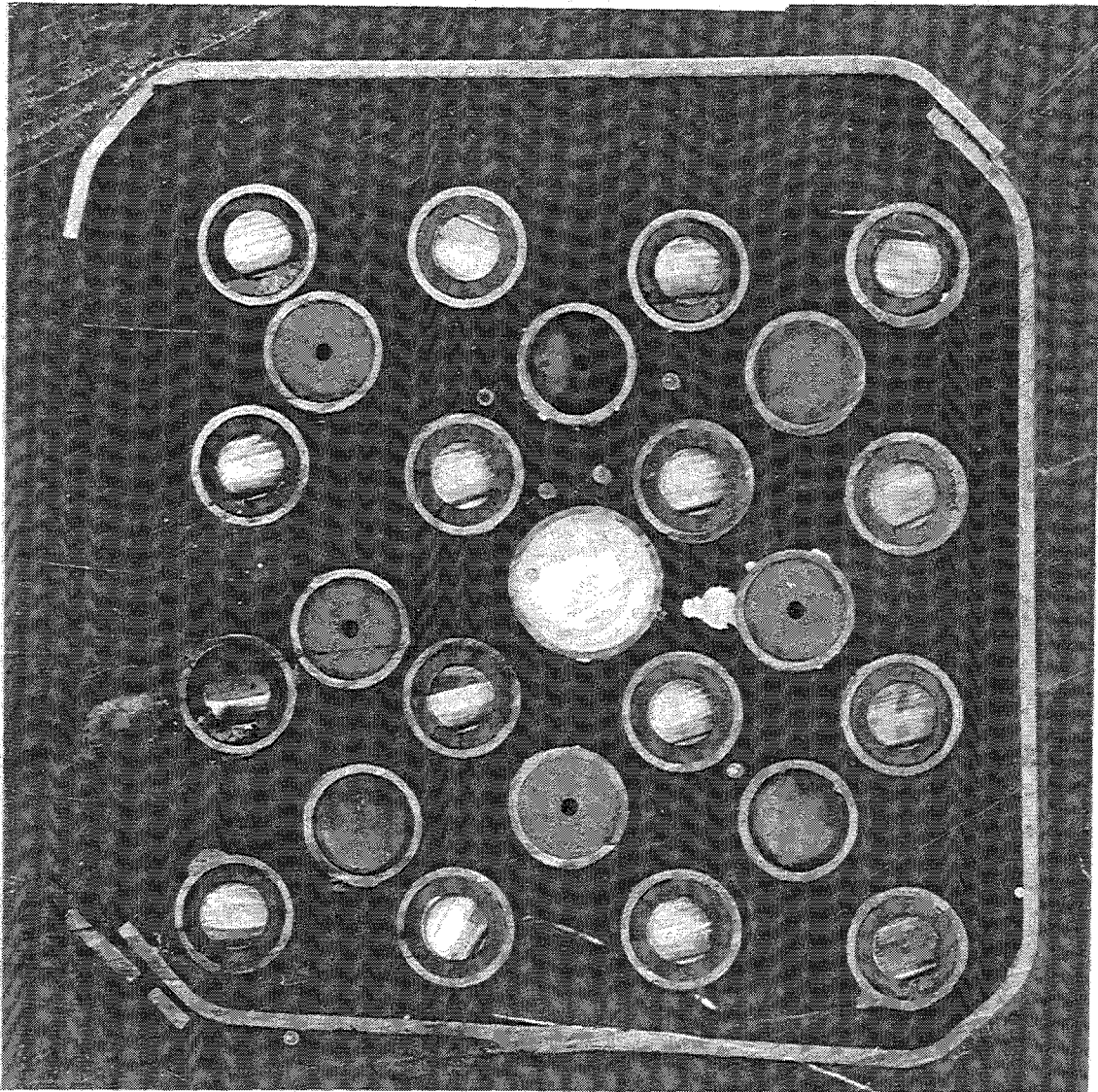
Fig.9: Cross section of bundle CORA-5. The re-solidified material has filled the gap inside the guide tube.
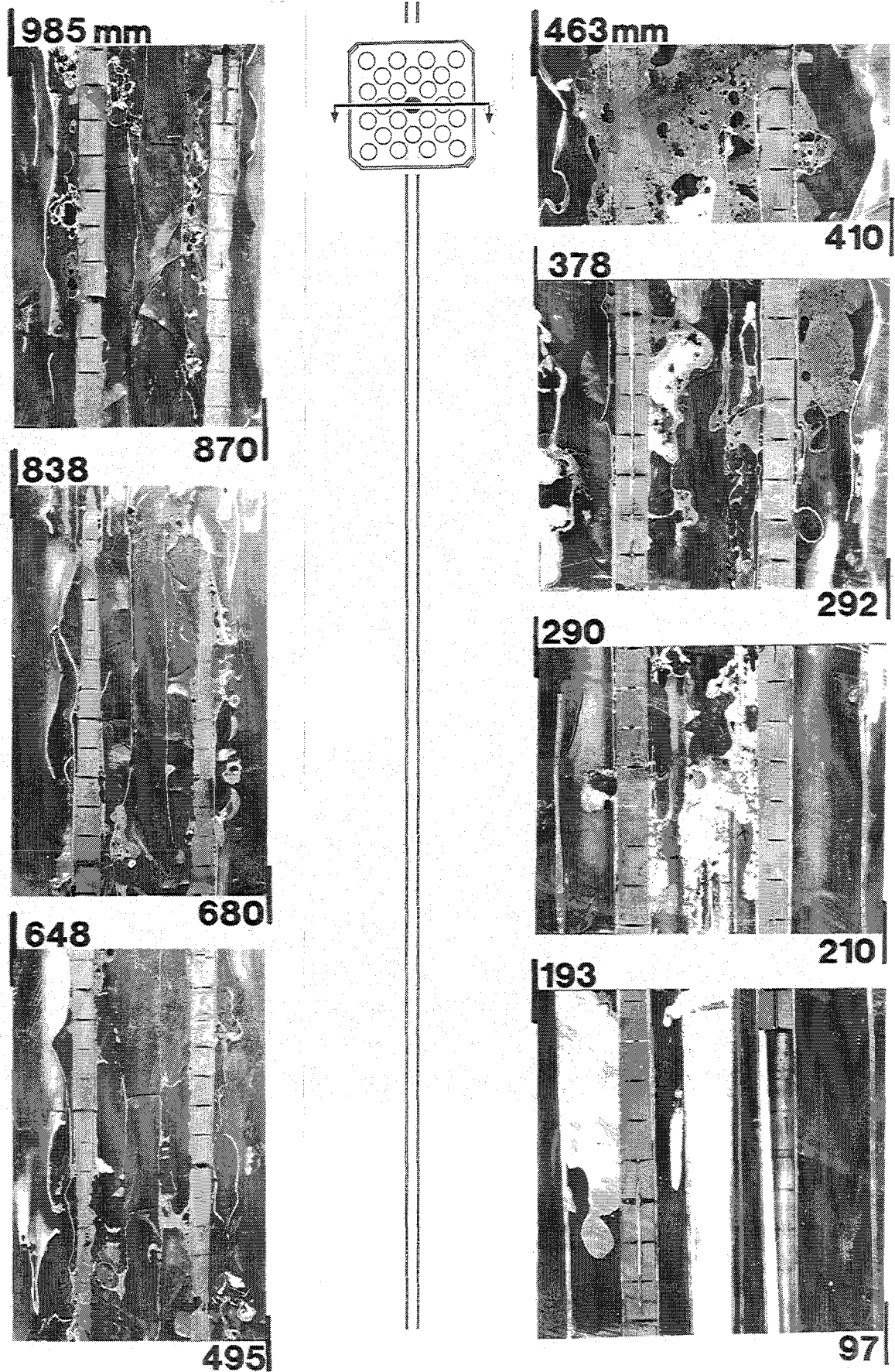
Fig.10: Vertical cross section of bundle CORA-5 showing the absorber rod destruction.
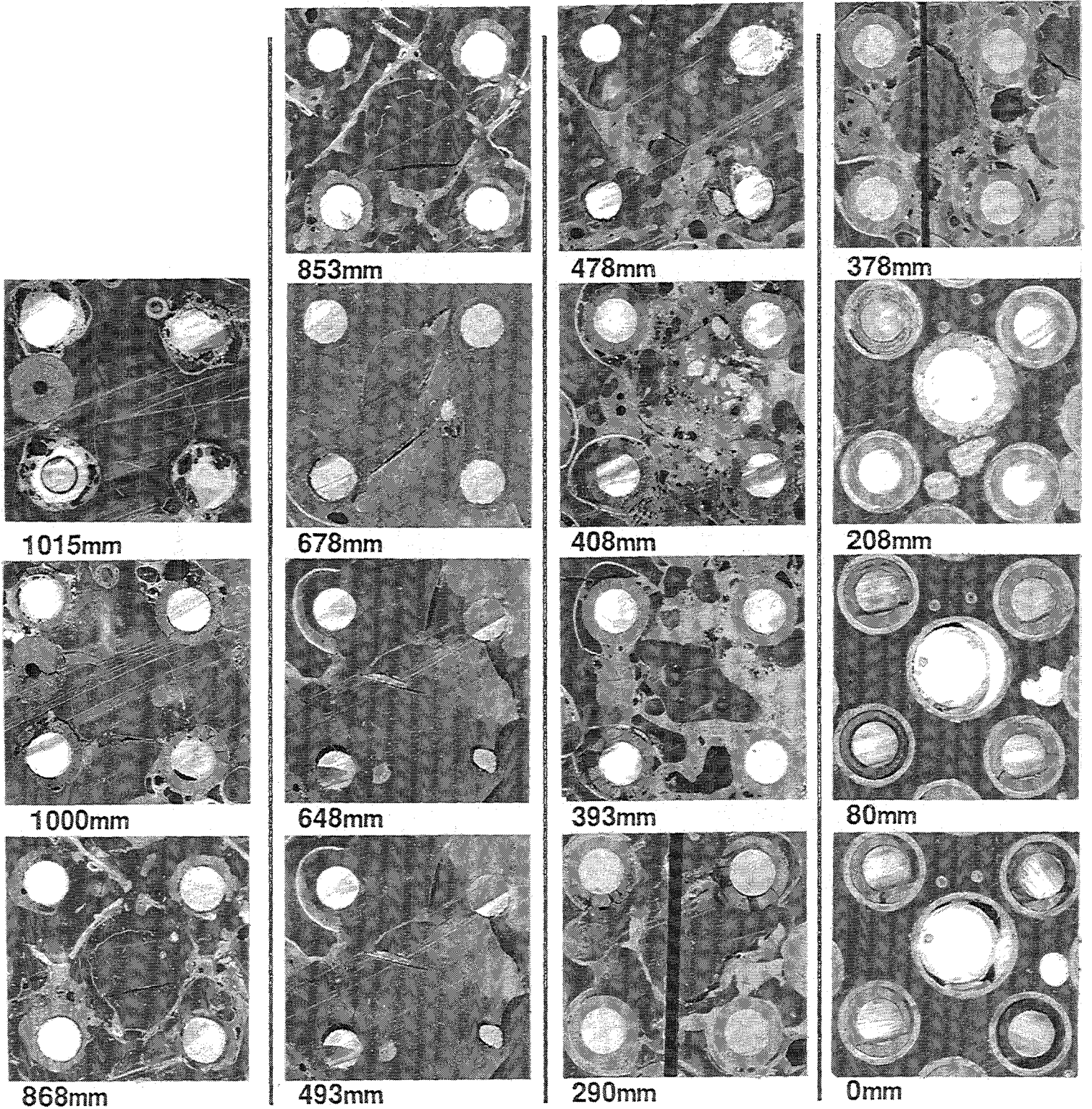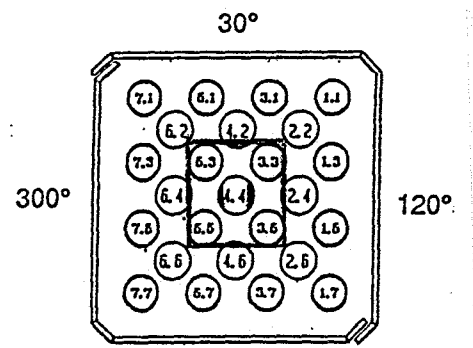
Fig.11:Horizontal cross sections of bundle CORA-5 with the absorber rod and its four neighbours

175 mm

120 mm
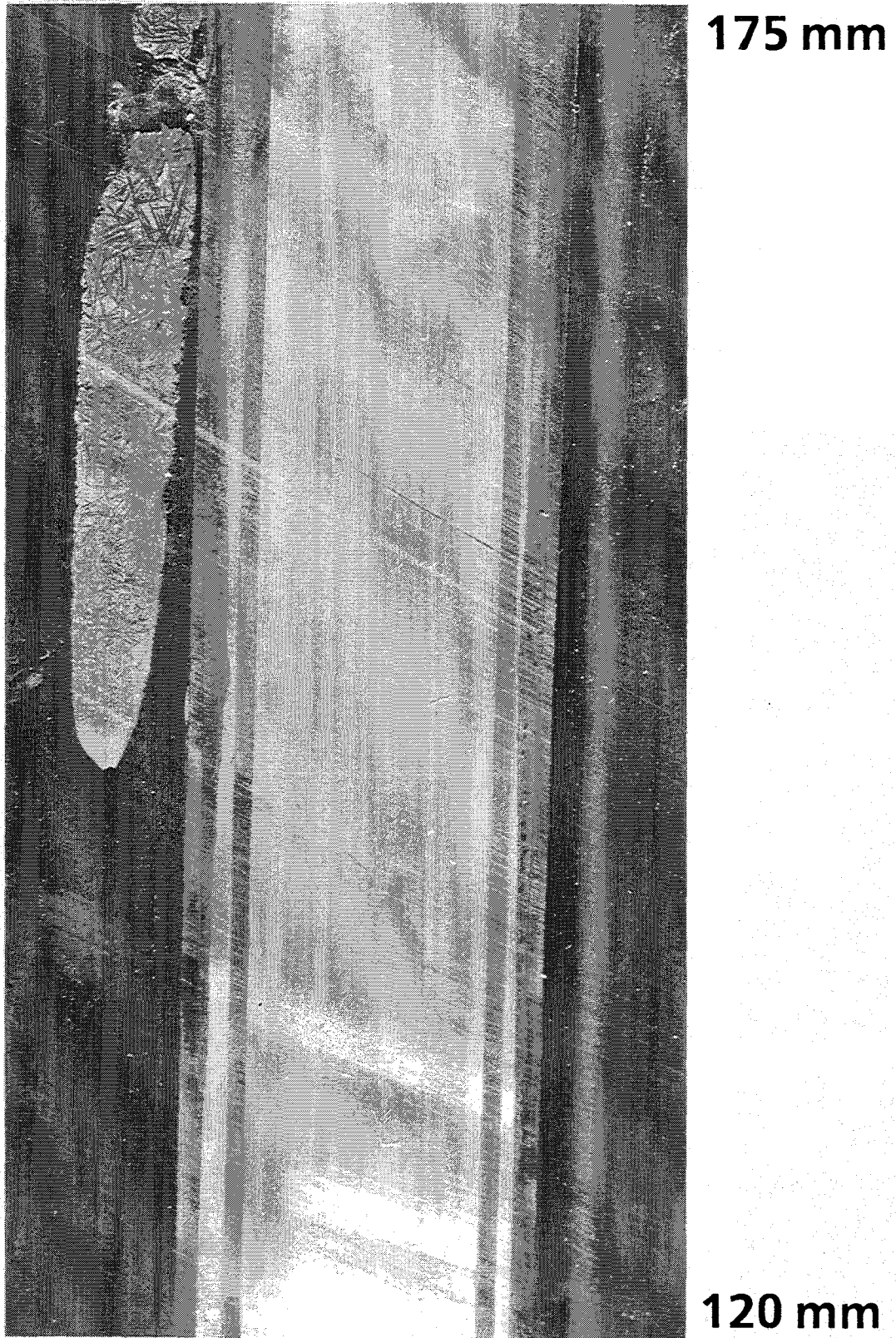
Fig.12: Dissolution of the guide tube by absorber material (CORA-5)

285 mm

230 mm

d
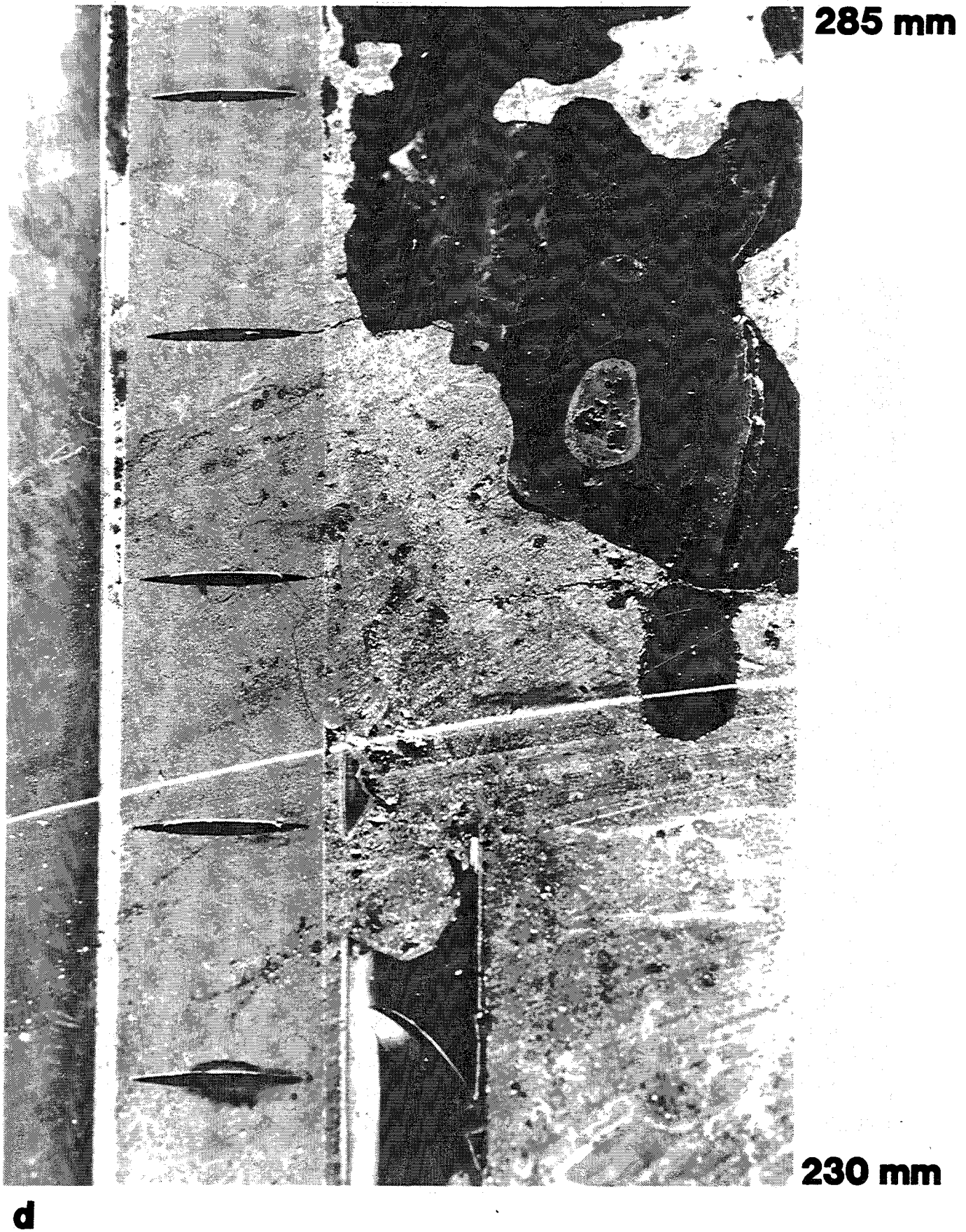
Fig. 13: Attack on the Zry-cladding by the absorber material

290 mm
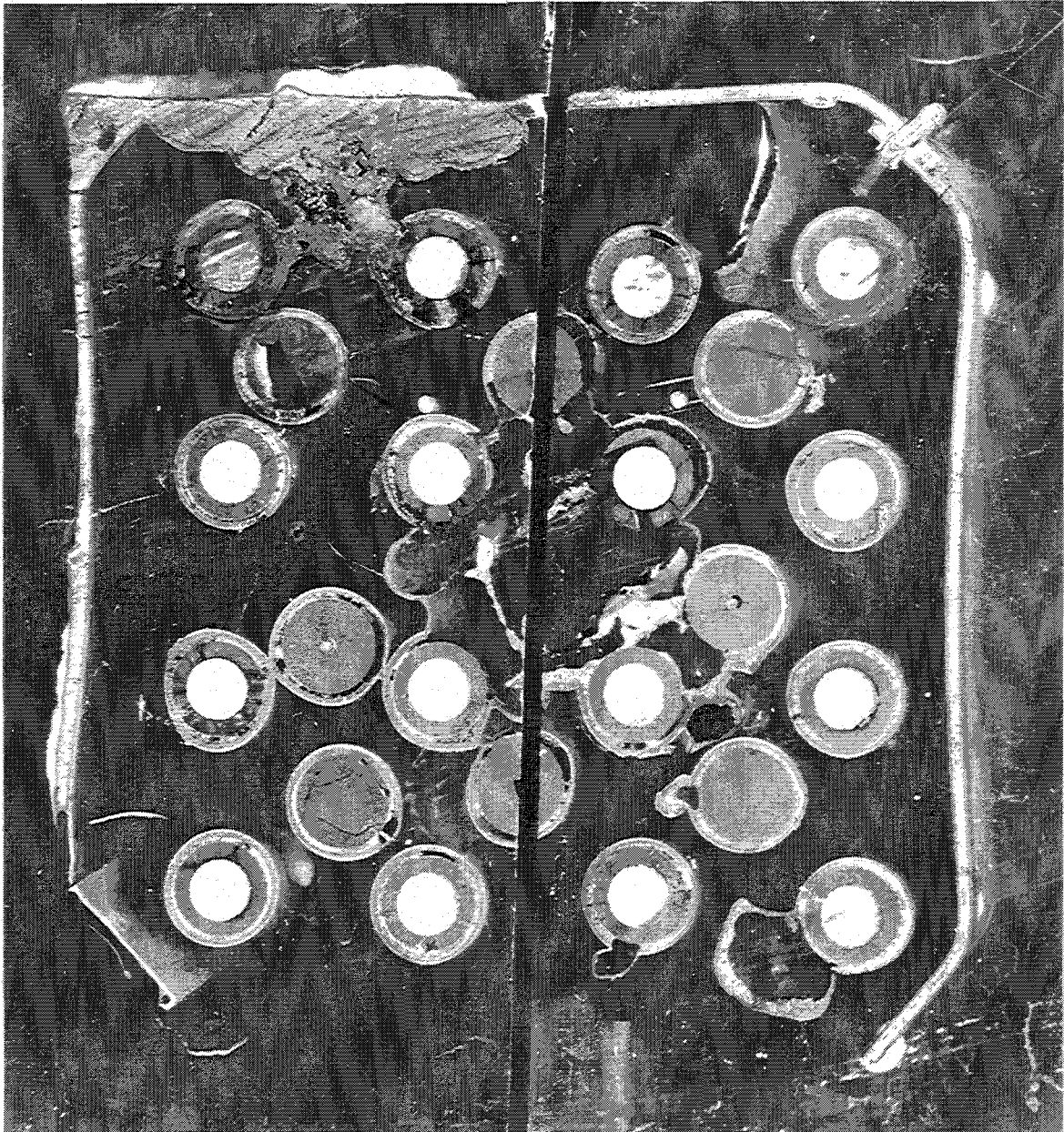
Fig. 14: Attack on the fuel rod claddings surrounding the missing absorber rod (CORA-5)
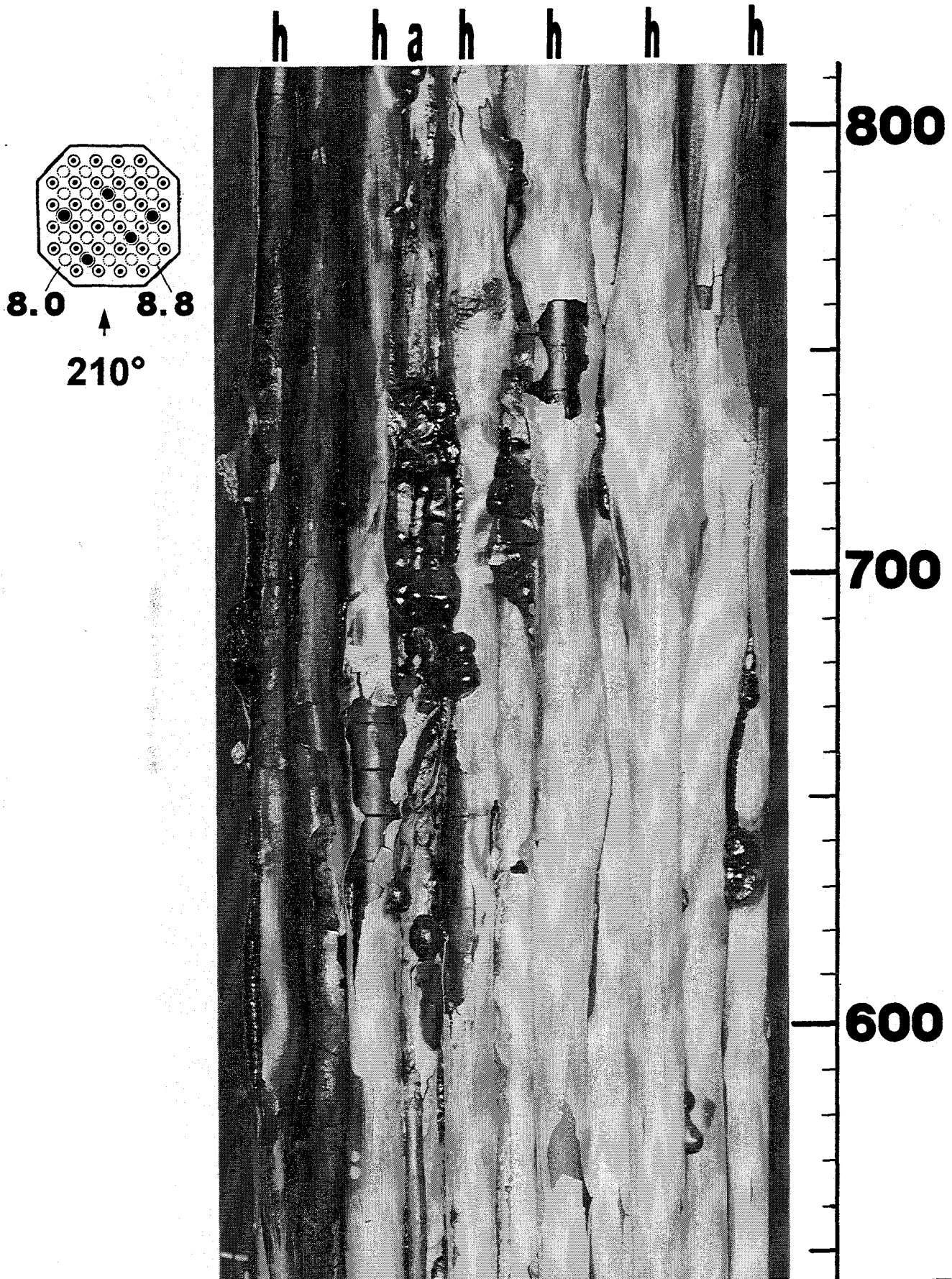
Fig.15: Melt formation in the neighbourhood of the
absorber rod (CORA-7)

42
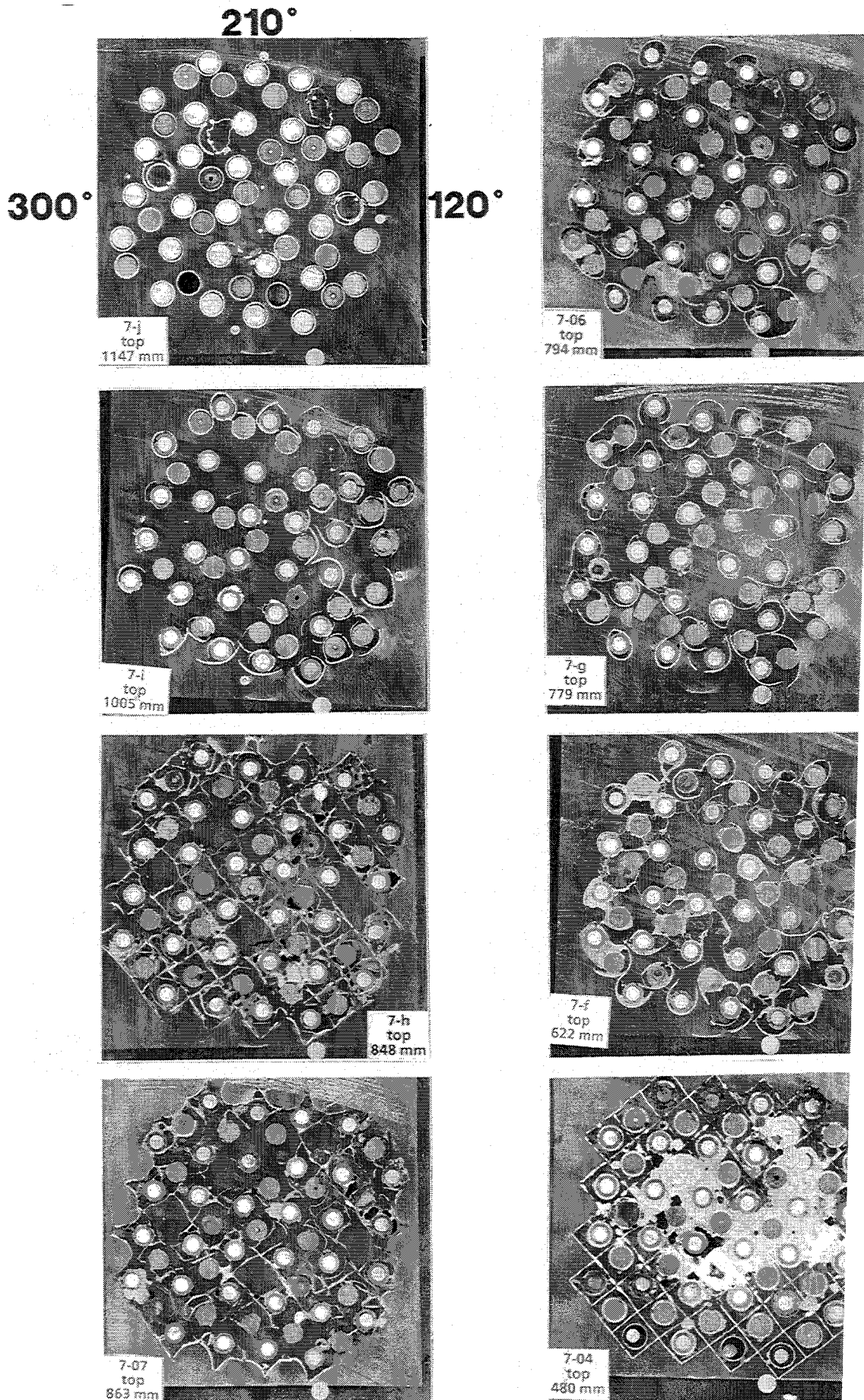
Fig.16: Melt distribution in the upper half of bundle CORA-7
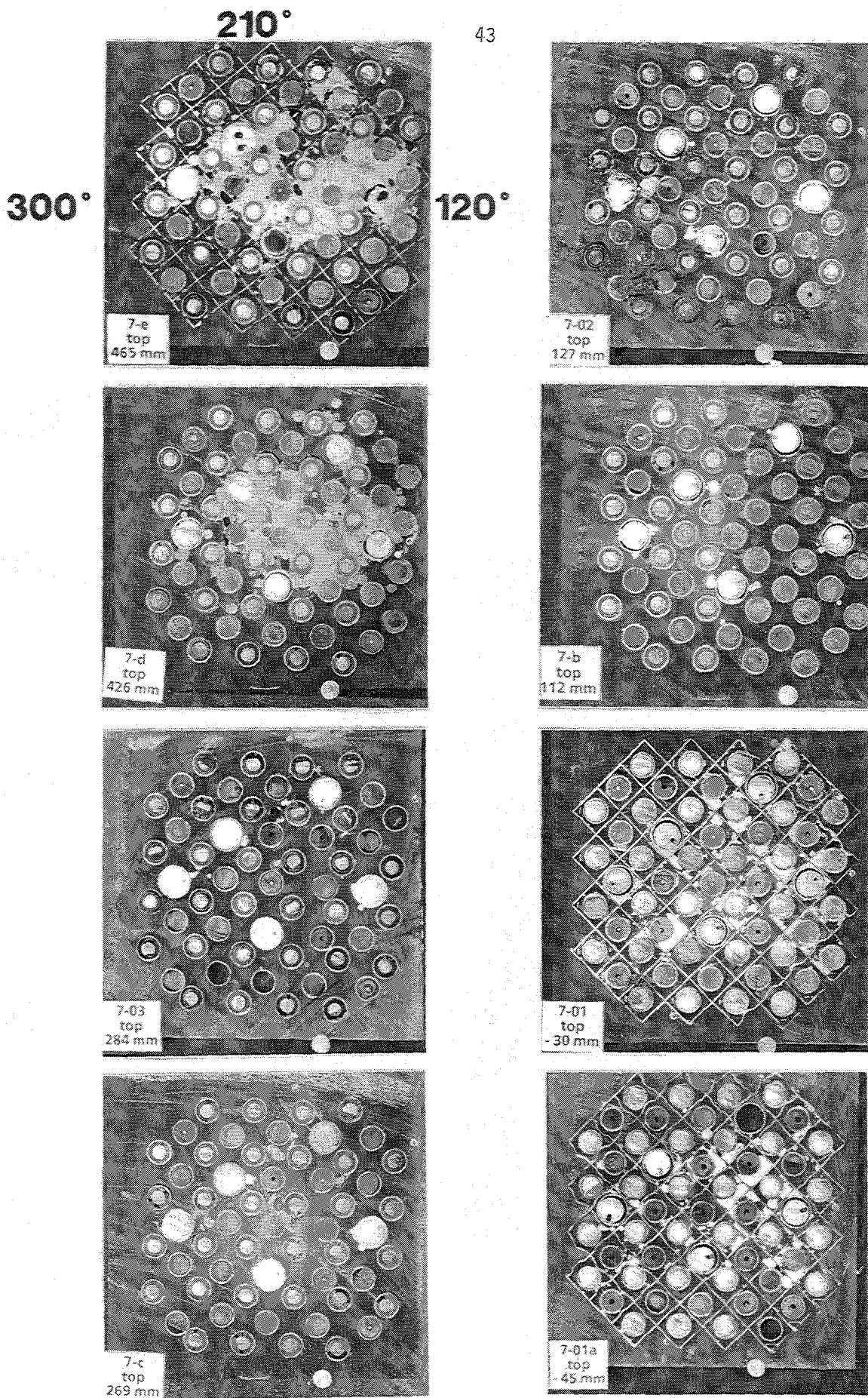
Fig.17: Melt distribution in the lower half of bundle CORA-7

(mm) *(°C)*

622 *1845*

1760

482 *1555*

465 *1405*

428
426 *1160*

980

286 *895*
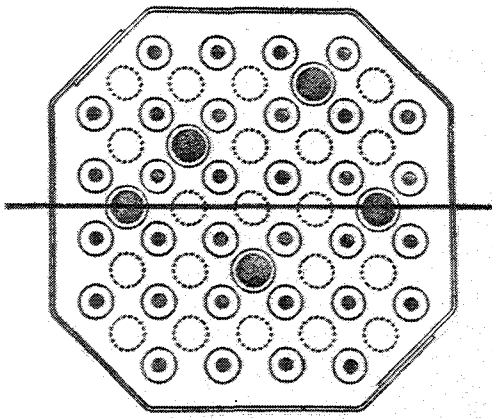
210°

300°   120°

30°
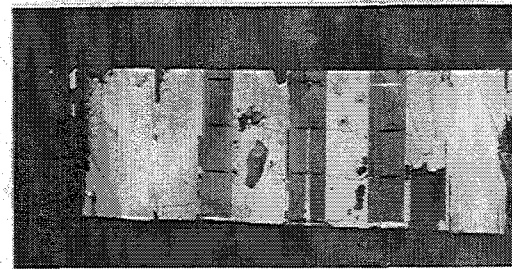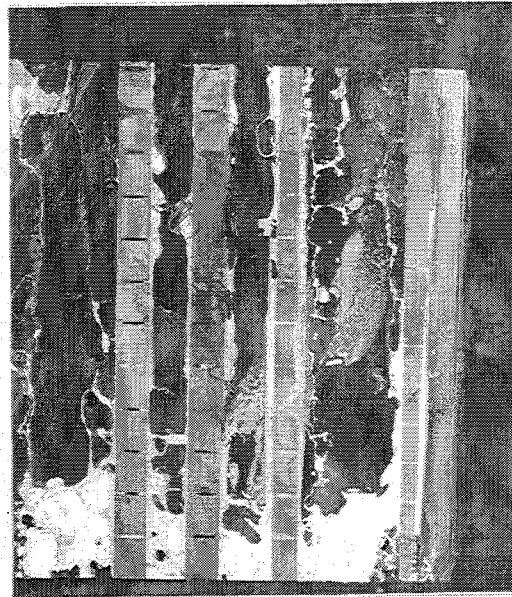
Fig.18: Vertical distribution of re-solidified melt in bundle CORA-7

Pressure Loss Measurement		Video Analysis	
Failure of rods		Start of Melt Movement	
Absorber rod 4.6	3980 s		
		3982 s	800 mm
		3982 s	600 mm
Absorber rod 6.2	3990 s		

Fig. 19: Failure time of absorber rods determined by video recordings (CORA-10)
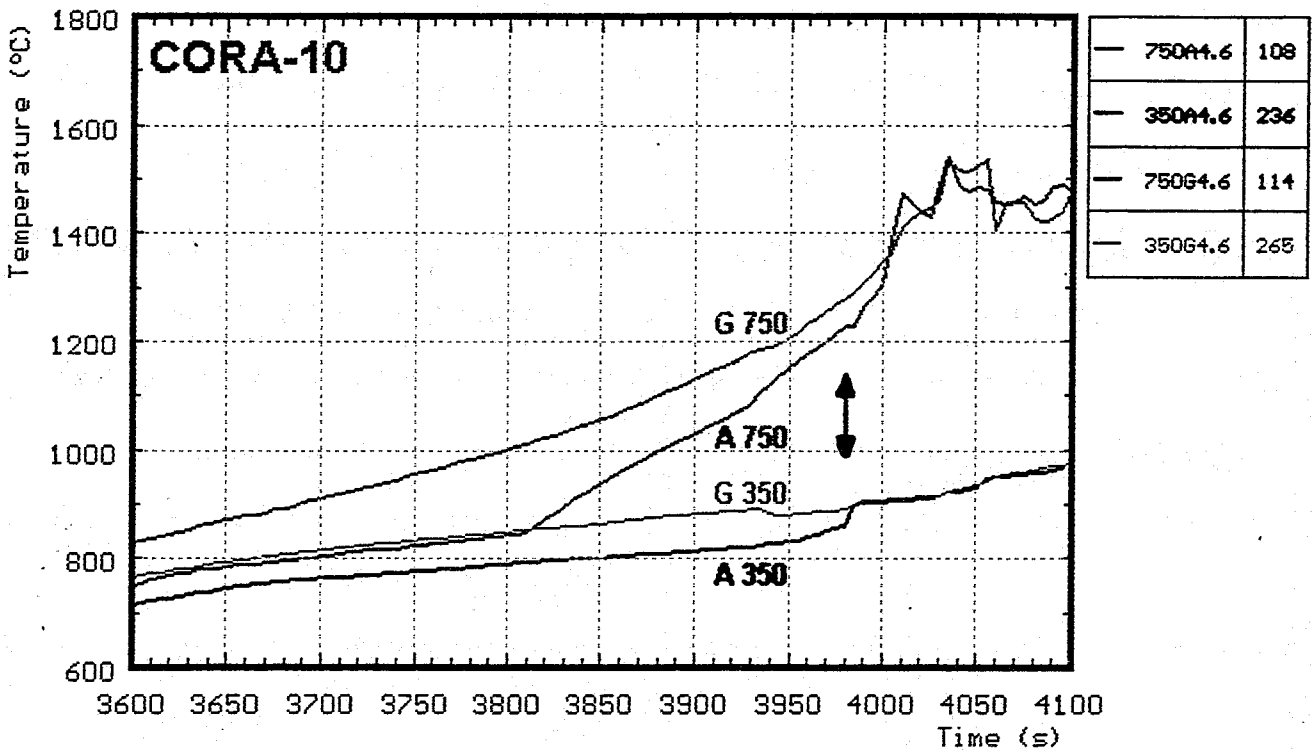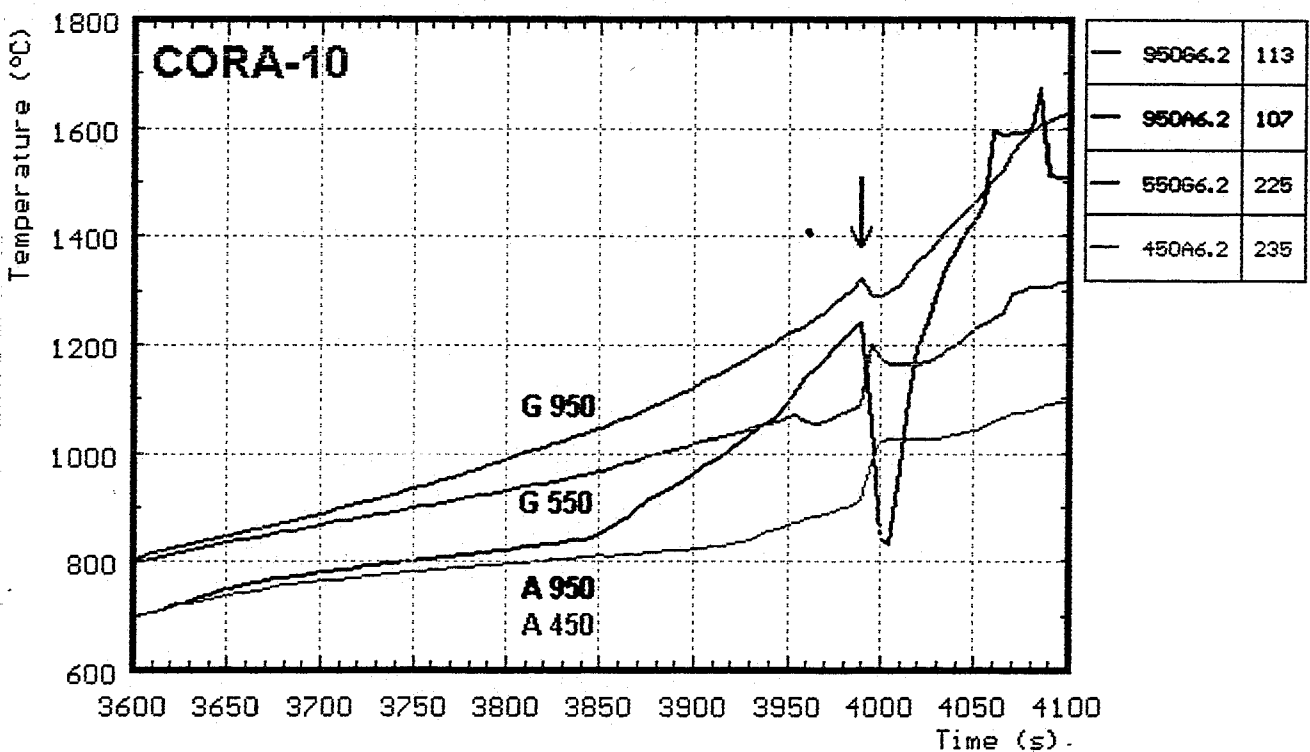
Fig.20 : Determination of failure time and temperature
by irregularities in the temperature measurement
(CORA-10)

Failure temperatures:

Rod 4.4: 1280 °C
Rod 6.4: 1310 °C
Rod 6.6: 1330 °C
Rod 3.3: 1450 °C
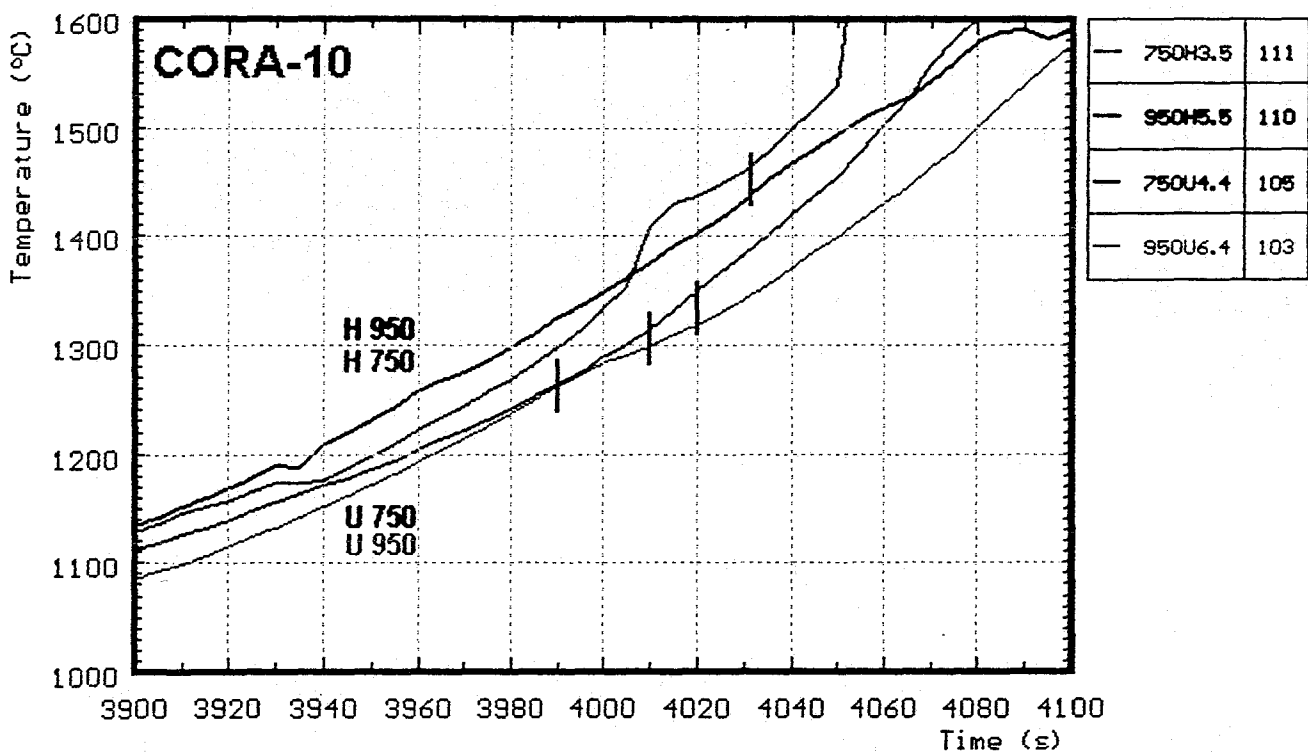
Fig. 21: Failure temperatures of heated (H) and unheated (U) fuel rods, determined by rod internal pressure measurement (CORA-10)

Interaction:
boron carbide
stainless steel blade
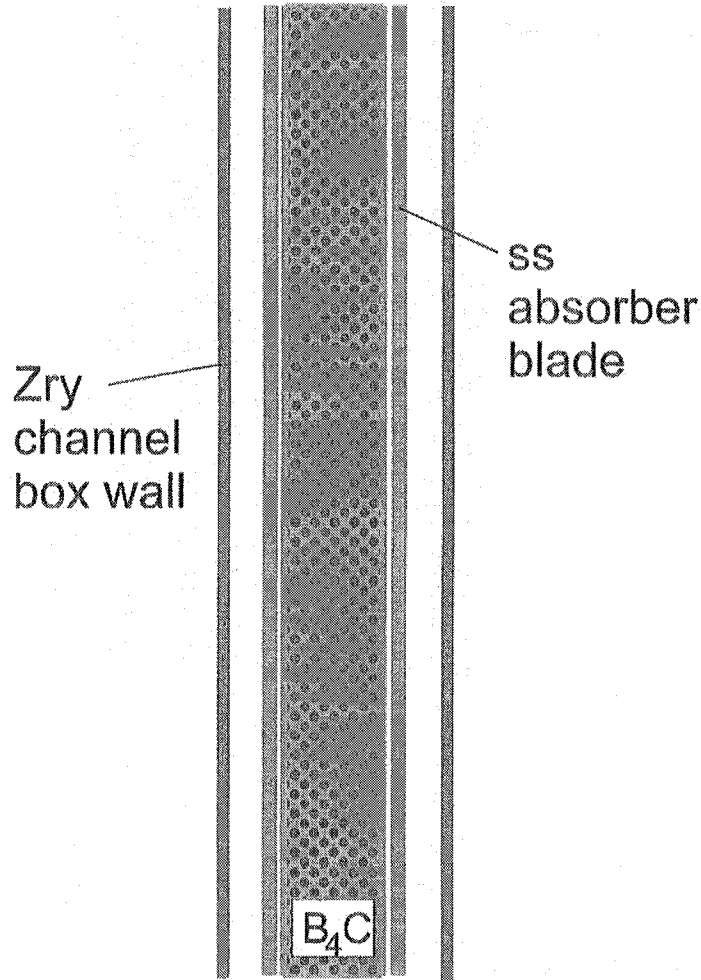
Interaction:
B_4C/ss - melt
Zry channel box wall
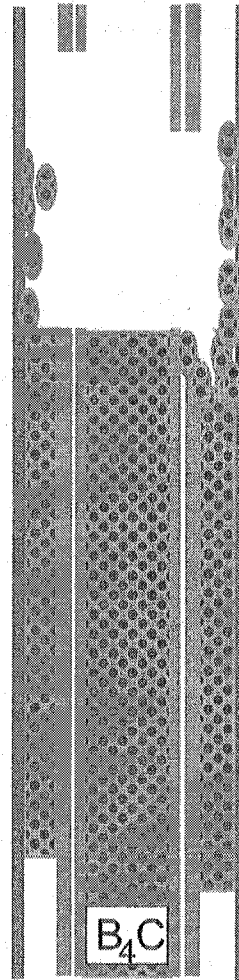
Interaction:
B_4C/ss - melt
Zry fuel cladding

ss
absorber
blade

Zry
channel
box wall

ss

Zry

B_4C

B_4C

B_4C

UO_2
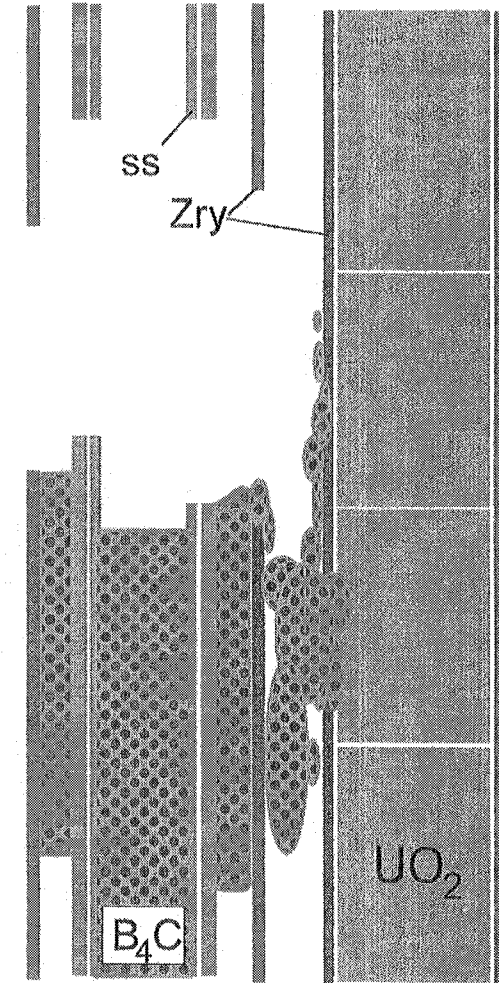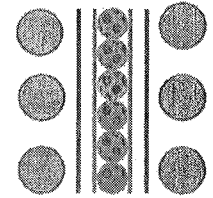
Fig.22: Steps of (B_4C - ss) attack on Zry-channel box wall and Zry cladding (BWR)

300°
View   Absorber blade missing
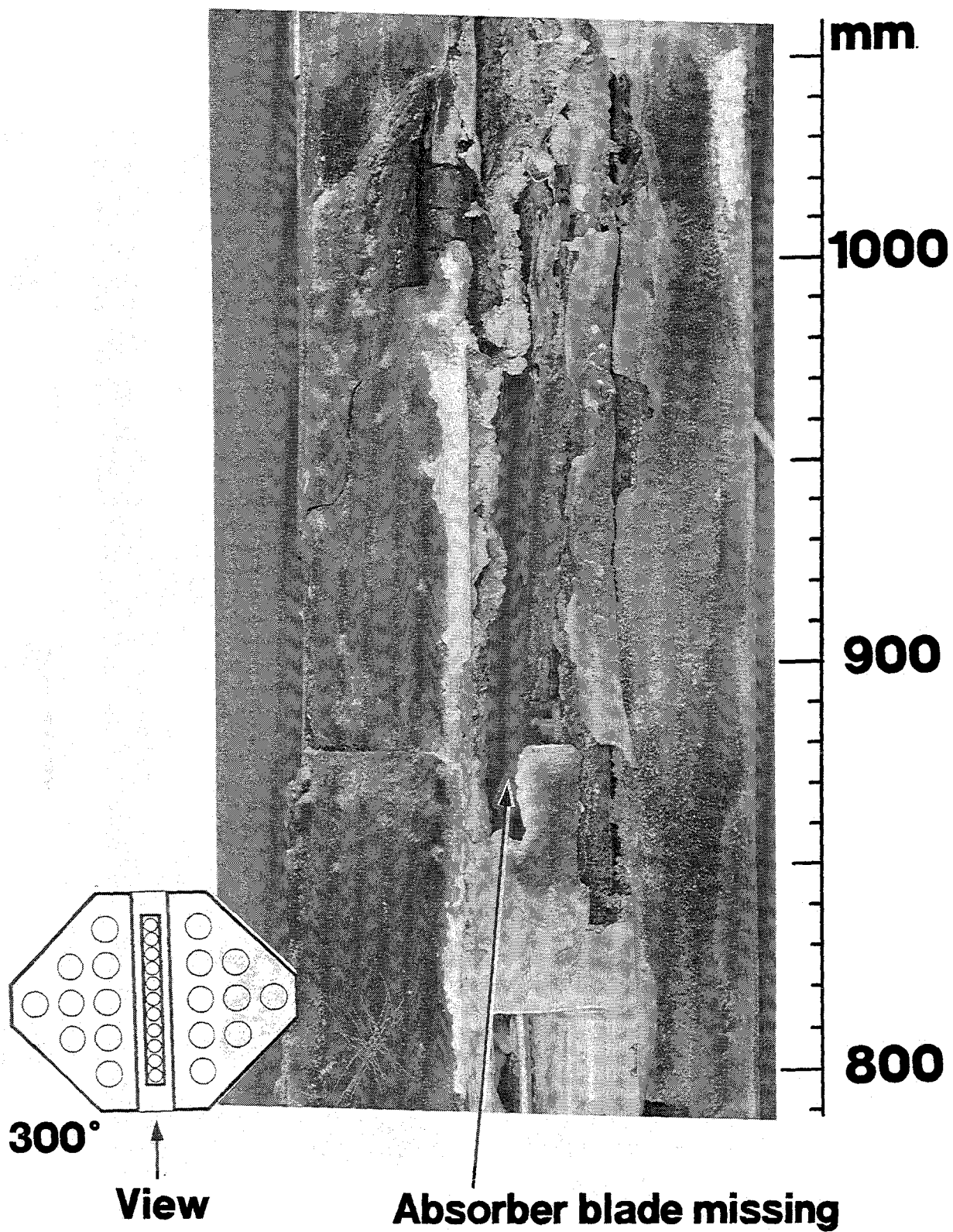
**Fig. 23: Posttest appearance of bundle CORA-16
showing the missing absorber blade**
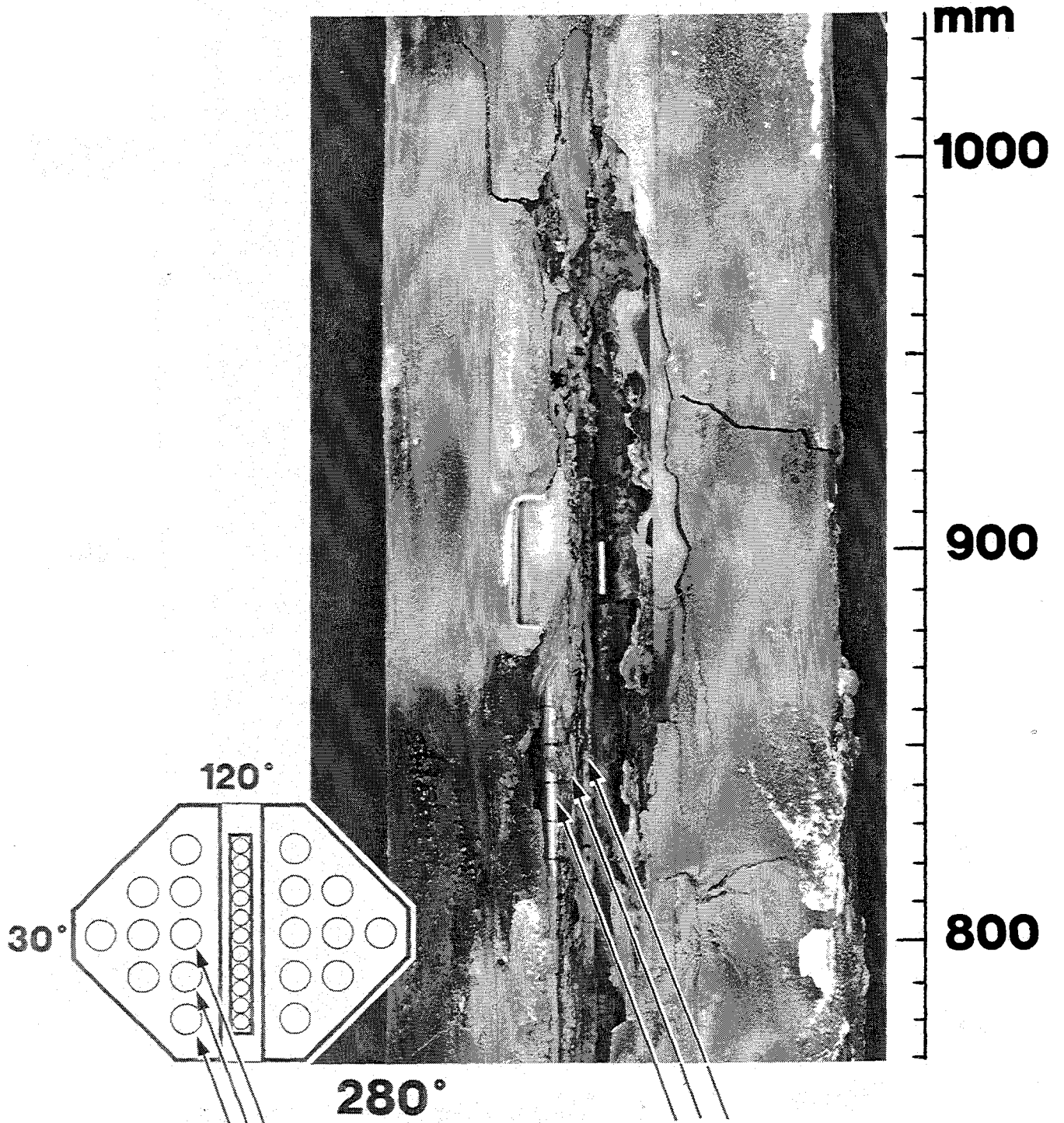
Fig.24: The posttest appearance of bundle CORA-16 shows the disappearance of absorber blade and channel box wall
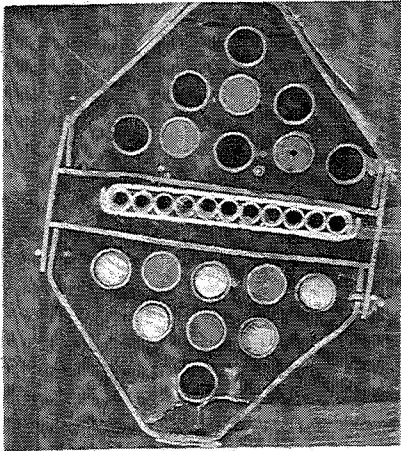
1145 mm
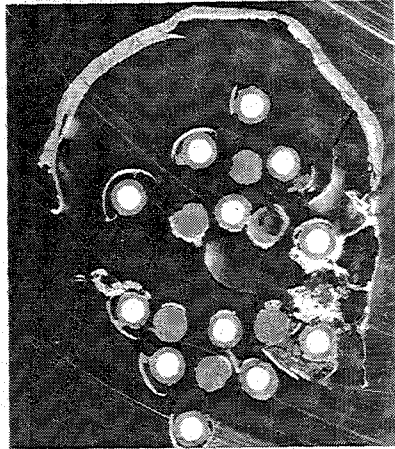
612 mm
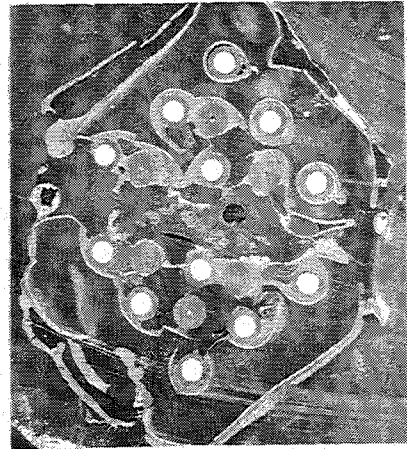
197 mm
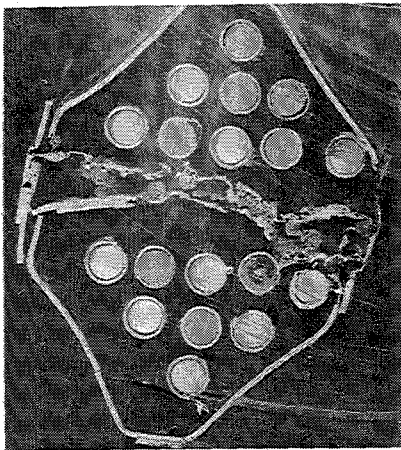
1052 mm
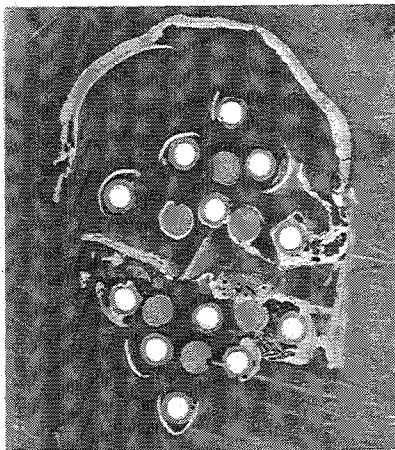
597 mm
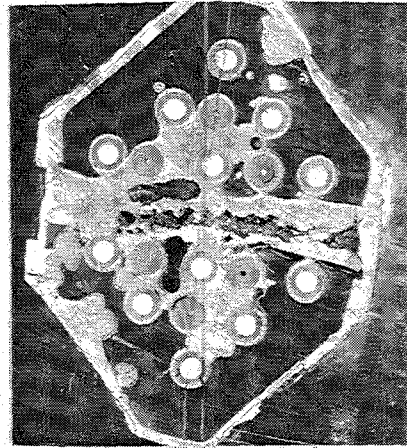
112 mm
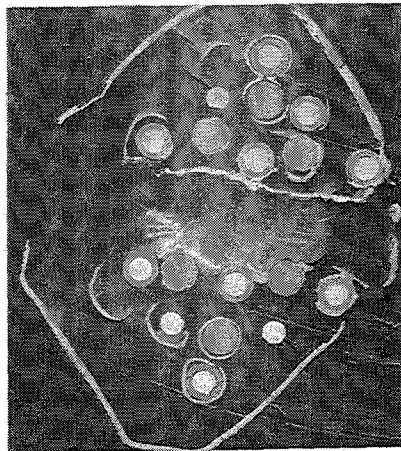
836 mm
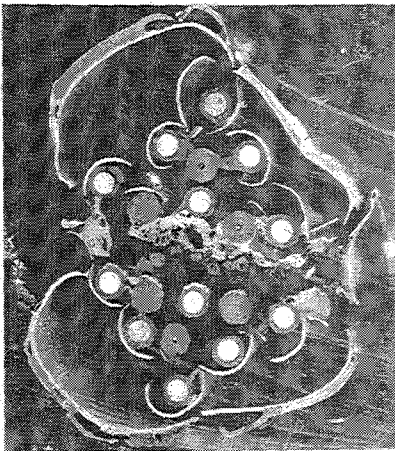
412 mm
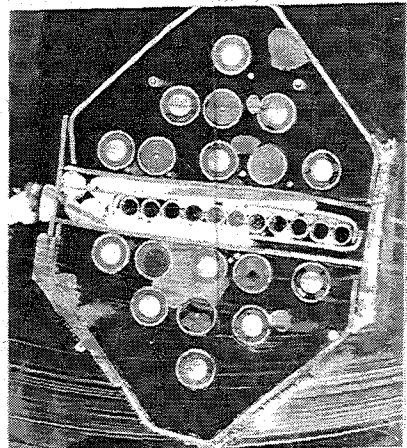
65 mm

bottom view

Fig.25: Horizontal cross section of test bundle CORA-16

195mm

112

95

65

210°

Fig.26: Vertical cross section of test bundle CORA-16

120°

1100 °C

1158mm

120°

1530 °C

1016mm
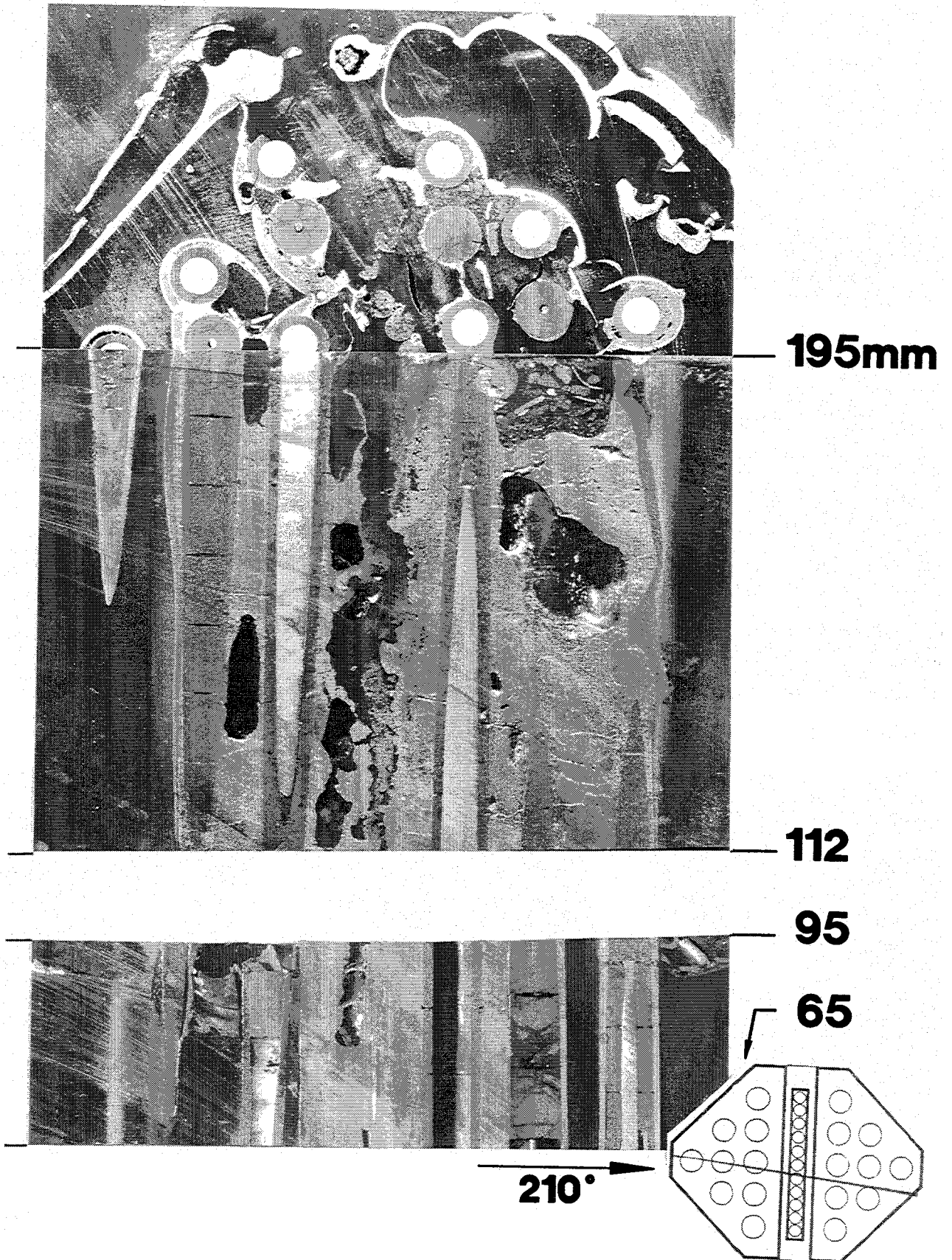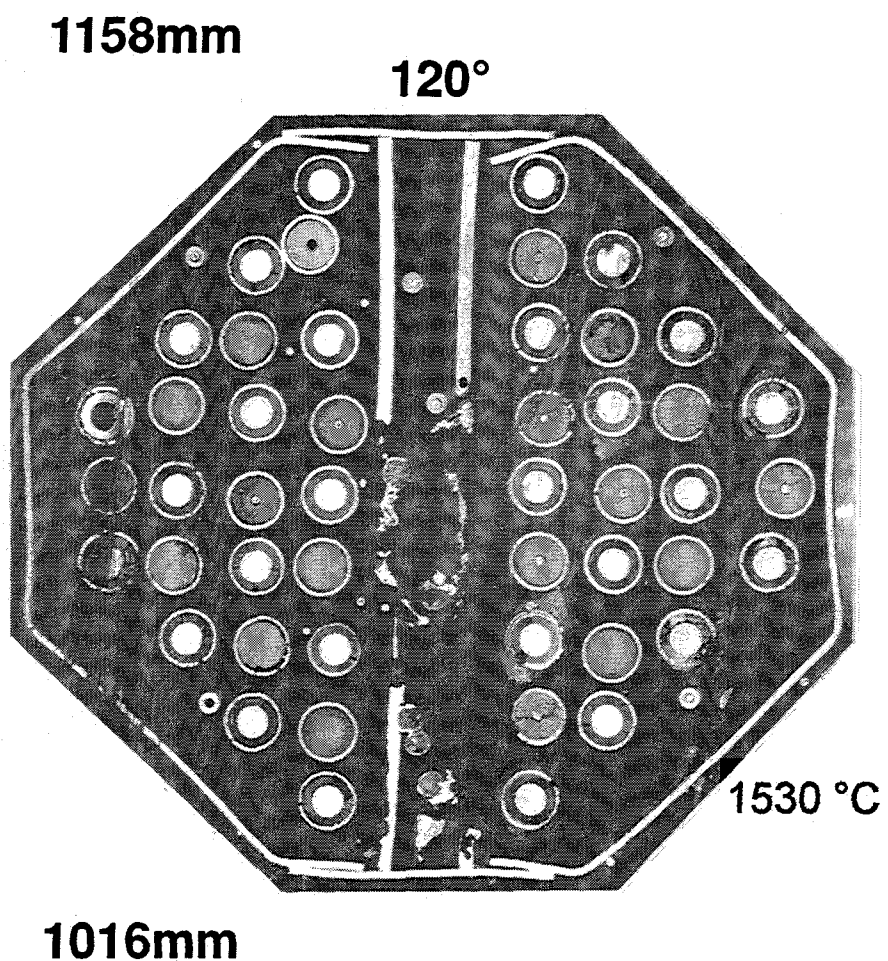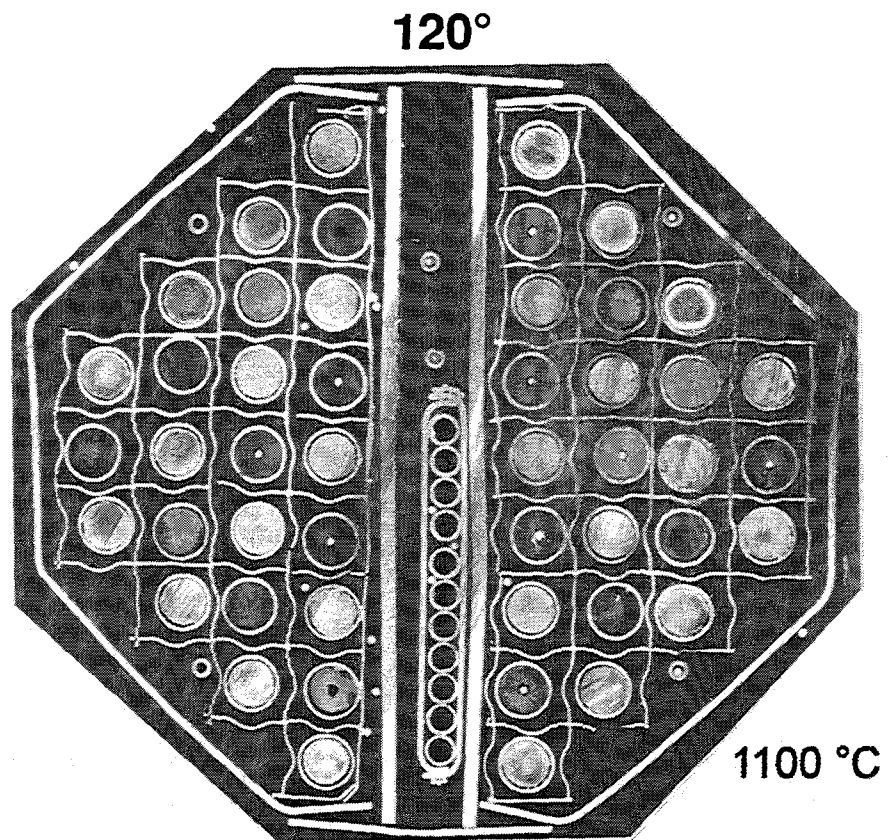
Fig.27: The cross sections at the upper end of bundle CORA-18
show the initiation of damage of the channel box wall
that occurs by contact to the absorber blade.
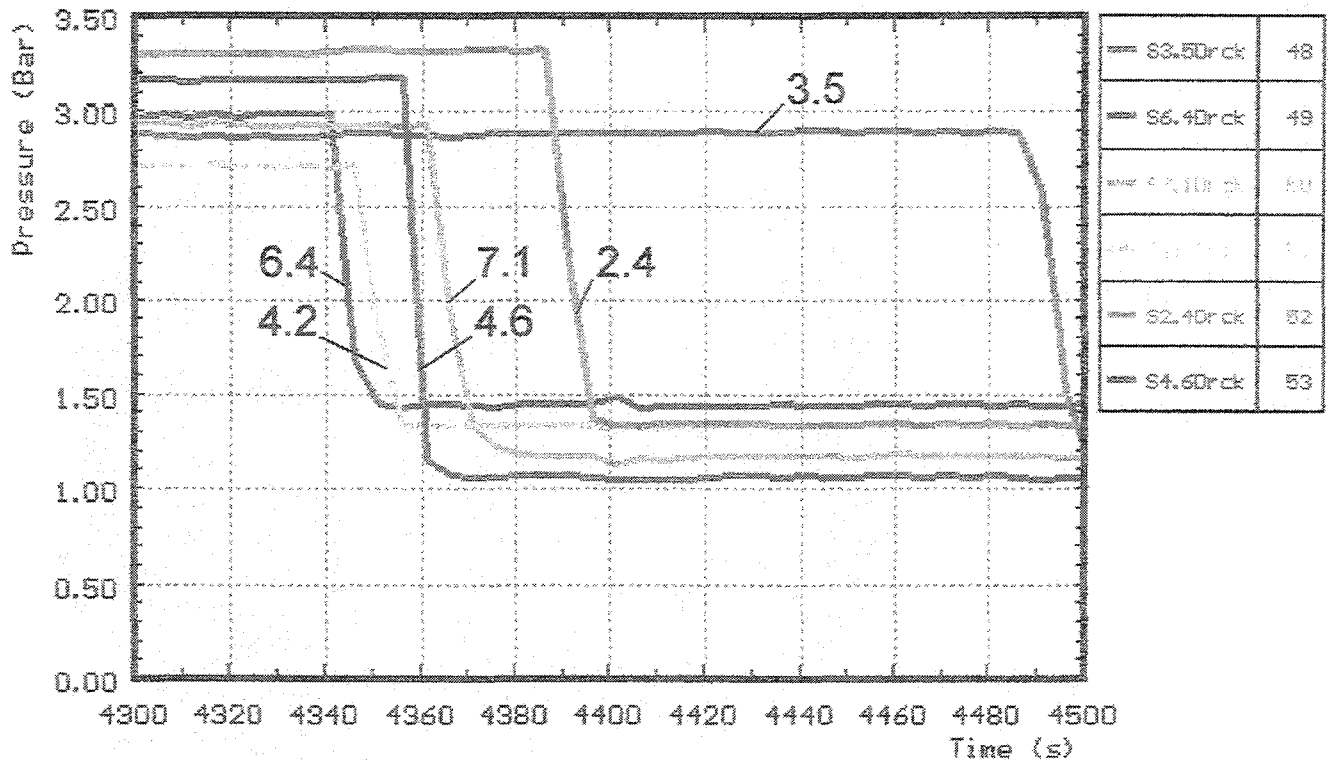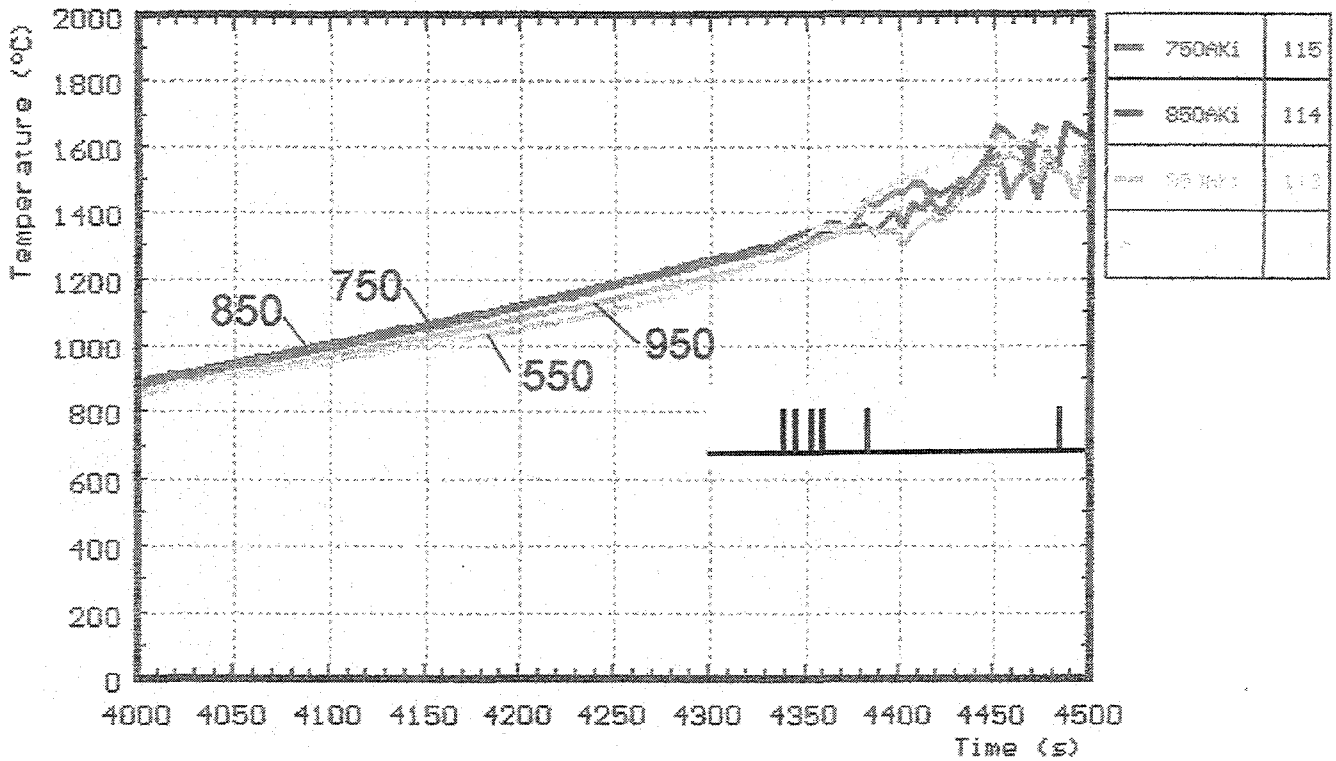
Fig.28: Irregularities in the temperatures of the absorber blade in comparison to failure of fuel rod simulator claddings used for estimation of absorber failure time (CORA-28).

Interaction:
B_4C boron carbide
stainless steel
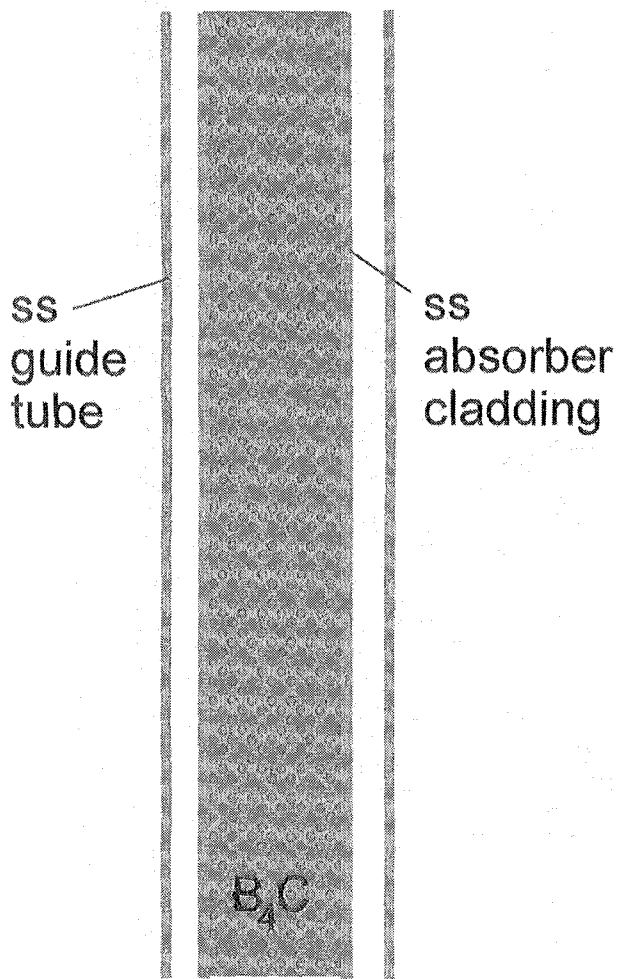
Interaction:
B_4C / ss - melt
ss - guide tube
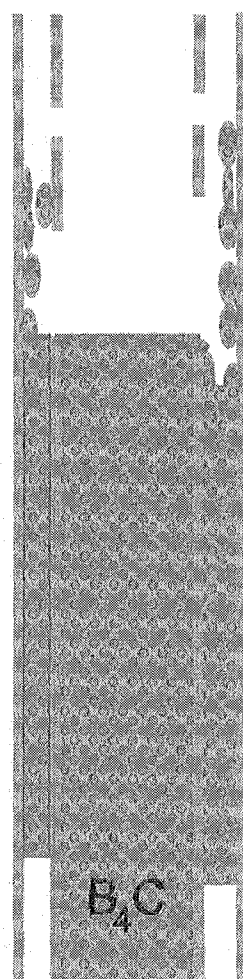
Interaction:
B_4C / ss - melt
ZrNb fuel cladding

ZrNb

ss
guide
tube

ss
absorber
cladding

B_4C

B_4C

B_4C

UO_2
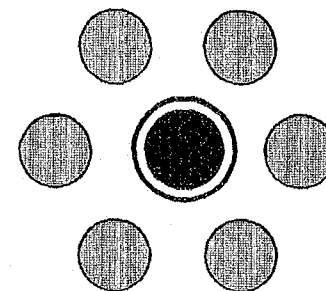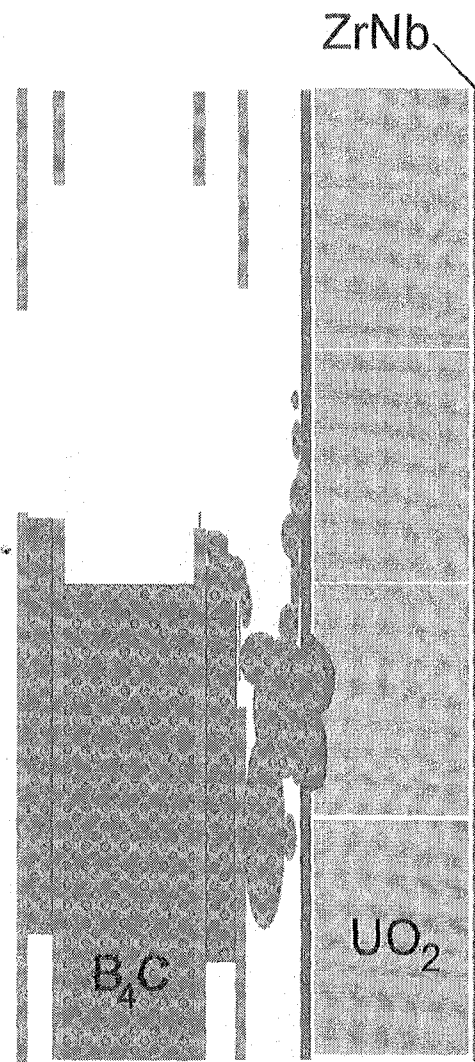
Fig. 29: Steps of (B_4C - ss) attack on Zr1%Nb cladding (VVER)

120° / 200mm / 400mm / 600mm / 800mm
(30x30mm)

13 heated rods

6 unheated rods

CORA-W1

300° / 900mm
(30x30mm)

120° / 600mm / 800mm
(30x30mm)

13 heated rods

5 unheated rods

1 absorber rod
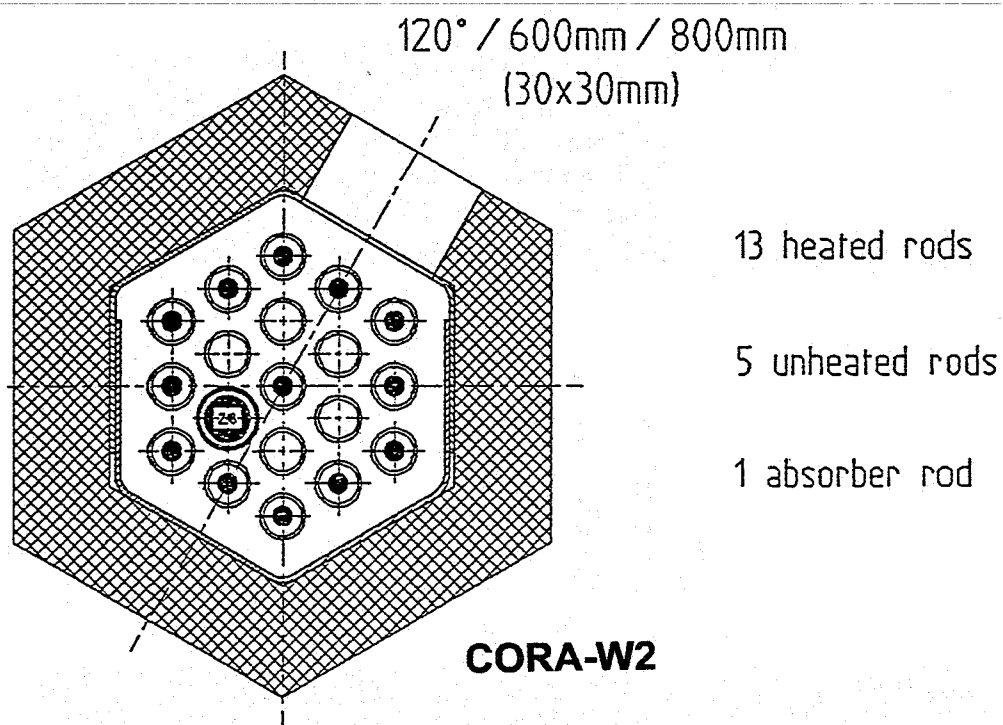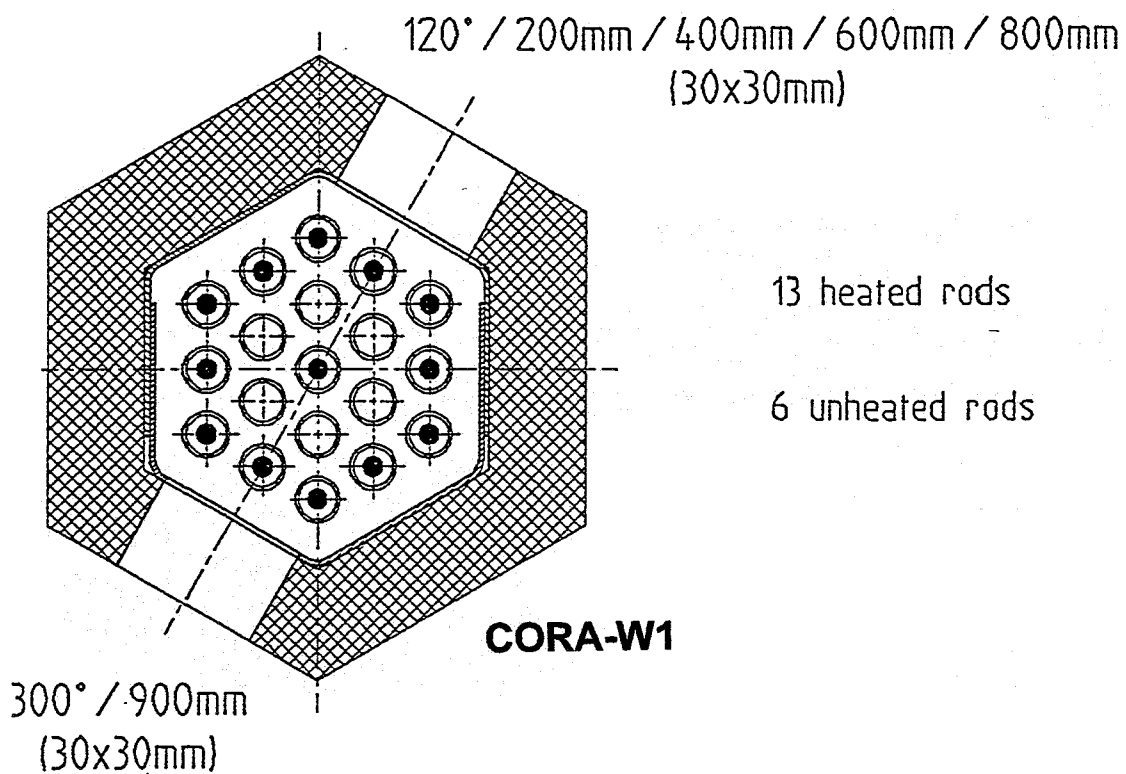
CORA-W2

Fig. 30: Test rod arrangement for bundles CORA-W1 and CORA-W2

Bundle flange

1471 mm

Thermocouple

End plugs (Ni alloy)

SS guide $\phi 12{,}6 \: / \: \phi 11$

1000 mm

SS cladding $\phi 8{,}2 \: / \: \phi 7$

Absorber (B_4C)

0 mm
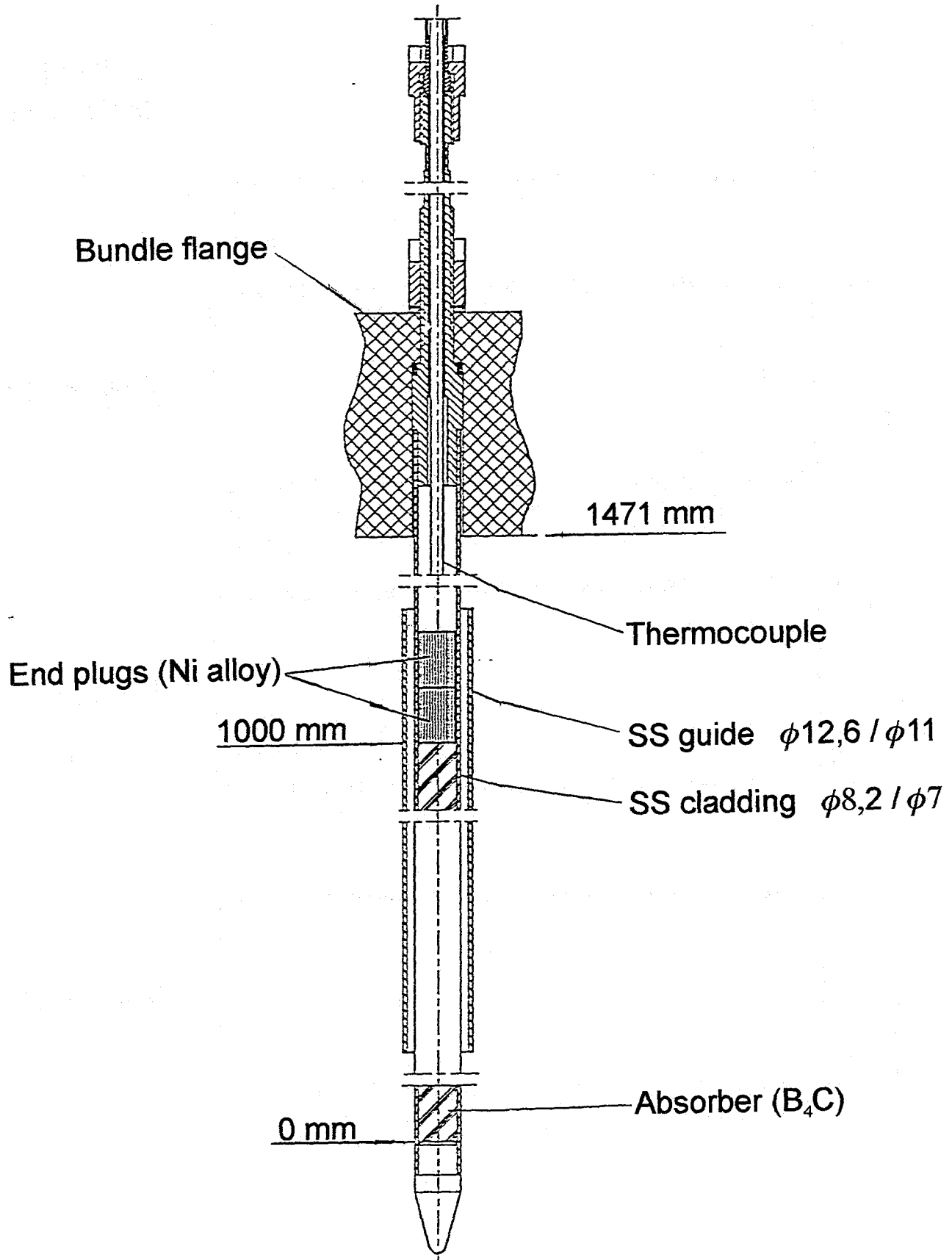
Scale 1:1

Fig. 31: Absorber rod of CORA-W2 experiment
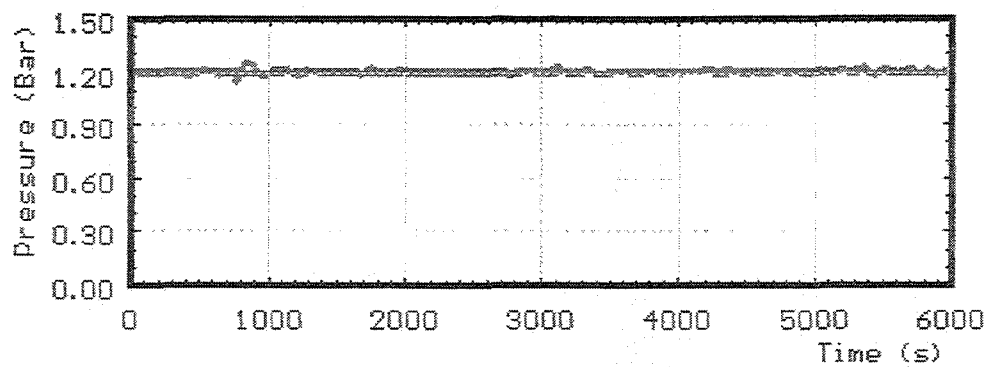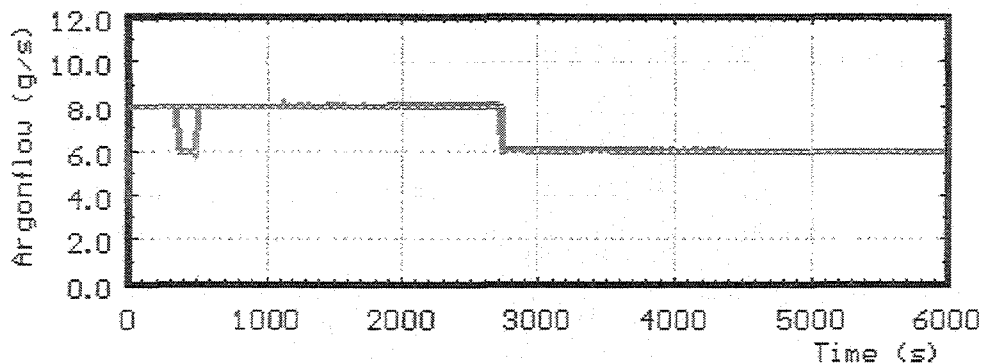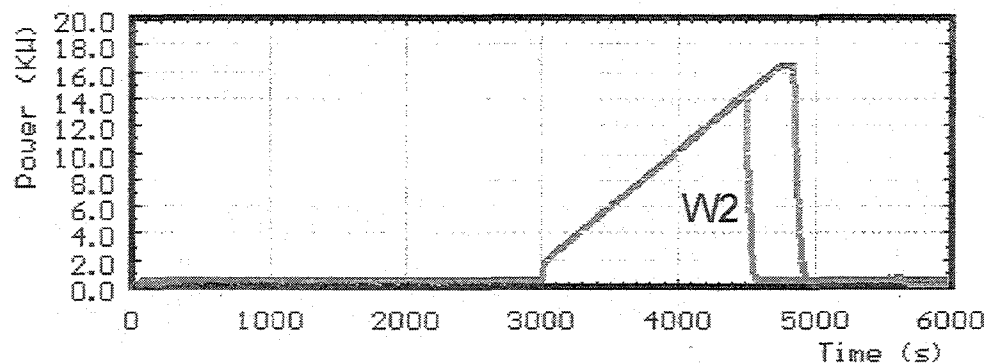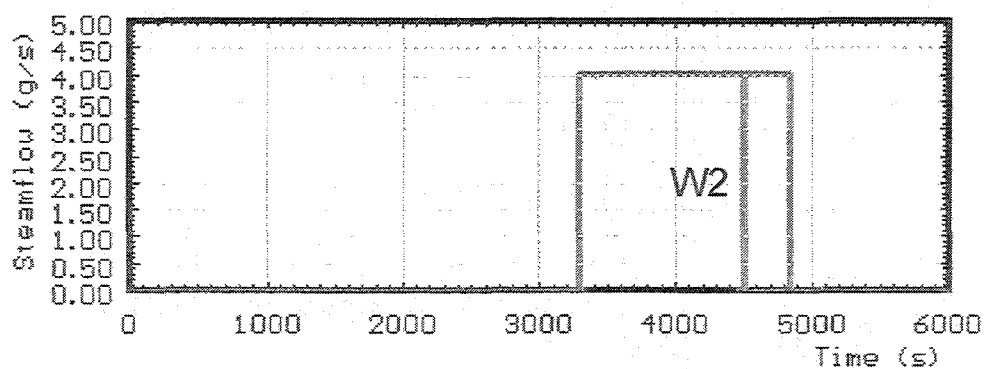
Fig. 32: Test conditions of CORA-W1 and CORA-W2
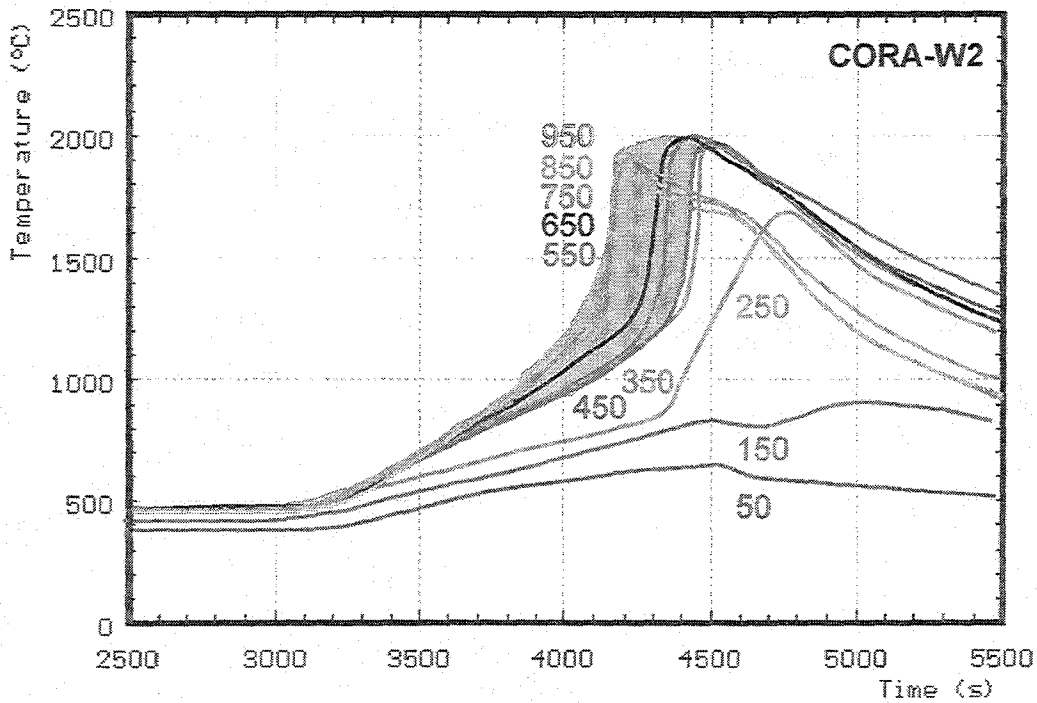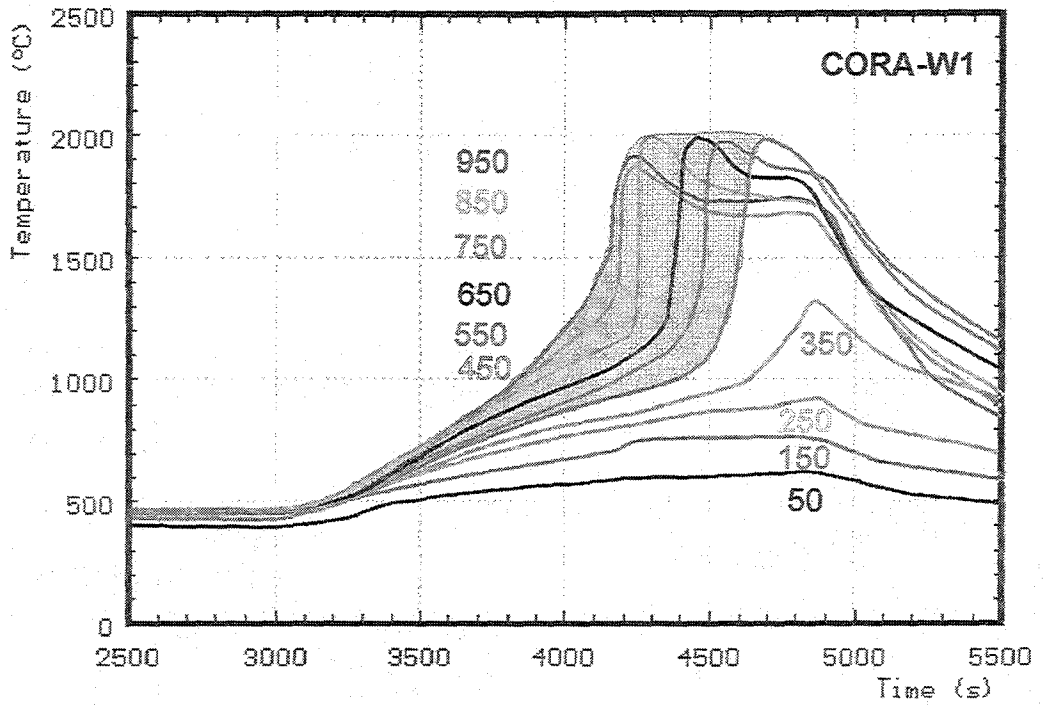
Fig. 33: Test CORA-W2 (with absorber material) shows a faster vertical propagation of the temperature escalation in comparison to test CORA-W1 (without absorber)
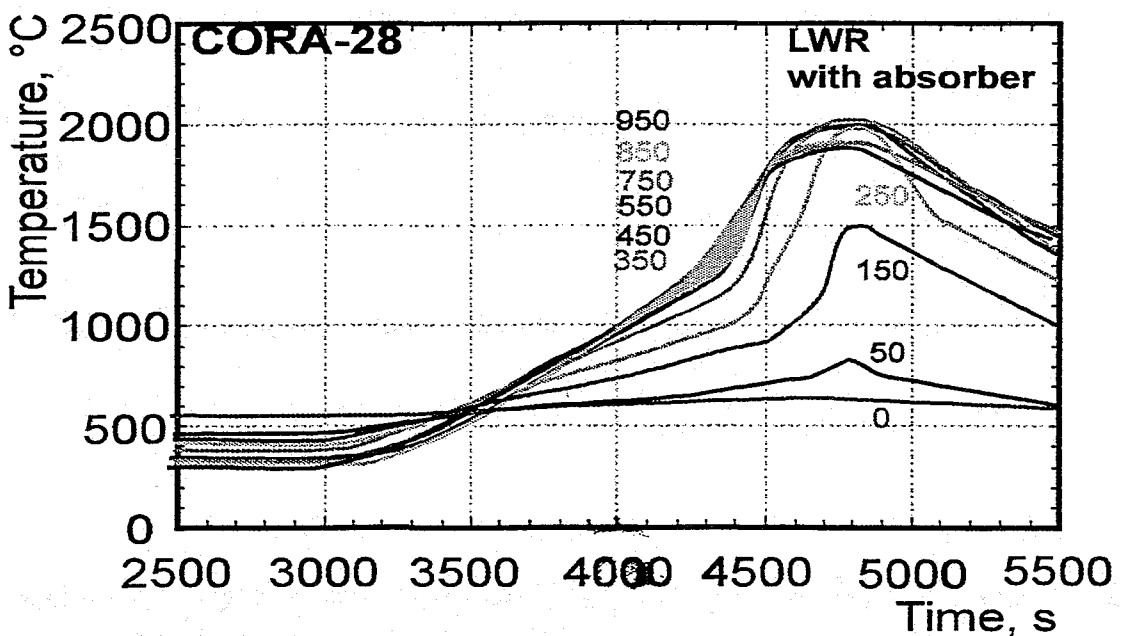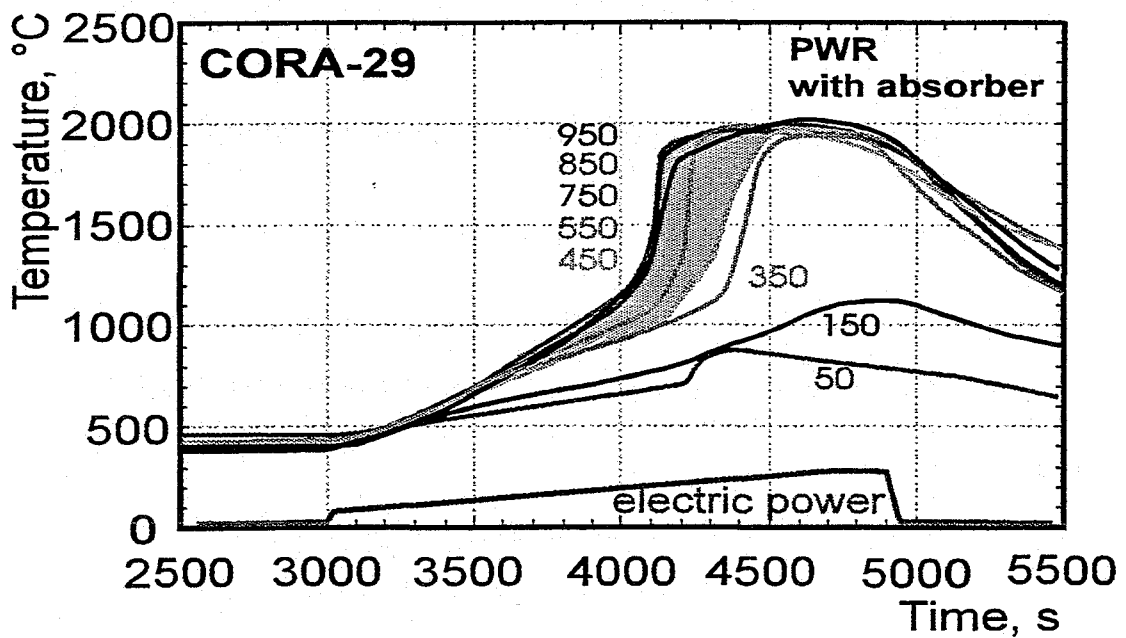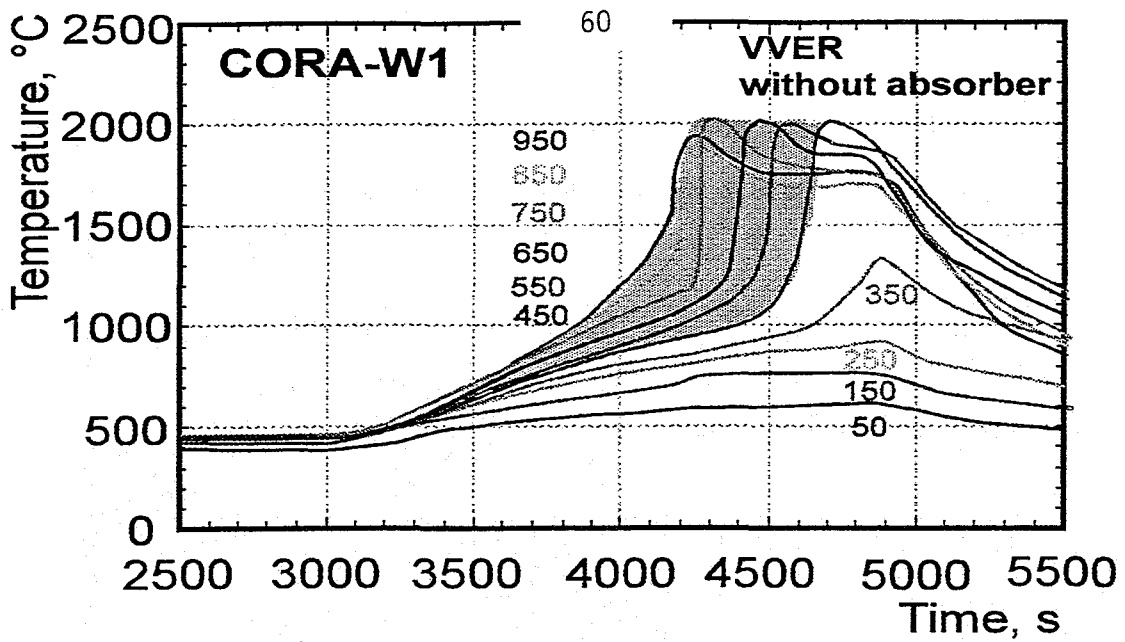
Fig. 34: The vertical temperature escalation in absorber test 29 (PWR) and 28 (BWR) is faster than in test W1 without absorber
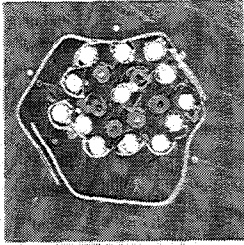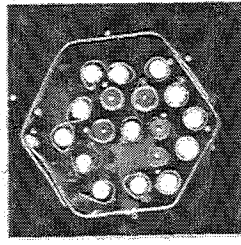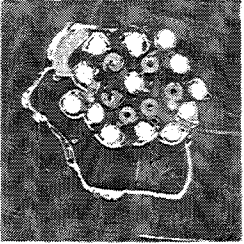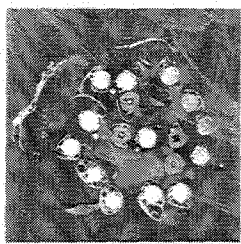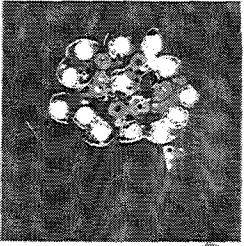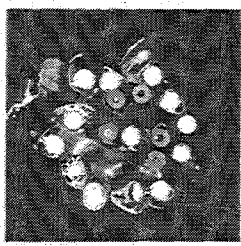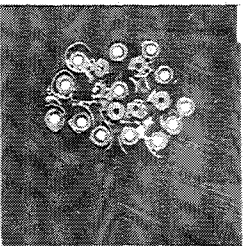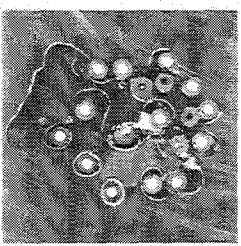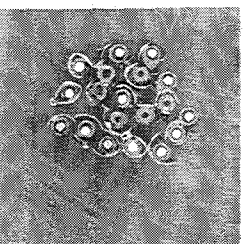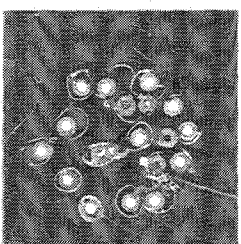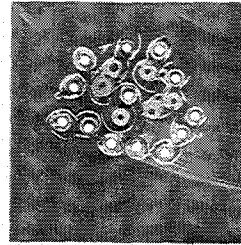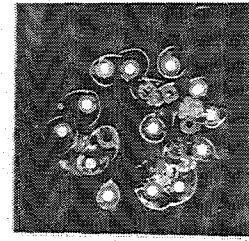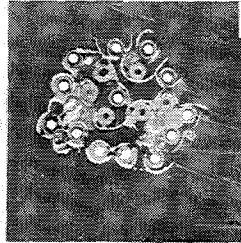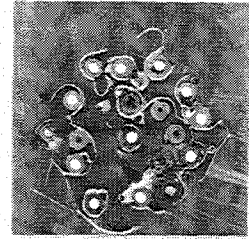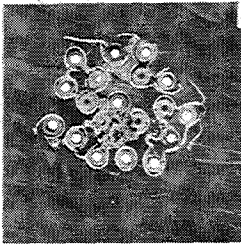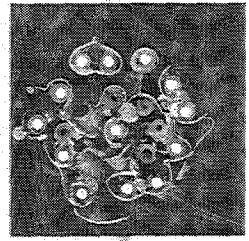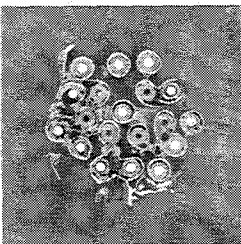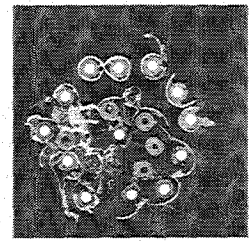
Fig. 35a: Comparison of cross sections CORA-W1 / CORA-W2

W1   **W2**   **W1**   **W2**

768 mm   739 mm   560 mm   563 mm

716 mm   724 mm   508 mm   511 mm

664 mm   672 mm   493 mm   496 mm

612 mm   620 mm   441 mm   444 mm

597 mm   605 mm
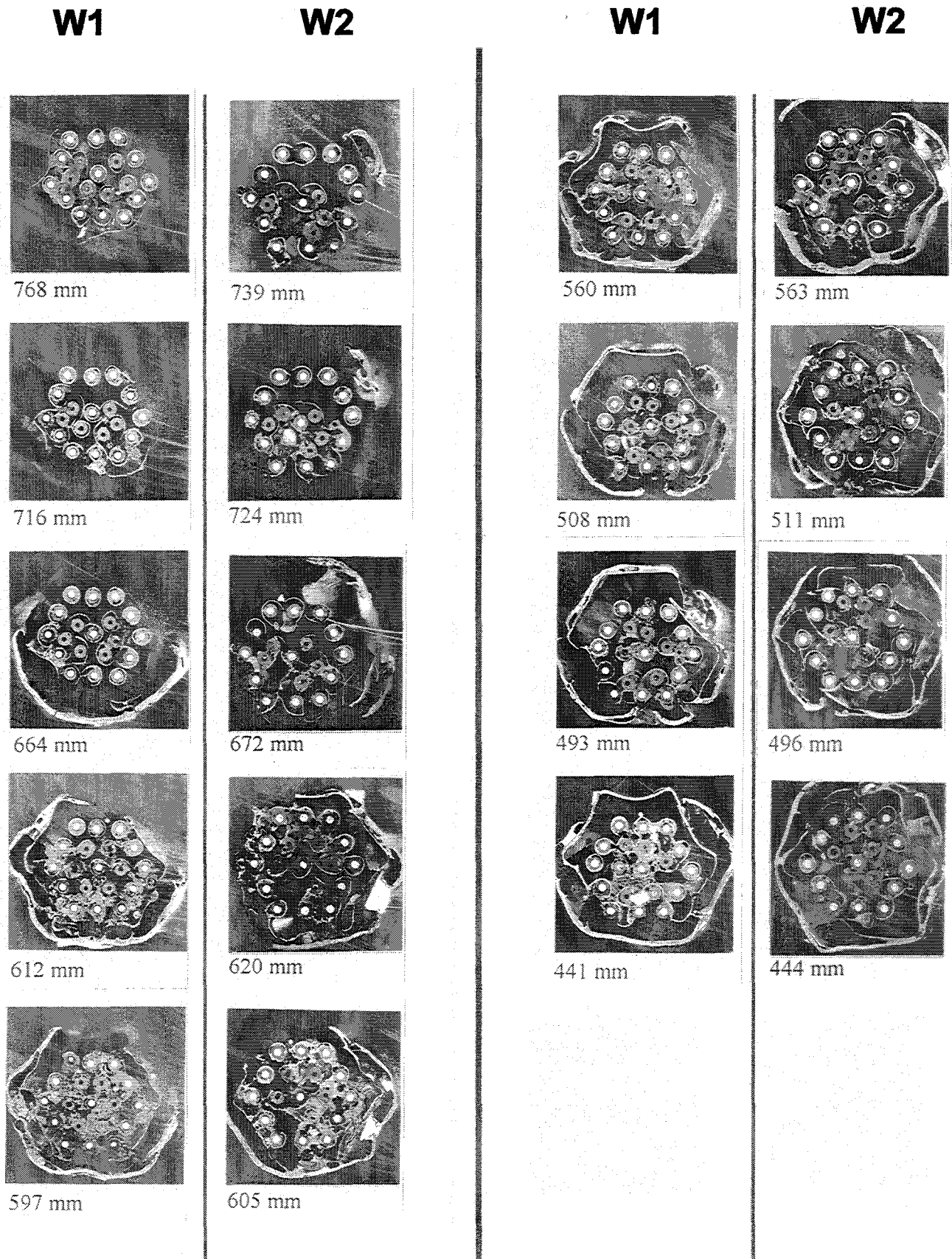
Fig. 35b: Comparison of cross sections CORA-W1 / CORA-W2

W1 **W2** **W1** **W2**
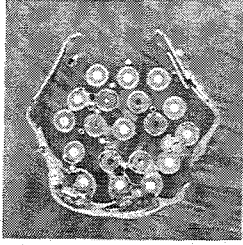
389 mm
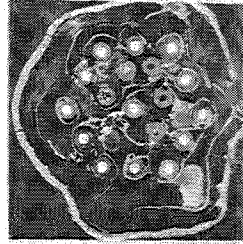
392 mm
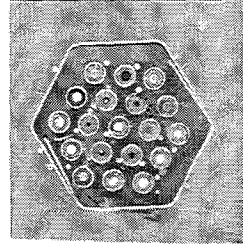
218 mm
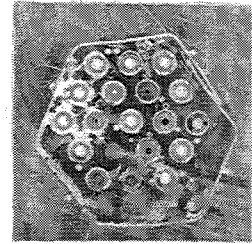
221 mm
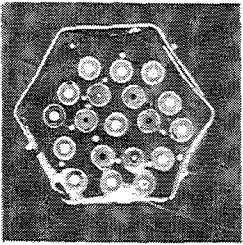
374 mm
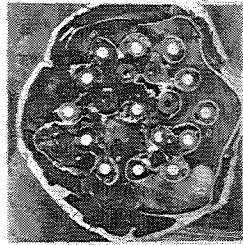
340 mm
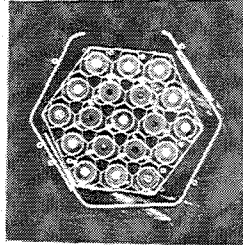
203 mm
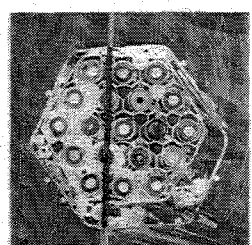
206 mm
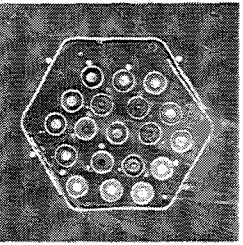
322 mm
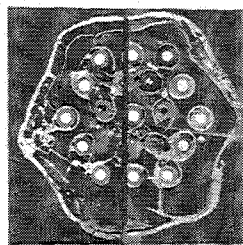
325 mm
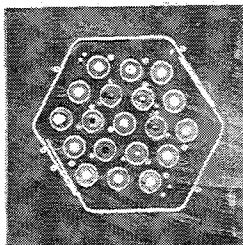
171 mm
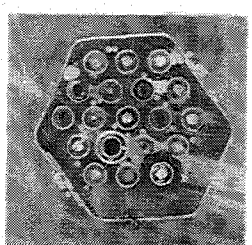
154 mm
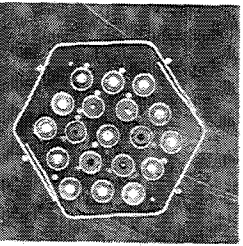
270 mm
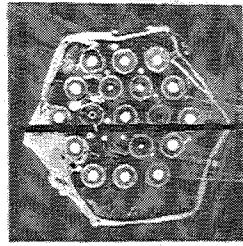
273 mm
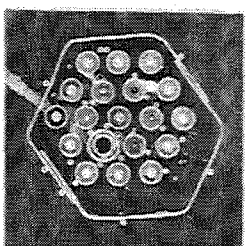
139 mm

Fig. 35c: Comparison of cross sections CORA-W1 / CORA-W2

CORA-W1   CORA-W2
(without B$_4$C-   (with B$_4$C-SS
SS absorber)   absorber)

time of electric
heatup
1800 s   1500 s

heatup rate
1 K/s   1 K/s

total input of
electric energy
19,7 MJ   14,2 MJ

main blockages formed at
500 mm   200 mm
elevation
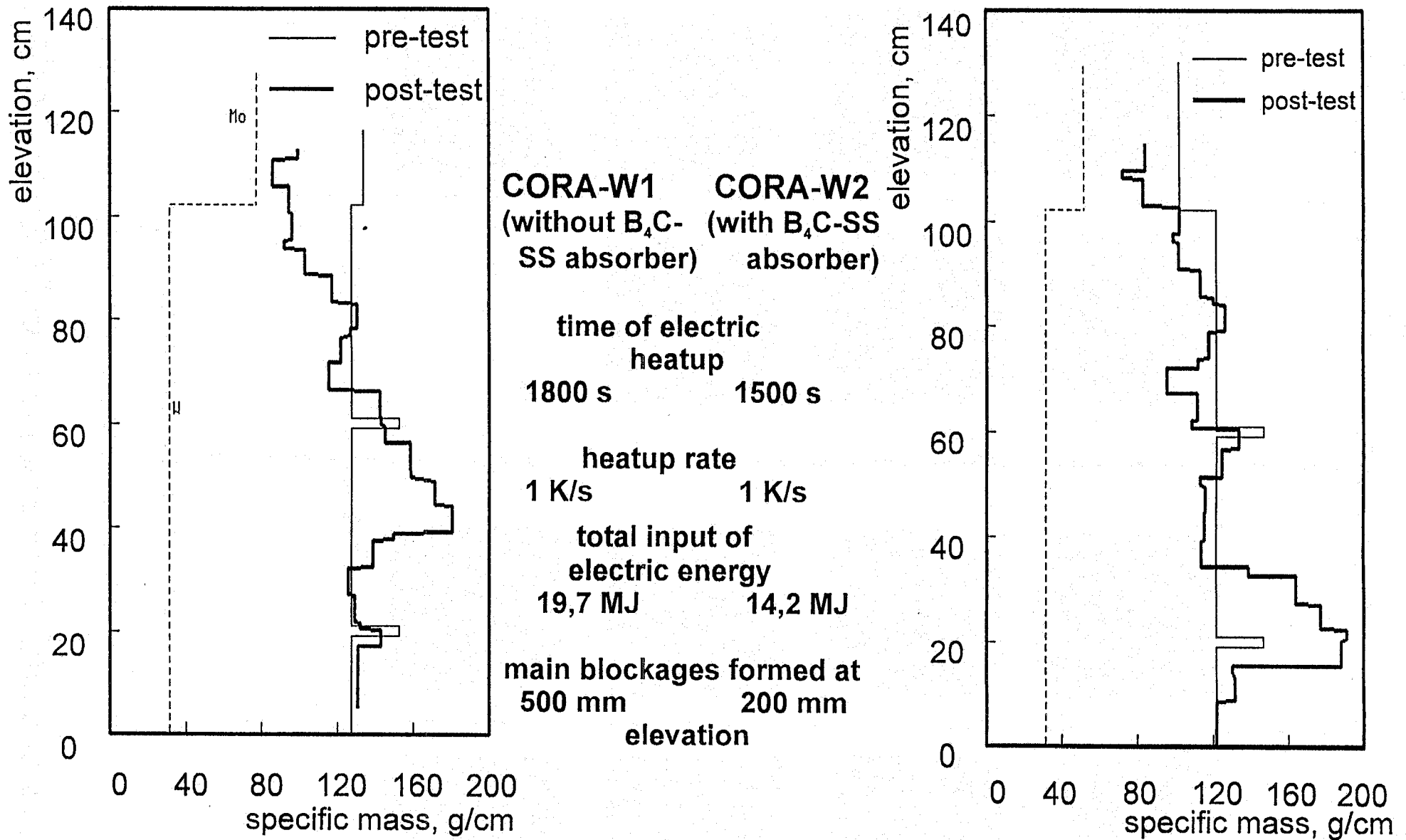
Fig.36: Influence of ss-B$_4$C absorber on posttest material distributions in the VVER - CORA tests.

CORA-W1
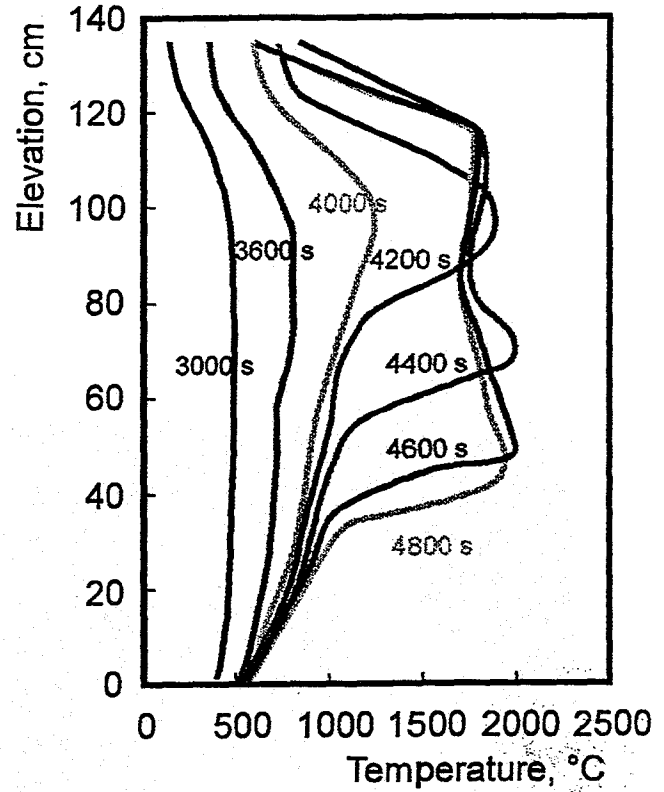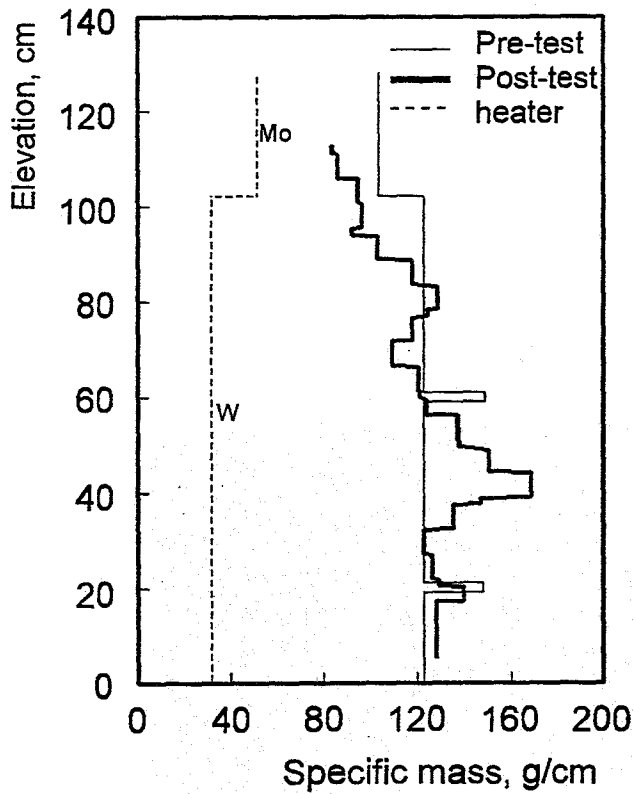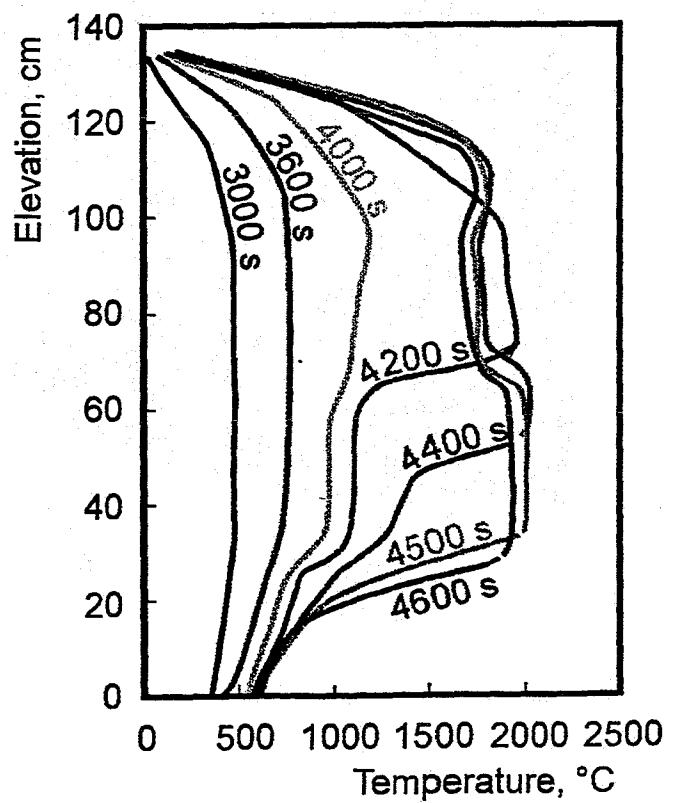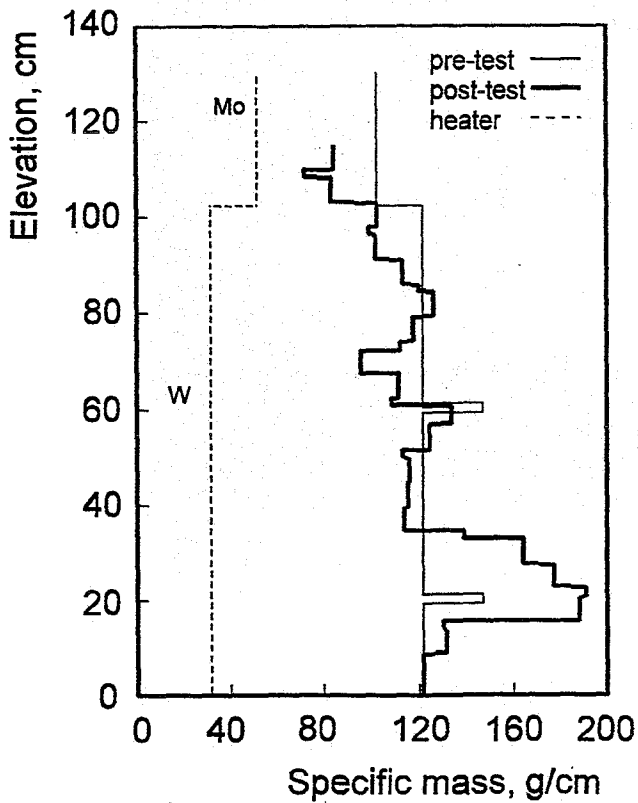
CORA-W2

Fig.37: Posttest material distribution compared to axial bundle temperature for CORA-W1 and CORA-W2.
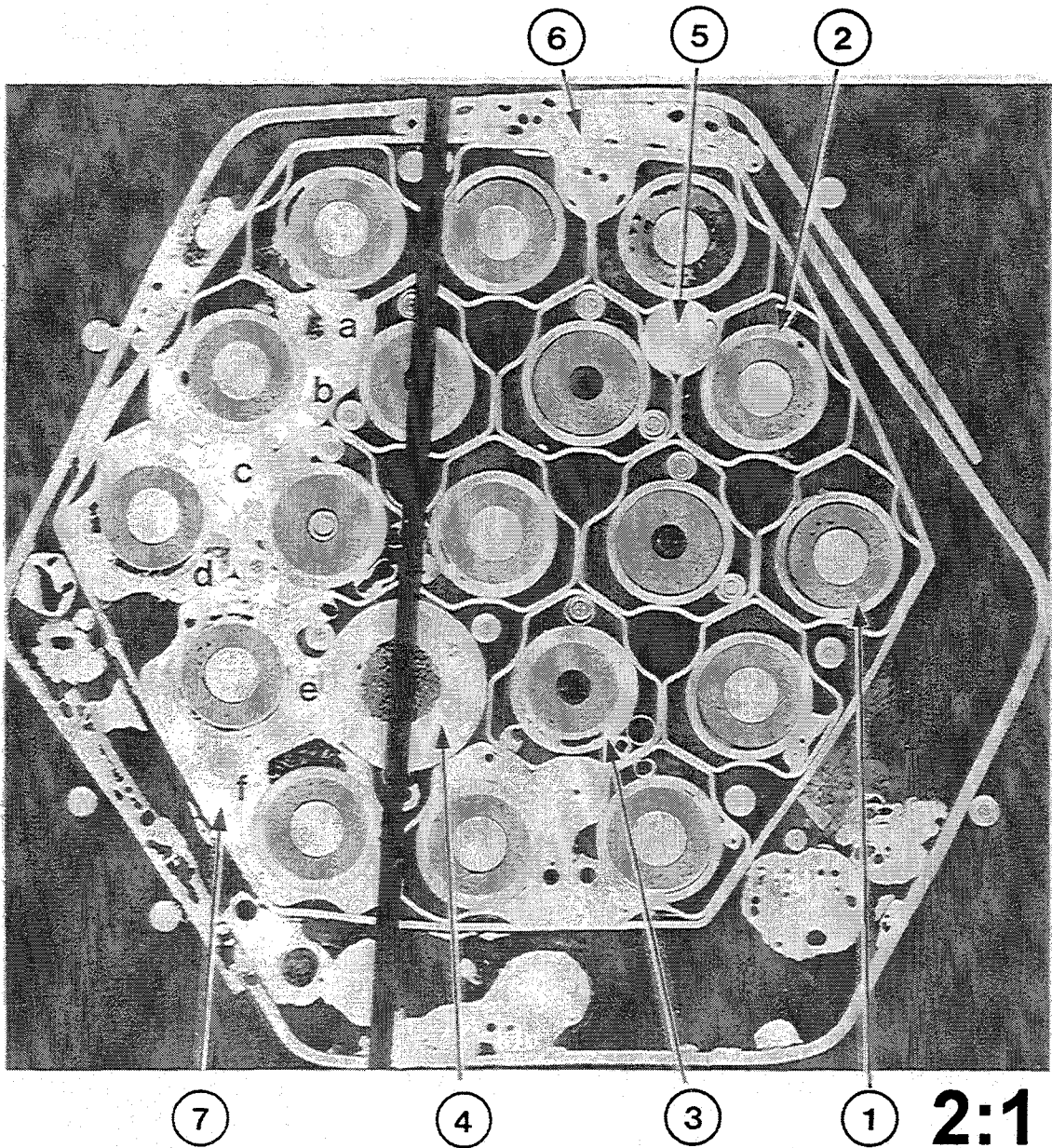
Fig. 39: Cross section of test CORA-W2 at 206 mm with positions of analysis.

Zr   Zr: 85 w-%
U   B: 15 "
Fe
Cr
Ni
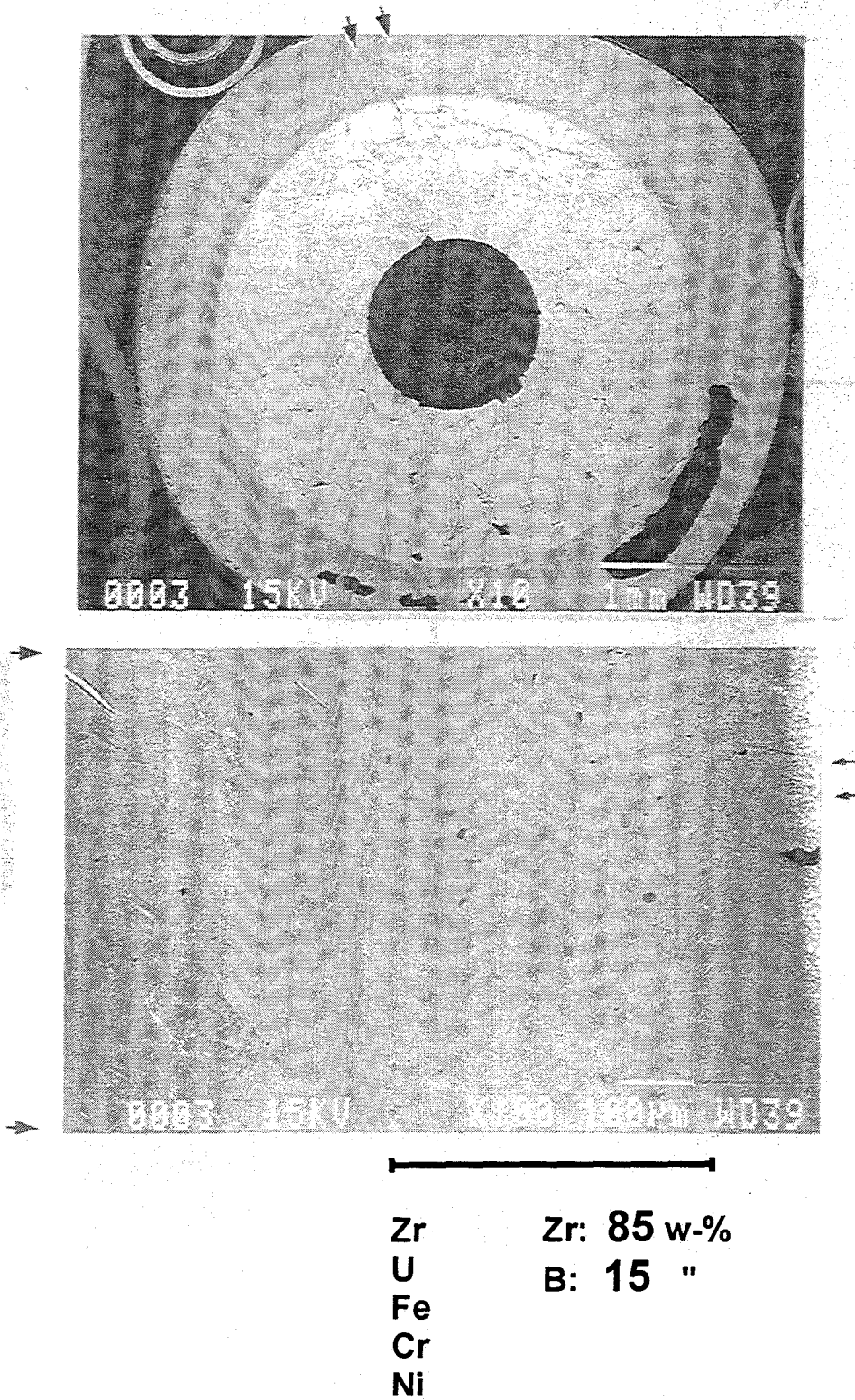
Fig. 40: Internal liquefaction of cladding in the neighbourhood of absorber CORA-W2, 206 mm, pos. 3
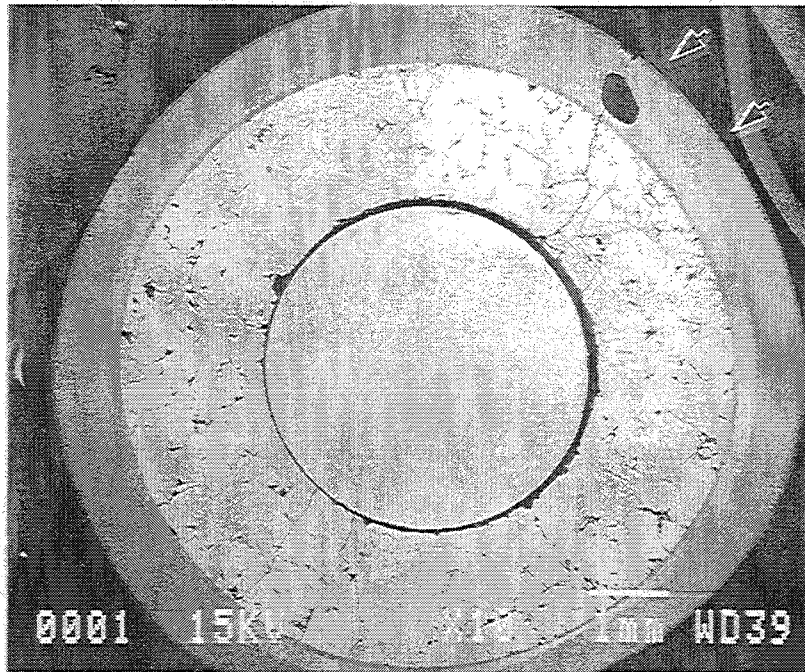
Zr: **76** w-%
U: **14**   "
Fe: **7**   "
Cr: **1.4** "

Fig. 41: Internal liquefaction of cladding (CORA-W2, 206 mm, pos. 3)
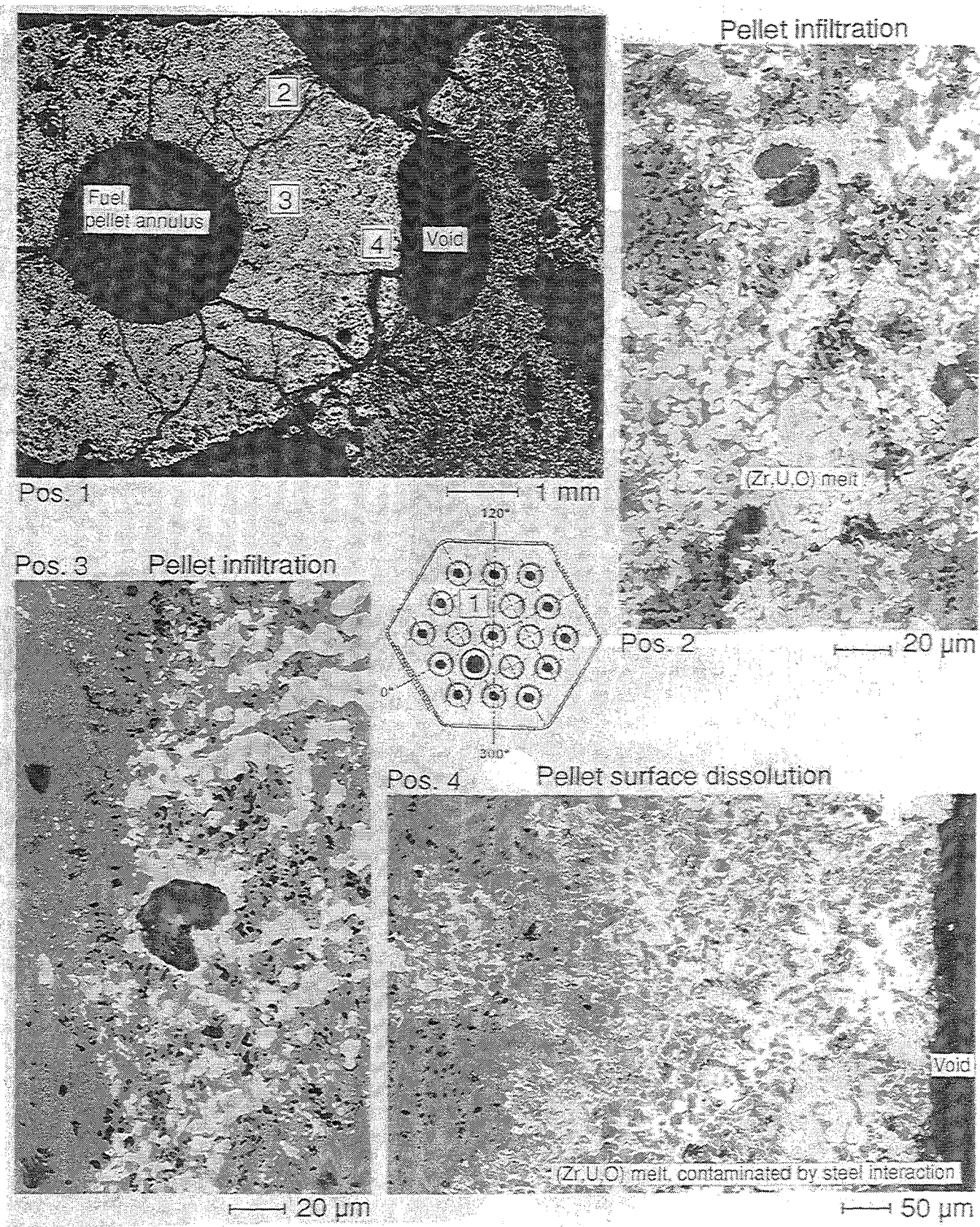
Fig. 42: Dissolution of a UO₂ pellet (CORA-W2, 206 mm)